Understanding the role of Uip4p, a novel NE/ER protein, in the maintenance of nuclear organization and cellular homeostasis in *Saccharomyces cerevisiae*

Thesis submitted for the degree of

Doctor of Philosophy

work carried out by

Pallavi Deolal

Reg. no. 15LBPH02

under the supervision of

Prof. Krishnaveni Mishra

DEPARTMENT OF BIOCHEMISTRY
SCHOOL OF LIFE SCIENCES
UNIVERSITY OF HYDERABAD
HYDERABAD – 500 046
INDIA

UNIVERSITY OF HYDERABAD
SCHOOL OF LIFE SCIENCES
DEPARTMENT OF BIOCHEMISTRY

DECLARATION

I, Pallavi Deolal, hereby declare that this thesis entitled "**Understanding the role of Uip4p, a novel NE/ER protein, in the maintenance of nuclear organization and cellular homeostasis in *Saccharomyces cerevisiae***" submitted by me under the guidance and supervision of Prof. Krishnaveni Mishra, is an original and independent piece of research work. I also declare that it has not been submitted previously in part or in full to this University or any other University or Institution for the award of any degree or diploma.

Date: 17-Jan-2022

Name: Pallavi Deolal

Reg. No. 15LBPH02

Pallavi Deolal

Signature of the student

CERTIFICATE

This is to certify that the thesis entitled "**Understanding the role of Uip4p, a novel NE/ER protein, in the maintenance of nuclear organization and cellular homeostasis in *Saccharomyces cerevisiae***" submitted by **Pallavi Deolal** bearing registration number **15LBPH02** in partial fulfilment of the requirements for award of Doctor of Philosophy in the School of Life Sciences is a bonafide work carried out by her under my supervision and guidance.

The thesis is free from plagiarism and has not been submitted previously in part or in full to this or any other University or Institution for the award of any degree or diploma.

The student has following publications prior to submission:

- **Deolal, P.,** and K. Mishra. 2021. Regulation of diverse nuclear shapes: pathways working independently, together. Commun. Integr. Biol. 14:158–175. *doi:10.1080/19420889.2021.1939942.*

- **Deolal, P.,** G. Male, and K. Mishra. 2021. The challenge of staying in shape: nuclear size matters. *Curr. Genet.* 1–8. *doi:10.1007/s00294-021-01176-1.*

Part of this work has been presented in the following conferences:

- GSA-The Allied Genetics Conference (TAGC); April 2020 *(Online)*
- XI-International Conference on Biology of Yeasts and Filamentous Fungi, November 2019, 10th Conference on Yeast Biology, February 2018
- International Congress of Cell Biology, January 2018
- Bangalore Microscopy Course, September 2017 (Zeeshan Khan Memorial Award for Best Poster Presentation)
- 6th meeting of the Asian Forum of Chromosome and Chromatin Biology, March 2017

Further the student has passed the following courses towards fulfilment of coursework requirement for Ph.D.

Course code	Name	Credits	Pass/Fail
BC 801	Analytical techniques	4	Pass
BC 802	Research ethics, Data analysis and Biostatistics	3	Pass
BC 803	Lab Seminar and Records	5	Pass

Supervisor

Prof. KRISHNAVENI MISHRA
Department of Biochemistry
School of Life Sciences
University of Hyderabad
Hyderabad-500046. (TS), INDIA

Head of the Department

HEAD
Dept. of Biochemistry
SCHOOL OF LIFE SCIENCES
UNIVERSITY OF HYDERABAD
HYDERABAD-500 046.

Dean of the School 17/1/2022

DEAN
School of Life Sciences
University of Hyderabad
Hyderabad-500 046.

TABLE OF CONTENTS

ACKNOWLEDGEMENT

I always find myself caught up in a fret when it comes to writing! And while I did not anticipate this, writing acknowledgement **is** *hard. However, I feel very grateful as I type this and reflect on my PhD journey. I, therefore, take this space to show my* **gratitude** *to people who have been a part of my research journey and made this thesis possible.*

Prima facie, I express my profound gratitude to my **supervisor** *Dr. Krishnaveni Mishra, Professor, Department of Biochemistry, SLS-HCU. Ma'am, thank you for accepting me as a PhD student and allowing me to have this amazing experience. Thank you for instilling good research practices, organizational habits, and presentation and communication skills. I am a work in progress but your fine blend of guidance and independence has allowed me to become better professionally as well as personally. I greatly value the amount of time that you spend listening to my (confounding) ideas, troubleshooting queries, discussing infinite possibilities- limitations and other challenges. Also, thank you for the comforting tea !*

While the idea for this thesis was nucleated by my supervisor, my **doctoral committee members**, *Prof. KVA Ramaiah and Prof. MBV Sepuri, have been very vital in chaperoning and powering the project. They have shown great interest in the prospects of the project right from its inception and continue to provide their constructive insights. Thank You Prof. Ramaiah and Prof. Naresh for your valuable time, participation and motivation. I look forward to your guidance beyond this thesis.*

It goes without saying that infrastructure and funding are key to research. **Funding** *bodies- Council of Scientific and Industrial Research (CSIR), Department of Biotechnology (DBT) and University Grants Commission (UGC) are highly acknowledged. I am very thankful to the Dean-School of Life Sciences and Head-Department of Biochemistry for ensuring the sufficiency of funds and maintenance of central research facilities. I would also like to thank my supervisor for the well-equipped lab space and provision for accessing best resources. I would like to acknowledge Dr. Helge Ewers and his lab for hosting me as part of ERASMUS exchange. I extend my thanks to CSIR for the research fellowship.*

A significant amount of time is spent in the lab during the course of PhD journey. I am very grateful to **my colleagues** *who made this tenure worthwhile. I owe gratitude to my seniors Dr. Imlitoshi, Dr. Hita, Dr. Neethu and Dr. Gurranna for their acceptance and assistance. We have had some great science and non-(sense) science discussions in lab, over tea and the extended lunch-breaks. Kathir, thank you for being the constant over these years! From fixing my broken gels to helping with RT-PCRs, lending me reagents as well as your ears- for my novel ideas AND rants with unvarying attention, you have been a great colleague and friend. Chhaya, you are a very accommodating person and make the lab very lively. Thank you for letting me slide into your imaging slots! Hitakshi, do not let PhD dull your sparkle. Vidya, you bring a lot of calm to the lab! Dr. Renu, thank you for periodically bringing my awareness to the life beyond PhD and of course, for ghar ka khana! Dr. Naresh, Swati and Dipika, thank you for your contribution to the other aspects of this project. Your efforts are deeply acknowledged. Bhaskar, you are the next avenger in this pursuit of deciphering the role of Uip4. Thank you for your interest in taking up the challenge! Anil bhaiya, thank you for all the daily chores that enable us to carry out our experiments efficiently. Thank you Srinivas for all your assistance in making the paperwork hassle free.*

My friends *are very dear to me and I would like to thank them for enriching my life. Kathir and Harita, you were home! Thank you for the beautiful time spent together. Chandani, everything was so effortless and easy with you! Fiza- you always uplift my mood and spirit! Himani, you make me a better person! Praveen- (un) thank you for turning my working Wednesdays in to weekends. Amita, all the conversations during the imaging and chai-paani session were indeed very therapeutic. I also thank Kanika and Shreemoyee for always cheering me on.*

My family *has always been very supportive of my career choices. I am thankful to them for having faith in me and giving me the independence and encouragement to pursue research.* ईजा बुबू तुमोरो आशीर्वाद छ यो। *M'mma, thank you for your endurance during difficult times, and enabling me to grow and explore. Papa, you teach me to be tolerant and approach life with flexibility. Rashi, thank you for all your affection, entertainment and constructive-criticism! Rashi, Cheena, Riya, Rini- you make everything pleasant!*

Thank You

-the thesis is now complete!

LIST OF ABBREVIATIONS USED

AMP	Ampicillin
BSA	Bovine serum albumin
CEN	Centromere
CHX	Cycloheximide
DAPI	4', 6-Diamidino-2-phenylindole
DNA	Deoxyribonucleic acid
dNTP	Deoxyribonucleotide
DMSO	Dimethyl sulfoxide
DTT	Dithiothreitol
EDTA	Ethylene-diamine-tetra acetic acid
ELYS	Embryonic Large Molecule Derived From Yolk Sac
ER	Endoplasmic reticulum
ESC1	Establishes silent chromatin1
FG	Phenylalanine- glycine
G418	Geneticin
GAA	Glacial Acetic Acid
GFP	Green fluorescent protein
h	Hour(s)
HeLa	Henrietta Lacks
HIS	Histidine
HGPS	Hutchinson–Gilford progeria syndrome
HRP	Horse-radish peroxidase
IF	Immunofluorescence
INM	Inner nuclear membrane
KASH	Klarsicht-Anc1-Syne1 homology
L	Litre
LB	Luria-Bertani broth
LEU	Leucine requiring
LINC	Linker of nucleoskeleton and cytoskeleton
LiAc	Lithium Acetate
LMNA	Lamin A
LMNB	Lamin B
µ	micro
m	Mili
M	Molar
MAT	Mating type
MDa	Megadalton
min	Minute (s)
mRNA	Messenger RNA
NE	Nuclear envelope
NUPS	Nucleoporin(s)
NPC	Nuclear pore complex
OD	Optical density
ONM	Outer nuclear membrane
PCR	Polymerase chain reaction
PEG	Polyethylene glycol
POM	Pore membrane protein

PVDF	Polyvinylidene Fluoride
PAGE	Polyacrylamide gel electrophoresis
PIPES	Piperazine-1,4-bis(2-Ethanesulphonic Acid)
RanGTP	Ran guanosine tri phosphate
RITE	Recombination induced tag exchange
RPM	Rotations per minute
SC	Synthetic complete
SDS	Sodium dodecyl sulphate
sec	Second(s)
SOB	Super optimal broth
SPB	Spindle pole body
STED	Stimulated emission depletion
ssDNA	Single-stranded DNA
TCA	TriChloro acetic acid
UIP4	Ulp1 interacting protein 4
UV	Ultraviolet
WB	Western Blot
WT	Wild type
YPD	Yeast extract-Peptone-Dextrose

LIST OF FIGURES

LIST OF TABLES

CHAPTER 1 INTRODUCTION

Cells are the basic unit of life. Coordination of cellular activity is essential for the survival of an organism. In order to carry out various metabolic processes efficiently, cells compartmentalize the space within them. Biomolecules are known to cluster in defined territories within the simplest of bacterial cell too (Yeates et al., 2008; Cheng et al., 2008). However, unlike prokaryotes, eukaryotic cells have an organized endomembrane system that results in well-defined organelles (Cohen et al., 2018). This compartmentalization ensures that the metabolic processes are spatially separated within membrane-bound organelles (Fig1). The major organelles present in a eukaryote system are the nucleus, mitochondria, endoplasmic reticulum (ER), Golgi, chloroplast (only in plants) and lysosomes (vacuole in plants and fungi). The form and function of every organelle are interdependent. Maintenance of organelle architecture is essential to execute biological processes in a regulated and coordinated fashion. The function of an organelle in a cell is linked to its structure and overall organisation of its sub-compartments. Improper spatial placement and altered levels of essential skeletal proteins affect not only the normal geometry, but often even the function, of an organelle.

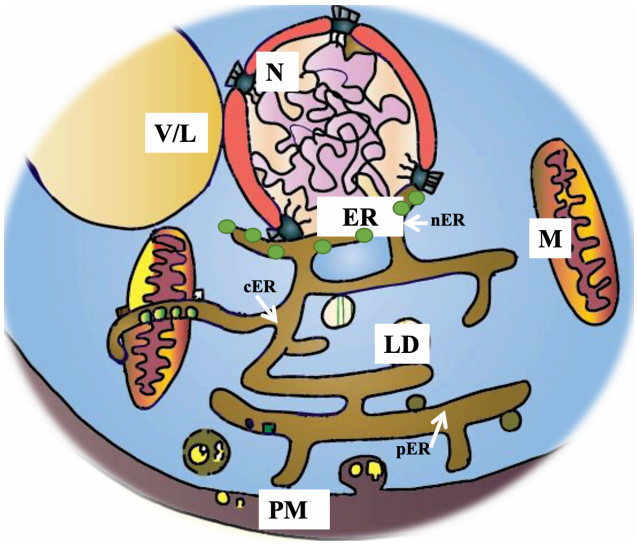

Fig1. Intracellular landscape of a typical eukaryotic cell.
This cartoon represents various cellular organelles. Each organelle has a distinct morphology, is strategically placed within the cell and contacts other organelles physically. N-nucleus, ER-endoplasmic reticulum, nER- perinuclear ER, cER- cytoplasmic ER, pER- peripheral/cortical ER, LD- lipid droplets, M-mitochondria, V/L- Vacuole/Lysosome PM- Plasma membrane

Changes in the shape of an organelle can have functional consequences (Fig2). Altered morphology affects inter and intra-organellar interactions, physical properties of the organelle, and their movement and relative positioning (Fig2, black arrows). Reversibly, perturbed protein interactions, membrane properties and restricted movement can also manifest as architectural and geometric alterations (Fig2, blue arrows).

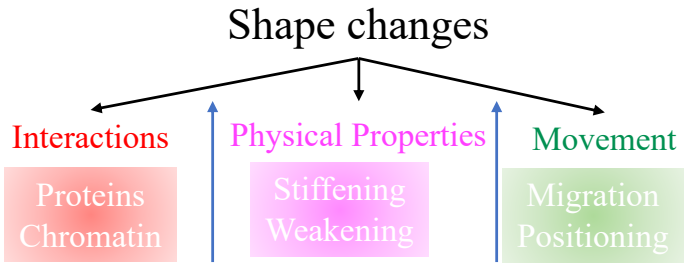

Fig2. Co-dependency between form and function of an organelle

1.1 NUCLEAR ORGANISATION

Nucleus is one of the most prominent organelles in a eukaryotic cell. Spatial organization of nucleus into various sub-compartments within the double membrane bilayer is one of the salient features of eukaryotes. The genome is organized within the nucleus in a non-random fashion resulting in the formation of discrete nuclear bodies associated with a specific function (Bortle and Corces, 2012). Chromosome ends (telomeres) are usually clustered and anchored at the NE in yeast. The nucleolus is the site of regulation for transcription of rRNA genes and assembly if ribosome subunits (Thiry and Lafontaine, 2005). The inner nuclear membrane (INM), acts as a site of regulation for various nuclear processes including transcription, mRNA export and DNA repair. Several INM associated proteins also provide structural support to the nucleus (Katta et al., 2014; Mekhail and Moazed, 2010). Of the various INM proteins, lamins are one of the most well studied and notable class of structural proteins. Lamins are intermediate filament class of cytoskeletal proteins that form a network beneath the INM and provide mechanical support to the nucleus (Dittmer and Misteli, 2011). Besides, they are involved in a multitude of nuclear functions such as supporting the nuclear structure, regulating genome organisation, DNA repair and transcription regulation, and nuclear mechanics (Dechat et al., 2010). While lower metazoans and plants have conserved lamin-like protein, the homologs of lamins have not been reported in yeast and other fungi (Deolal and Mishra, 2021).

The outer nuclear membrane (ONM) is continuous with the ER which extends up to the cell periphery in yeast (Fig1). The selective exchange of macromolecules between nucleus and cytoplasm occurs through the macro-molecular assemblies called the nuclear pore complexes (NPCs). NPCs are embedded in the NE where the inner and outer nuclear membrane fuse. Nuclear function is associated with changes in its morphology, which is in turn responsive to cellular processes such as growth, development, aging and movement. Conversely, functional defects in the proteins of the nuclear matrix and INM are associated with aberrations in nuclear organization (Méndez-lópez and Worman, 2012; Rempel et al., 2019), and lamins (Lattanzi et al., 2016). Of the various internal and external factors that determine nuclear shape, studies have reported the roles of genome size and ploidy, functional requirements of the cell, lifespan, chemical environment and signalling (Bahmanyar and Schlieker, 2020; Deolal and Mishra, 2021; Cantwell and Dey, 2021)

1.2 DIVERSE NUCLEAR SHAPES AND THEIR SIGNIFICANCE

Nuclei are often represented as spherical/round organelles. However, deviations from this morphology are seen across the eukaryotic supergroups (Fig3). Shapes as diverse as ovoid, lobed or condensed nuclei are seen in mammalian cells (reviewed by Skinner and Johnson, 2017). For instance, the nuclei of granulocytes and monocyte lineage of the mammalian immune system are multi-lobed or kidney-bean shaped while lymphocytes have a spherical, round nuclei (Theera-Umpon and Dhompongsa, 2007; Manley et al., 2018). Heterophils, the equivalent of neutrophils in birds, show species-specific differences in the presence or absence of nuclear lobes (Blofield et al., 1992). Lobed nuclei have their genetic material packaged in more than one sphere-like organisation giving the NE a lobulated appearance (Leitch, 2000). Multiple lobes are often connected with a thin chromatin-containing filamentous structure. Spermatozoa also exhibit wide variations in nuclear shapes in animals (Gu et al., 2019). The highly condensed sperm nucleus has asymmetric shapes depending on the shape of the sperm head since the nucleus occupies most of the sperm head. Most mammalian sperms including those of whales and dolphins have oval or paddle-shaped nuclei whereas birds display either tubular or worm-like nuclei (Miller et al., 2002; Santiago-Moreno et al., 2016; Gu et al., 2019). Plants too exhibit a tissue-specific diversity of nuclear shapes (reviewed by Meier et al., 2016). Spindle-shaped nuclei are seen in differentiated root epidermal and cortical cells (Chytilova et al., 1999). Meristematic and vascular tissues have spherical and rod like nuclear shapes,

respectively (Dittmer et al., 2007). Nuclei may have grooved surfaces, as in epidermal cells in onion and invaginations of NE produce lobed nuclei (Collings et al., 2000). In many instances, nuclei of circulating cells such as neutrophils are either lobed (neutrophils) or spindle shaped (fibrocytes) (Barzilai et al., 2017).

Though a nucleus typically holds a firm shape, the shape can change in response to internal and external stimuli. Nuclear shape normally changes during periods of cell division, migration, development and apoptosis. In cells undergoing open mitosis, the NE disassembles into vesicles and chromosomes are released into the cytoplasm for the duration of M-phase. In cells undergoing closed mitosis, the generally spherical/oval nucleus is stretched into various shapes until it finally splits into two spherical/oval nuclei (Wang et al., 2016). Shifting budding yeast cells to a less preferred carbon source also results in reduced circularity (Wang et al., 2016). Migration of mammalian cells through confined spaces affects the geometry of the entire cell and its organelles, including the nucleus (Chen et al., 2015; Makhija et al., 2016; Hobson et al., 2020). Nuclear morphology may change during physiological states like nuclear division, nuclear fusion during mating, development, differentiation, and cell migration (Deolal and Mishra, 2021). For instance, the round nuclei of budding yeast become dumbbell or spindle-shaped as they transition from S phase to G2 (Wang et al., 2016). During the plant root development, cellular elongation is accompanied by elongation of nuclei (Ketelaar et al., 2002). In *Drosophila*, the change of spherical to elliptical nuclear shape is critical during the cellularization stage, wherein asynchronous cytokinesis in the syncytial blastoderm leads to formation of uninucleate cells (Brandt et al., 2006). Thus, it appears that maintenance of cell-type specific nuclear morphology is highly regulated.

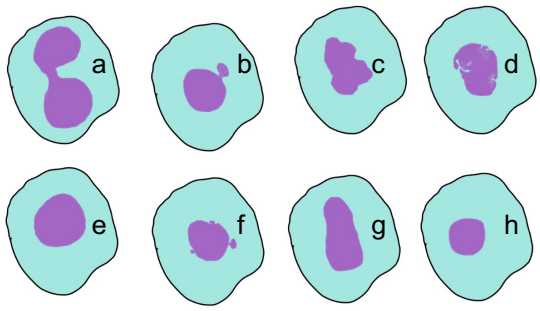

Fig3. Diverse nuclear morphologies associated with various physiological and pathological conditions

A graphical representation of the various kinds of nuclear morphologies (magenta) is shown. Such nuclei are referred to as: a- bilobed, b-blebbed, c-distorted, d-invaginated, e-quasi-round, f-flared, g-elongated, h-round, spherical

Alterations in nuclear shape are correlated with progression of essential processes like DNA repair, signalling, cell health and homeostasis; however, it is not clear whether distortion of nuclear shape is a cause or consequence of a change in the physiological status of a cell. NE protrusions that result in compartmentalization of the nucleus can give a lobular appearance to the nucleus (Taimen et al., 2009). Lobed nuclei are generally fragile and aid in mobility of the cells during processes like cell metastasis or differentiation (Manley et al., 2018). Evagination or excessive outward growth of either INM or ONM or both can result in a bleb like nuclear growth. The size and origin of such NE out growth or herniation can depend on various factors (Thaller and Patrick Lusk, 2018). Blebs are also often associated with regions of NE deficient in lamins and therefore prone to rupture. NE can show invaginations, with membrane projecting inwards. Such structures are also termed 'nucleoplasmic reticulum' and can originate either at the INM or cytosol. In plants, placental cells in Lilium ovaries have infoldings of INM continuous with the ER lumen, while onion epidermis and tobacco invaginations originate in the cytoplasm (Collings et al., 2000). An imbalance of forces along the nuclear axes can cause elongation of a quasi-round nuclei (MESEROLL and Cohen-Fix, 2016). Similarly, lack of factors that maintain a normally elongated nuclei can result in rounding of the nucleus. Sometimes, the nucleus can get abnormally shaped without falling into these defined deformities and form 'tail-like' membrane extensions or distorted NE (Fig3).

There is growing evidence of association between abnormal nuclear morphology, sub-nuclear organization defects and several human diseases. Loss-of-function mutations in nuclear proteins such as lamins, MAN1, Nesprin-1, Emerin and Torsin1 results in diseases characterized by abnormal nuclear morphology. These diseases, broadly referred to as nuclear envelopathies, include osteopoikilosis, sclerosing bone dysplasias, cerebellar ataxia, X-linked Emery-Dreifuss muscular dystrophy and DYT1 dystonia (Worman et al., 2010; Janin et al., 2017). Altered nuclear morphology associated with viral infection has been used as a diagnostic measure. For example, flower-like lobulated nuclei are used to diagnose adult T-cell leukemia caused by human T-cell leukemia virus type 1 (Matsuoka, 2005). HIV infection of terminally differentiated macrophages produces nuclear herniations that are induced by the HIV-1 Vpr protein (De Noronha et al., 2001). Nuclear dysmorphia and lobulation is also seen in various cancers such as lung and adenocarcinomas (Tolksdorf et al., 1980; reviewed in Zink et al., 2004). Nuclear blebs have also been reported in macrophages infected with *Mycobacterium tuberculosis* (Castro-Garza et al., 2018). Atypical nuclear shape is also observed in other pathological conditions, such as striated muscle laminopathies, Hutchinson-Gilford Progeria

Syndrome and mandibulofacial dysplasia (Tolksdorf et al., 1980; Goldman et al., 2004; Filesi et al., 2005; Alvarado-Kristensson and Rosselló, 2019). Patients of Hutchinson-Gilford Progeria Syndrome and mandibuloacral dysplasia show cells with aberrant nuclear morphology (Goldman et al., 2004; Filesi et al., 2005). Aberrant distribution of NPCs as a result of shape abnormalities has also been implicated in several human pathologies, including autoimmune diseases, viral infections, cardiomyopathies and various cancers (Capelson and Hetzer, 2009; Patel et al., 2015). These observations highlight the potential of nuclear morphology to affect multiple processes in the cell and reflect its disease status in some cases. Understanding signals which regulate the nuclear shape under normal conditions holds the potential to provide clues for deciphering mechanisms that deform and reshape the nucleus under physiological and pathological conditions.

1.3 INTERDEPENDENCE OF NE MORPHOLOGY AND NPC DISTRIBUTION

The transport of macromolecules between nucleoplasm and cytoplasm takes place through the massive protein assemblies called NPCs (Fig4). Proteins that are part of NPCs vary greatly in their size, structure and other bio-physical properties (Kabachinski and Schwartz, 2015). All these constituent proteins are referred to as nucleoporins or nups. The overall NPC structure is conserved across eukaryotes, and there are a core set of constituent conserved proteins (Belgareh et al., 2001; Mansfeld et al., 2006; Rasala et al., 2006). However, there are species specific additions and loss of protein components as well suggesting a tremendous amount of plasticity within this conserved structure (Chopra et al., 2019). The NPCs in yeast are made up of ~30 different nups which are assigned to various classes primarily depending on their relative position in the entire complex (Rout et al., 2000). The scaffold nups are the ones that nucleate the NPC assembly and hold the entire complex in place resulting in a cylindrical core. These are also called membrane nups due to the presence of trans-membrane domains in their structure that allows the anchoring of these proteins to the membrane at the pore. The inner and the outer ring nups decorate the diameter of the channel. The phenylalanine glycine (FG) repeat containing nups are present along the inner side of the channel and are key regulators of the direction and flux of transport. The entire NPC structure is stabilised by a combination of interaction of certain filament nups with the cytoskeletal components and membrane proteins (Krull et al., 2004).

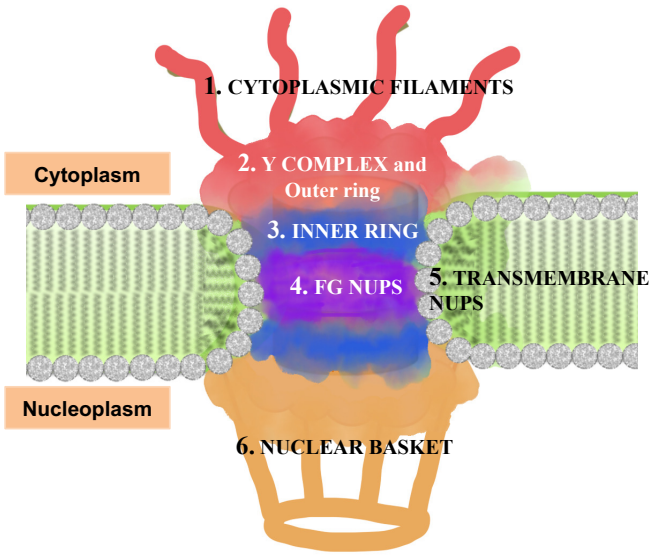

1. Nup159, Nup42
2. Nic96, Nup82, Nup133, Nup84, Nup85
3. Nup188, Nup170, Nup157
4. Nup116, Nup100, Nsp1, Nup49
5. Pom152, Pom34, Ndc1
6. Nup60, Nup1, Nup2, Mlp1, Mlp2

Fig4. Graphical representation of yeast NPC
Various subunits of yeast NPC and some of their constituents are shown here.

NPC assembly

NPCs are inserted into the NE at the site of inner and outer nuclear membrane fusion (Dawson et al., 2009). Previous studies have reported an intricate dependence of nuclear shape and NE dynamics on the distribution of NPCs (Schneiter and Cole, 2010). Mutants that have aberrant NPC distribution are often accompanied by nuclear shape abnormalities. In yeast, several integral ER proteins such as Brr6, Brl1, Apq12 and reticulons-Rtn1, Yop1 are important for the formation and stabilisation of membrane curvature at this site of pore formation. The current understanding is that the biogenesis of NPC begins when nups with amphipathic helices and membrane binding properties begin to associate with the pore membrane (Marelli et al., 2001; Zhang et al., 2021). This nucleates the process of NPC assembly. The exact sequence of events governing the assembly of NPCs has not been deciphered yet. Several possible pathways and mechanisms have been proposed by various groups trying to understand the principles governing initiation of assembly, site selection, recruitment of nups and their turnover. Based on the available literature, there are two distinct mechanisms operating in higher eukaryotes (Doucet et al., 2010; Otsuka and Ellenberg, 2018). Metazoans undergo open mitosis. The nuclear envelope, which begins to disassemble during prophase, is re-assembled after the two daughter nuclei are separated. When the nuclear envelope begins to disassemble, the peripheral NUPs are the first ones to dissociate from the NPC. The remaining skeleton which has members of the inner ring, FG and transmembrane Nups stays attached to the ER membrane. This

facilitates quick resealing of nuclear envelope and assembly of NPCs at the pores post mitosis (Knockenhauer et al., 2016). The interaction between various proteins in this entire process is largely dependent on their phosphorylation state (De Noronha et al., 2001). Cyclin/CDK complexes regulate the key members of this signalling cascade (Maeshima et al., 2010). NPC disassociation is accompanied by lamin depolymerization (De Noronha et al., 2001). *In vitro* studies that use assembled nuclei have identified formation of a Y shaped structure of Nup107-160 and ELYS components (Franz et al., 2007; Rasala et al., 2008). This is followed by recruitment of membrane associated nups. This pre-pore then serves as the nucleating centre for recruitment of other nups such as inner ring and nuclear basket proteins. This post mitotic assembly is thought to be driven primarily by RanGTP promoted ELYS localization to the chromatin (Rasala et al., 2008).

In contrast to the assembly of NPCs following mitosis, the number of pores grow continuously on the nuclear membrane during the interphase (Maeshima et al., 2011). This interphase assembly requires fusion of the double membrane bilayer and the insertion of a NPC takes about one hour to completion unlike the post mitotic assembly that requires around ten min only (Doucet et al., 2010; Otsuka and Ellenberg, 2018). Since yeast undergoes closed mitosis, the mechanism of NPC assembly is similar to the interphase assembly in mammalian cells. The density of NPCs on the nuclear envelope increases continuously during the growth. An inside-out mechanism of NPC growth has been proposed by Otsuka, S. *et al* (2016). According to this mechanism, the nucleation begins on the INM and the pre-pore grows out towards the ONM like a mushroom, followed by fusion of the two membranes. Immediately after the membrane fusion, the pre pore undergoes rapid rearrangement to form the mature NPC with an eight-fold structural symmetry.

Association between NE morphology and NPC distribution

Proteins with membrane deforming and curvature sensing abilities are shown to be important for initiating the assembly of NPC(Lone et al., 2015). Examples of such proteins include members of reticulon and DP1/Yop1 family proteins (Dawson et al., 2009). The inner nuclear membrane protein Sun1 is also found to be important for this in U2OS cells (Talamas and Hetzer, 2011). A study which examined the organization of NPCs in some of the chromatin remodelling mutants also reported changes in shape of budding yeast nucleus (Titus et al., 2010). The mutants had abnormal NE morphology as well as mislocalization of NPCs.

Interestingly, addition of benzyl alcohol, an agent that increases membrane fluidity, restores the nuclear shape in these mutants, indicating mechanical reasons behind the shape changes (Titus et al., 2010). In addition, members of the membrane remodelling machinery- the endosomal sorting complex required for transport (ESCRT), have also been shown to play a role in proper NPC assembly in yeast (Scourfield and Martin-Serrano, 2017; Gu et al., 2017; Koch et al., 2020). Genetic analysis reveals that there is epistatic interaction between ESCRT members and proteins involved in NPC biogenesis (Frost et al., 2012; Webster et al., 2014). In yeast, ESCRT-III component-Chm7, is shown to be important for maintenance of pore homeostasis and quality control by removal of misassembled NPC subcomplexes (Webster et al., 2014, 2016; Koch et al., 2020). Chm7, along with INM proteins -Heh1/Heh2, and ESCRT-III associated protein- Vps4, is necessary for sequestration of nups away from the NE (Webster et al., 2016; Koch et al., 2020). While a direct participation of ESCRTs in pore stability or biogenesis is not reported in higher eukaryotes, downregulation of ESCRT components is characterized by deformed nuclei and aberrant membrane proliferation (Arii et al., 2018; Olmos et al., 2015). Cell cycle delay and aberrant NPC distribution are other accompanying defects reported upon depletion of ESCRT-III subunits in humans (Carlton et al., 2012).

The *de novo* assembly of an NPC requires INM and ONM fusion and as such the process is inextricably linked to the NE architecture (Maeshima et al., 2006; Fernandez-Martinez and Rout, 2009; De Magistris and Antonin, 2018). Nups with membrane binding regions play crucial roles in insertion and stabilization of NPC at the site of pore formation. ScNup1 and ScNup60 support the INM via their amphipathic domains; overexpression of these nups induces membrane curvature and distortions in the NE (Mészáros et al., 2015). The membrane binding regions of nucleoporins (Nup133, Nup53, Pom121, gp210) contribute significantly to the NE stability (Kim et al., 2014). Upon silencing of a transmembrane protein gp210 in HeLa cells, along with clustered NPCs, aberrant nuclear membrane structures are observed (Cohen et al., 2003). Another vertebrate transmembrane nup, Pom121, also contributes to nuclear membrane stabilization and assembly of functional NPCs by regulating the spacing between INM and ONM during fusion to nucleate NPC assembly (Antonin et al., 2005; Yavuz et al., 2010).

The distortion of nuclear shape observed in overexpression, complete loss or downregulation of nups further underscores the importance of NPCs in nuclear shape maintenance. For instance, depletion of ELYS/Mel28, a nucleoporin essential for post-mitotic NPC assembly,

results in aberrant distribution of lamin A/C and other INM proteins in HeLa cells (Clever et al., 2012). Similarly, reduced expression of Nup153 in HeLa cells results in nuclear membrane invaginations and lobulation, and punctate lamin A/C distribution (Zhou and Panté, 2010). Depletion of Nup53 or Nup93 in HeLa cells also results in abnormally shaped nuclei albeit without affecting lamin distribution along the NE (Hawryluk-Gara et al., 2005). Budding yeast cells lacking nups or with other defects in NPC assembly show herniations of the NE (Wente and Blobel, 1990; Titus et al., 2010; Webster et al., 2014). The overexpression of Nup53 in *S. cerevisiae* leads to formation of intranuclear double-membrane lamella, which is lined beneath the INM (Marelli et al., 2001). In *Arabidopsis*, cells lacking the nucleoporin Nup136 show spherical instead of normal ellipsoid nuclei (Tamura et al., 2010); these mutants have a shorter major axis length compared to the elongated nuclei of wild type. Plant cells that overexpress Nup136 display extremely elongated nuclear structures instead (Tamura and Hara-Nishimura, 2011). This shows that levels of Nup136 are critical for regulation of nuclear morphology in *Arabidopsis*.

While it remains to be resolved if these distortions are a primary outcome of subunit depletion, it is also possible that the nuclear shape changes are a secondary consequence of the effect of altered complex stoichiometry on nuclear size and the interaction of members with other structural determinants.

NPC stability and cellular health

Deterioration of NE integrity and NPC function is concomitant with the increasing organismal age and decline of cellular health (Capelson and Hetzer, 2009; Robijns et al., 2018). NPCs are the sole conduits of regulated nucleo-cytoplasmic transport. Mis-localization and altered stoichiometry of nucleoporins has been linked to aging and clinical pathologies (D'Angelo et al., 2009; Lord et al., 2015). Malfunctional NPCs are implicated in pathology of multiple neurodegenerative and cardiovascular diseases (Capelson and Hetzer, 2009). Nuclear inclusions have been reported in neurological disorders and dystonia (Woulfe, 2007). Regulation of starvation and aging induced nucleoporin turnover is also of particular interest in the field of neurodegenerative diseases (Sakuma and D'Angelo, 2017; Rempel et al., 2019; Lord et al., 2015). The protein constituents of NPCs, which are among the longest-lived protein complexes of the cell, undergo turnover (Daigle et al., 2001; Fernandez-Martinez and Rout, 2009; Toyama et al., 2013). While the scaffold nucleoporins are more stable, cytoplasmic and

FG nups are turned over more rapidly in metazoans and yeast (Daigle et al., 2001; Toyama et al., 2019; Rempel et al., 2019, 2020). Dysfunctional NPCs are associated with cellular aging and loss of proteostasis (Martins et al., 2020). Recent work has contributed to our understanding of how NE integrity and NPC turnover is regulated under specific conditions such as either nitrogen or carbon starvation (Tomioka et al., 2020; Lee et al., 2020). This response is important for coordinating overall stability and function of NPCs.

The megadalton NPCs have several sub-components. Various nuclear and non-nuclear components are important in regulating the assembly, turnover and function of NPCs. Defective assembly of NPC intermediates and dysregulation of nuclear quality control pathway results in abnormal nuclear shape (Wente and Blobel, 1993; John J. Scarcelli et al., 2007; Webster et al., 2016). NE extension or herniations have been observed in yeast as a result of such failed nuclear protein quality control pathways (Wente and Blobel, 1993; Webster et al., 2016). When the surveillance machinery fails to optimally monitor the early steps of NPC assembly, nups mislocalize and are stored in cytoplasm along with members of the ESCRT machinery (Webster et al., 2016). Cells showing aberrant cytosolic nups also have accompanying growth defects. Yeast mutants that have nuclear morphology and NPC assembly defect, such as *nup116*Δ*,* display strong exacerbated phenotype when combined with loss of nuclear components involved in NPC surveillance machinery such as Heh1, Heh2 and Chm7. The ONM is known to share several proteins with the ER. Many such ER proteins also contribute to NPC biogenesis and assembly (Casey et al., 2015; Dawson et al., 2009; Scarcelli et al., 2007; Lone et al., 2015). A non-essential integral membrane protein of the yeast ER-Apq12, in concert with two proteins Brl1 and Brr6, is essential for NPC biogenesis (Lone et al., 2015). These proteins are believed to act as local sensors and regulators of membrane homeostasis thereby positively regulating NPC assembly. About 40% of the *apq12*Δ cells also have cytosolic spots containing nups and these mutants are sensitive to reduced temperature (Scarcelli et al., 2007). The presence of amphipathic helix in Apq12 is required for promoting phosphatidic acid accumulation at the NE and regulating function of Brr6 and Brl1 (Zhang et al., 2021). Suppressing expression of essential proteins of Brr6 and Brl1, renders the cells sensitive to increased membrane fluidity as encountered during increased growth temperatures or addition of membrane fluidizing agents such as benzyl alcohol. Since Brr6 and Brl1 directly interact with nups at the NE, this growth defect is proposed to be related to NE remodelling and other membrane related functions, rather than via lipid homeostasis (Zhang et al., 2018). Interestingly, lipid droplets (LDs) have recently been shown to act as reservoirs for nups

(Kumanski et al., 2021). This study identified several nups as part of the cytosolic LD proteome. However, the exact function of this association remains elusive.

These studies underscore the importance of both, the components of the NE including, proteins of the NE, NPC and components of other organelles like ER, LD in the regulation of the shape, architecture and function of the nucleus.

1.4 SCOPE AND AIM OF THE CURRENT STUDY

Despite the knowledge of basic structural components of NE, a clear understanding of the mechanisms that contribute towards the maintenance of shape of NE and integrity of the associated complexes is lacking. To understand how the nuclear organization is achieved and the nuclear architecture is maintained, it is important to know the key players and components involved in the process. A genome-wide screen holds the potential to look for all the components spread throughout the genome. The approach used in our lab involved screening deletion mutants of all the non-essential genes in yeast for defects in localization of an inner nuclear membrane protein and distribution of the nucleoporins on the nuclear envelope. Live cell imaging was done using fluorescent tagged marker proteins. Yeast is easy to handle, non-pathogenic, has a rapid growth cycle and is easy to manipulate genetically. The basic cellular mechanisms and key players are conserved between yeast and higher eukaryotes. Importantly, unlike metazoans it undergoes closed mitosis and the yeast nuclear membrane does not disassemble during mitosis (Rout and Wente, 1994).

In order to identify novel components involved in maintaining nuclear morphology we initiated a fluorescence microscopy-based genome-wide screen approach in budding yeast. Loss of genes that reside in various non-nuclear spaces, have distorted nucleus suggesting that several pathways and processes contribute to nuclear shape regulation and perturbing them can cause nuclear shape distortions (Male et al., 2020; Deolal and Mishra, 2021). While some of the candidates obtained could be mapped to known biological pathways, we also found several uncharacterized genes. In this thesis one such uncharacterized protein, Uip4p, was studied for its effect on the assembly and distribution of nuclear pore complexes. We show that Uip4 localizes predominantly to the NE/ER and loss of Uip4 results in dramatic mis-localization of the NPCs. Furthermore, we also find that Uip4 expression is increased when the cells transition to stationary phase of growth. In this work, we have investigated the role and regulation of

Uip4 in *Saccharomyces cerevisiae.* This work opens up avenues for understanding multiple ways in which cellular components can contribute towards maintenance of the nuclear shape, integrity and thereby function.

1.5 SPECIFIC OBJECTIVES OF THE STUDY

The key goals of the study are as follows:

1. To understand the role of Uip4 (Chapter 3 and 4)

a) Establish the role of Uip4 in maintenance of nuclear shape
b) Examine the effect of loss of *UIP4* on the organization of nuclear complexes
c) Examine the localization of multiple nucleoporins in *uip4*Δ
d) Address how Uip4 affects localization and distribution of NPC

2. To understand the regulation of Uip4 in yeast (Chapter 5)

a) Identify domains and sequence features of Uip4
b) Determine the localization of Uip4
c) Analyse the expression of Uip4
d) Investigate the regulation of expression of Uip4

3. To identify the biological pathways where Uip4 functions (Chapter 6)

a) Identify novel physical interactors of Uip4
b) Analyse the pathways

CHAPTER 2 MATERIALS AND METHODS

2.1 MOLECULAR BIOLOGY TECHNIQUES

Plasmid isolation from bacteria

Plasmid isolation from bacteria was done by Alkaline Lysis method. A single colony of bacteria was inoculated in 3mL of LB broth containing appropriate antibiotic for selection. The culture was allowed to grow overnight at 37ºC with shaking at 220rpm. 2mL of culture was harvested in an Eppendorf tube and cells were pelleted by spinning at 13000rpm for 1min. Next, the media was decanted and the tube was inverted on a tissue to ensure excess liquid is removed. 200µl of ice-cold Sol I was added to the pellet and the pellet was dissolved either by pipetting or vortexing the tube for 5-10 sec at maximum speed. This was followed by addition of 200µl of Sol II and gently inverting the tube to mix. 200µl of Sol III was added after this and the contents were mixed by inverting the tube 4-5 times. After this the tube was placed immediately in ice for 5min. Next, the tubes were spun at 13000 rpm for 10 min at 4ºC. The supernatant was collected and added to a fresh Eppendorf tube containing 420µl of isopropanol. Mixing was done by inverting the tube 4-5 times. The DNA was precipitated by spinning the tube at 13000 rpm for 10 min at room temperature. This was followed by washing the pellet with 70% ethanol and air drying it to remove the residual alcohol. Finally, the plasmid DNA was resuspended in 40µl of TE-RNase and incubated at 37ºC for 30 min. The concentration and purity of plasmid was checked either spectroscopically or by agarose gel electrophoresis.

Solution I	25mM Tris-Cl pH8.0
	10mM EDTA pH8.0
Solution II	0.2%NaOH
	0.2% SDS
Solution III	3M Potassium Acetate
	11.5% Glacial Acetic Acid
TE-RNase	10mM Tris-Cl pH7.4, 1mM EDTA pH8.0, 0.1mg/mL RNase

Agarose gel electrophoresis

Agarose Gel	0.8% in 0.5X TAE buffer
TAE (1X)	40mM Tris
	20mM Glacial Acetic Acid
	1mM EDTA

Genomic DNA isolation from yeast

A single colony of yeast was inoculated in 5mL of YPD/SC and grown overnight. The cells were harvested by centrifugation at 3000rpm for 5 min. The supernatant was discarded and cells were resuspended in 500µl of breaking buffer. The cells suspension was transferred to a 2.0mL microfuge tube containing glass beads up to ~200µl mark. To this, 200µl of Phenol:Chloroform:Isoamylalcohol (25:24:1) solution was added. The tubes were sealed with parafilm tape and vortexed at high speed for 2 min. Next, 200µl of TE-pH8.0 was added to the same tube and vortexed briefly for 15-20 sec at high speed. The tube was centrifuged at 13000rpm for 5 min and the top aqueous layer was transferred to a clean microfuge tube and 1mL of 100% ethanol was added to it. The contents were mixed by gently inverting the tube and then centrifuged at 13000rpm for 5 min. The supernatant was discarded and DNA pellet was allowed to air dry. The pellet was resuspended in 30-50µl of TE-RNase. The quality and approximate concentration of DNA was assessed by agarose gel electrophoresis.

Breaking Buffer:

10mM Tris-Cl pH8.0
1mM EDTA pH8.0
100mM NaCl
2% TritonX-100
1% SDS

Plasmid isolation from yeast

A single colony of yeast was inoculated in 5mL of YPD/SC and grown overnight. The cells were harvested by centrifugation at 3000rpm for 5 min. The supernatant was discarded and cells were resuspended in 200µl of breaking buffer. The cells suspension was transferred to a 2.0mL microfuge tube containing glass beads up to ~200µl mark. To this, 200µl of Phenol:Chloroform:Isoamylalcohol (25:24:1) solution was added. The tubes were sealed with paraffin and vortexed at high speed for 2 min. The tube was centrifuged at 13000rpm for 10 min and the top aqueous layer was transferred to a clean microfuge tube and equal volume of chilled 95% ethanol was added to it. The contents were mixed by gently inverting the tube and then placed in -20ºC for 30min. The DNA was precipitated by spinning the tube at 13000 rpm

for 10 min at room temperature. This was followed by washing the pellet with 70% ethanol and air drying it to remove the residual alcohol. The pellet was resuspended in 20µl of TE-RNase. 10µl of this yeast plasmid DNA was transformed into ultra-competent bacterial cells.

RNA isolation from yeast

A primary culture of desired strains was grown overnight. Next day, appropriate volume of inoculum was taken and secondary culture was set up to an initial OD600 of 0.15-0.20. A 5mL culture containing cells equivalent to 1unit OD600 were harvested after desired growth or treatment. The cell pellet was washed with cold, sterile water, transferred to a microfuge tube and snap frozen in liquid nitrogen. The pellet was then stored in -80ºC. To begin RNA isolation, the pellet was resuspended in TES buffer prepared freshly. This suspension was added to another microfuge tube containing equal volume of water saturated acidic phenol preheated to 65ºC. The tubes were then placed in thermomixer set at 65ºC and incubated for 1hour with intermittent mixing by gently inverting the tube. The tubes were then placed in ice for 5 min followed by centrifugation at 13000rpm for 5 min. The top aqueous layer was collected and added to an equal volume of chloroform to get rid of residual phenol. The solution was centrifuged again at 13000rpm for 5 min and aqueous layer was collected. To this, 2.5 volumes of chilled 100% ethanol and 0.10 volume of 3M sodium acetate (pH5.2) was added for precipitating RNA. The tubes were then placed in -80ºC for at least 2 hours (upto overnight). RNA was pelleted by spinning at 13000rpm for 10 min followed by washing the pellet with 70% ethanol. The pellet was allowed to air dry in the tube followed by resuspension in 100µl of RNase free water. The integrity of RNA was checked by agarose gel. DNase digestion of RNA was done by using RNase free-DNase and further DNA contamination was tested by PCR.

TES buffer
10mM Tris-Cl pH7.5
10mM EDTA pH8.0
0.5% SDS

Restriction digestion

For digestion of DNA using high-fidelity restriction enzymes from NEB, the cocktail was prepared as follows for 10µl reaction. Restriction digestion was carried out at 37ºC for a minimum of 20 min.

Table1: Setting up restriction digestion

Component	Volume
10X CutSmart Buffer	1µl
DNA (1-2µg)	2-5µl (depending on concentration)
Enzyme (4units)	0.2µl
Deionized water	3.8-6.8µl

Polymerase Chain Reaction

The PCR reaction for amplification was set as follows. Standard Taq Buffer was used for Taq Polymerase and ThermoPol Buffer was used with Vent Polymerase. All enzymes used were from New England Biolabs (NEB).

Table2: Setting up PCR

Component	Volume
10X Buffer	2.5µl
10mM dNTPs	0.5µl
10mM FP	0.5µl
10mM RP	0.5µl
Template DNA (50-100ng)	1µl
Polymerase	0.125µl
MiliQ water	19.875µl

PCR reaction was carried out as follows:

95ºC	Initial denaturation	
95ºC	Denaturation	25-35cycles
55-65ºC	Annealing	
72ºC	Extension	
72ºC	Final Extension	
4ºC	Hold	

Colony PCR

This protocol was used to do rapid screening of genomic DNA for gene deletions or epitope tagging. A small number of cells were picked from a single colony of yeast using a toothpick and resuspended in 40µl of 20mM NaOH in a PCR tube. Cells were lysed by heating at tube at 98ºC for 10min followed by placing on ice immediately. The tubes were spun at high speed for 15 sec and 1µl of the supernatant was used as a template for PCR. The PCR was set up as described above.

cDNA synthesis and qRT-PCR

cDNA was prepared by using Verso cDNA synthesis Kit by ThermoScientific using 1µg of RNA as template. The reaction mixture was prepared as follows:

Table3: Reaction mixture for cDNA synthesis

Component	**Volume**
5X cDNA synthesis Buffer	4µl
5mM dNTP Mix	2µl
RNA Primer	1µl
RT enhancer	1µl
Verso Enzyme Mix	1µl
Template (RNA)	1-5µl
Nuclease free water	to 20µl
Total Volume	**20µl**

The quality of cDNA was tested by PCR. Transcript levels were tested by qRT-PCR. ΔΔCt method was used to calculate fold change (Abraham and Mishra, 2018).

2.2 LIST OF PLASMIDS

The following plasmids and clones were used in the current study. All new DNA constructs were confirmed by restriction digestion and sequencing.

Table4: List of plasmids used in the study

Reference no.	Name	Description	Reference/ Source
CKM 32	pRS313	YC-type centromere vector	(Sikorski and Hieter, 1989)
CKM 35	pRS316	YC-type centromere vector	(Sikorski and Hieter, 1989)
CKM 74	pFA6a-13MYC-HIS3MX	Yeast genomic targeting	(Longtine et al., 1998)
CKM 338	SPC42-dsRED: URA3	Marker for SPB	(Conrad et al., 2007)
CKM 353	pUN100-GFP-NUP49	Marker for NE/NPC	(Belgareh and Doye, 1997)
CKM 361	pDZ45-GFP-ESC1	Marker for INM/NE	(Male et al., 2020)
CKM 362	pBEVY-L	Bi-directional expression vector for yeast	(Miller, 1998)
CKM 462	pADH1- NLS-GFP2X-P12: URA3	Construct for monitoring nuclear import	(Stade et al., 1997)
CKM 466	pUIP4-UIP4-pRS313	UIP4 cloned in pRS313 under its native promoter as BamHI/SalI fragment	This study
CKM 501	pGPD-UIP4-13MYC-pBEVY-L	UIP4-13MYC cloned in pBEVY-L with a constitutively active bi-directional promoter that consists of a fusion of the GPD promoter and a short derivative of the ADH1 promoter as XbaI/SalI fragment	This study
CKM 503	pUN100-Nup49-mCherry	Marker for NE/NPC	(Chadrin et al., 2010)
CKM 506	pGPD-UIP4-pBEVY-L	UIP4 cloned in pBEVY-L with a constitutively active bi-directional promoter that consists of a fusion of the	This study

		GPD promoter and a short derivative of the ADH1 promoter as BamHI/SalI fragment	
CKM 510	pUN100-mRFP-NOP1	Marker for nucleolus	(Ulbrich et al., 2009)
CKM 517	pADH1-GAL4BD-UIP4-pBGKT7	UIP4 cloned in pGBKT7 as SalI/PstI fragment	This study
CKM 594	pGBKT7	Yeast two-hybrid bait expression vector	(Louret et al., 1997)
CKM 616	pFA6a-His3MX	Yeast genomic targeting	(Longtine et al., 1998)
CKM 638	SFB-pCU-PDC1	SFB cloned in EcoRI/SalI site of pCU-PDC1 with a STOP codon for generating C terminal tag	(Kumar et al., 2020)
CKM 653	pUIP4-UIP4-SFB-pRS313	UIP4-SFB cloned in pRS313 with its native promoter as XbaI/SalI fragment	This study
CKM 670	pUIP4-UIP4-13MYC-pRS316	UIP4-13MYC cloned in pRS316 with its native promoter as XbaI/SalI fragment	This study
CKM 679	pUIP4-GFP-SFB-pRS313	GFP cloned in pRS313 with an SFB tag under UIP4 promoter	This study
CKM 707	pSH62-EBD	Yeast expression vector for estradiol-dependent expression of Cre recombinase	Addgene #49455
CKM 708	pKV015	Genome targeting for Recombination-Induced Tag Exchange (RITE) Cassette for HA-GFP to a T7-RFP tag	Addgene #64766
CKM 712	pFA6a-KanMX	Yeast genomic targeting	(Longtine et al., 1998)

2.3 BACTERIAL GROWTH AND MEDIA

Bacterial colonies were usually grown in LB media at 37ºC. In order to achieve high growth efficiency upon transformation, Super Optimal Broth (SOB) was used. Sterilization was performed by autoclaving at 121ºC for 20min.

LB broth 0.5% Yeast Nitrogen Base
1% Tryptone
1% NaCl

SOB 0.5% Yeast Nitrogen Base
2% Tryptone
10mM NaCl
2.5mM KCl
10mM $MgSO_4$ (added after autoclaving)
10mM $MgCl_2$(added after autoclaving)

Additionally, 2% agar was added for solid media.

Preparation of ultra-competent bacterial cells

Bacterial cells competent for transformation were prepared by Inoue method (Sambrook and Russell, 2006). A single colony of bacteria was inoculated in 3mL of SOB. The culture was allowed to grow overnight at 37ºC with shaking at 220rpm. Next day, secondary culture was set up by using $1/100^{th}$ volume of primary culture in 100mL of SOB broth and incubated at 18°C with shaking at 180rpm until the OD_{600} reached 0.4-0.5. Cells were cooled by placing the flask in ice and immediately harvested by centrifuging at 12000 rpm for 10 min at 4°C.The supernatant was discarded and pellet was washed with cold distilled water. The cell pellet was resuspended in 80mL of Inoue transformation mix, resuspended and spun at 12000 rpm for 10 min at 4°C. The supernatant was discarded and centrifuge tube was placed on ice immediately. The cells were then resuspended in 20mL of ice-cold Inoue transformation buffer and 1.5mL of DMSO was added and the contents were mixed by swirling the tube. The cell suspension was allowed to sit on ice for 10 min. 100µl of this suspension was aliquoted into 1.5mL microfuge tubes and snap frozen in liquid nitrogen. The tubes were stored at -80°C until further use.

Inoue transformation mix 50mM $MnCl_2.4H_2O$
15mM $CaCl_2.2H_2O$
250mM KCl
500mM PIPES pH6.7

Bacterial transformation

A single Eppendorf tube containing 100µl of ultra-competent DH5α cells was used for transformation. Competent cells stored in -80ºC were taken and placed on ice. 2µl of plasmid

DNA was added to the cells and allowed to thaw in ice for 20min. Heat shock was given to the cells for 90sec at 42ºC followed by placing the tube in ice for 5min. 900µl of LB media was added to the cells and they were kept for 40min in thermomixer set at 37ºC with mixing. 100µl of cell suspension was spread on LB plate and the plate was incubated at 37ºC.

When transforming ligated DNA construct, 900µl of SOB was used instead of LB media. Further, the cells were allowed to recover at 37ºC for 60min. The tube containing cell suspension was spun at 13000rpm for 1min. 800µl of supernatant was removed and the cells were resuspended in the remaining media and spread on LB plate containing appropriate antibiotic selection.

2.4 TECHNIQUES RELATED TO YEAST GROWTH AND STRAIN GENERATION

Yeast strains of BY4741/42 and W303 background were used. A fresh batch of parent cells were streaked out from the glycerol stock at -80º before starting an experiment. The cells were grown in either Synthetic Complete (SC) medium containing all amino acids or Yeast Extract-Peptone-Dextose (YPD) media. The media composition is given below:

YPD 1% Yeast Nitrogen Base
2% Peptone
2% Dextrose

SC media 0.75% SC omission powder
2% Dextrose

2% agar was added for solid media.

Preparation of Powder Omission Media Mix

In order to prepare dropout powder, the components given in the table below were weighed and mixed using a blender. To prepare omission powder, the amino acid not required was omitted.

Table5. Components of synthetic complete dropout mix

Component	Amount
Yeast Nitrogen Base without amino acids	50gm
L- Arginine Sulfate	150mg
L-Glutamic Acid	3.75gm
L-Histidine HCl	150mg
L-Isoleucine	225mg
L-Leucine HCl	450mg
L-Methionine	150mg
L-Phenylalanine	435mg
L-Tryptophan	150mg
L-Tyrosine	225mg
L-Valine	1.12gm
Adenine Sulfate	150mg
Uracil	150mg
Total	**50 g**

Growth assay and spotting

Liquid media:

Overnight cultures were sub-cultured to 200µl volume in 96 well plate. Biological triplicates for each strain were used. The OD600 was measured and cells were diluted to an initial OD600 of 0.1-0.12. The plate was incubated at 30ºC with mild shaking. OD600 was recorded using a multimode plate reader every 90-120 min and growth curve was plotted. The readings were taken until the growth curve flattened and cells ceased to divide.

Spotting on solid media:

Overnight cultures were sub-cultured to 5mL of fresh medium with equal number of cells. Each of them was allowed to grow in the liquid synthetic complete medium for approximately 4-5 hours at 30°C. The cells were spun and a 10-fold serial dilution was performed. 5µl of cells were spotted on SC plates and incubated for 2-3 days at desired temperature to assess growth differences.

Plasmid Transformation into yeast

Yeast transformation was performed using standard lithium acetate based protocol (Daniel Gietz and Woods, 2002).

2.4.1.1 RAPID TRANSFORMATION OF PLASMID DNA

A single colony of yeast was inoculated in 10mL of YPD/SC and grown overnight. The cells were harvested by centrifugation at 3000rpm for 5 min. The supernatant was discarded and cells were resuspended in 10mL of sterile double distilled water. The cells were pelleted again and resuspended in 1mL of 100mM LiAc. 150µl of this cell suspension was aliquoted in to a microfuge tube and cells were pelleted. To this pellet, 350µl of transformation mixture was added.

Table6. Components of transformation mix

Component	**Volume**
PEG 3500 50% w/v	240 µl
LiAc 1.0 M	36 µl
Boiled SS-Carrier DNA (2 mg/ml)	50 µl
Plasmid DNA (0.1 to 1 µg) + water	24 µl
Total Volume	**350 µl**

The tube was vortexed to resuspend the cells and incubated in water bath/ thermomixer at 42ºC for 40min. The cells were pelleted by centrifugation at 6000rpm for 2 min and the supernatant was removed using a pipette. The pellet was resuspended in 100µl water and spread on selection plate. The plates were allowed to dry inside the laminar hood and then incubated at 30ºC for 2-3 days.

2.4.1.2 HIGH-THROUGHPUT TRANSFORMATION OF GENOMIC LIBRARY INTO YEAST

The method described above was scaled up to 10X in order to obtain large number of transformants when doing large screens such as yeast two hybrid. A single colony of yeast was inoculated in 10mL of YPD/SC and grown overnight. Next day, appropriate volume of inoculum was taken and 100mL of secondary culture was set up to an initial OD600 of 0.15-

0.20. The cells were allowed to grow and harvested at mid-log phase (OD600 0.8-1.0) by centrifugation at 3000rpm for 5 min. The supernatant was discarded and cells were resuspended in 25mL of sterile double distilled water. The cells were pelleted again and resuspended in 3mL of 100mM LiAc. This cell suspension was aliquoted in to a 15mL tube and cells were pelleted. To this pellet, 3.50mL of transformation mixture was added.

Table7. Components of transformation mix for high throughput transformation

Component	**Volume**
PEG 3500 50% w/v	2.40 ml
LiAc 1.0 M	360 µl
Boiled SS-Carrier DNA (2 mg/ml)	500 µl
Genomic library (2-3 µg) + water	240 µl
Total Volume	**3.50 ml**

The tube was vortexed to resuspend the cells and incubated in water bath/ thermomixer at 42ºC for 1hour. The tube was vortexed for 5-10 seconds every 15minutes to prevent cells from settling at the bottom of the tube. The cells were pelleted by centrifugation at 5000rpm for 3 min and the supernatant was removed using a pipette. The pellet was resuspended in 1mL water and cell suspension was spread on four selection plates, 250µl each. The plates were allowed to dry inside the laminar hood and then incubated at 30ºC for 2-3 days.

2.4.1.3 HIGH-EFFICIENCY TRANSFORMATION OF PCR PRODUCT INTO YEAST

This method is employed to obtain high efficiency when transforming PCR or linearised plasmid DNA into yeast cells for homologous recombination based approach (Gardner and Jaspersen, 2014). A single colony of yeast was inoculated in 10mL of YPD/SC and grown overnight. Next day, appropriate volume of inoculum was taken and 50mL of secondary culture was set up to an initial OD600 of 0.15-0.20. The cells were allowed to grow and harvested at mid-log phase (OD600 0.6-0.8) by centrifugation at 3000rpm for 5 min. The supernatant was discarded and cells were resuspended in 25mL of sterile double distilled water. The cells were pelleted again and resuspended in 5mL of 1X TE. The pellet was vortexed briefly and cells were pelleted by centrifugation. The pellet was resuspended in 200-500µl of LiAc mixture. Meanwhile, an aliquot of frozen ssDNA stock was placed in boiling water for 5min and then placed on ice immediately. To the cell suspension in LiAc mixture, 1-5µg of linearised DNA

was added, followed by 100µg of ssDNA. Next, 700µl of 50% w/v PEG 3500 was added and the tube was vortexed to mix the constituents. The tube was incubated at room temperature for 20min. Then 48µl of DMSO was added to the mixture followed by brief vortexing. The tube was then placed in water bath/ thermomixer set at 42ºC for 15-20min. The cells were pelleted by centrifugation at 6000rpm for 2 min and the supernatant was removed using a pipette. The pellet was resuspended in 1mL water and cell suspension was spread on four auxotrophic selection plates, 250µl each. The plates were allowed to dry inside the laminar hood and then incubated at 30ºC for 2-3 days. For antibiotic selection, the pellet was resuspended in 1mL of YPD broth and transferred to a 15mL tube. Further, 2mL of YPD was added and the cells were allowed to recover for 4-6 hours by placing the tube in shaker incubator at 30ºC. Then cells were pelleted and resuspended in 1mL water. The cell suspension was spread on four antibiotic selection containing plates, 250µl each. The plates were allowed to dry inside the laminar hood and then incubated at 30ºC for 2-3 days.

Generating strains by Mating, diploid selection, sporulation and marker segregation

Parent strains with opposite mating type were crossed in a YPD plate by making streaks (+ or X) with significant intersection. The plate was incubated overnight at 30ºC. Cells were picked from the middle of the intersection using a toothpick and patched on an auxotrophic selection plate. After confirming, the selected diploids were patched on to a YPK plate (1% Yeast Extract, 2% Peptone, 2.5% Potassium acetate, 2% agar) and placed in 30ºC incubator. The spores begin to appear in 4-8 days and can be seen under a light microscope as 4 haploid cells bound within the ascus wall.

For dissecting the haploids, spores were taken from YPK plate using a toothpick and diluted in 50µl sterile water. The spore wall was digested by using Zymolyase (100µg/ml) at 30ºC for 30 sec-1min. After digestion of the ascus, the spores were diluted in 1mL sterile water and the tube was placed on ice immediately. 25-30µl of the digested spores were dropped along a vertical line at the diameter of a YPD plate. Dissections of the spore was performed using an Olympus BX41 dissecting microscope.

Yeast two- hybrid screen

We used the yeast two-hybrid system to identify binding partners of Uip4 protein (Fields and Song, 1989). The genomic library containing random genomic fragments fused to *GAL4*

activating domain of plasmid pGAD-UC(X) was used to screen for relevant protein-protein interactions. The 'bait' *UIP4* was cloned to in the plasmid pGBKT-7 with its open reading frame fused to the open reading frame of the *GAL4* DNA binding domain. The bait plasmid was confirmed by sequencing and its ability to self-activate the Gal4 expression was tested. To screen for interactors, the 'bait' plasmid and 'prey' library were co-transformed into PJ694-A reporter strain (James et al., 1996). This strain has *HIS3* and *ADE2* as reporter genes. The transformants were selected on SC-leu-trp-his medium plates. The transformants were then labelled and either patched or replica-plated on to SC-leu-trp-ade plates. Plasmid DNA was isolated from the yeast colonies showing positive interaction with Uip4. This plasmid was then transformed in to bacterial competent cells and colonies bearing the interacting plasmids were selected on LB plate containing ampicillin. Next, we isolated plasmid DNA from three random bacterial colonies and examined the insert by restriction digestion of the interacting library plasmid to release the genomic insert. The interacting plasmids were sent for sequencing and analysed further to identify the likely interactor using BLAST and sequence alignment. The interaction was confirmed further by retransformation into PJ694-A bearing 'bait' plasmid, followed by selection on reporter plates.

2.5 LIST OF STRAINS

The following strains were used in the current study. Strains generated by homology-based recombination were confirmed by multiple screening PCR.

Table8: List of yeast strains used in the study

Reference no.	Name	Genotype	Reference
KRY280	PJ694-A	MATa trp1-901 leu2-3,112 ura3-52 his3-200 *gal4*Δ *gal80*Δ LYS2::GAL1-HIS3 GAL2-ADE2 met2::GAL7-lacZ	Phil James et. al. (1996)
KRY436	W303-1A	*MATa ade2-1 leu2–3 -112 his3-11,15 trp1-1 ura3-1*	Thomas and Rothstein (1989)
KRY437	W303-1B	*MATα ade2-1 leu2–3 -112 his3-11,15 trp1-1 ura3-1*	Thomas and Rothstein (1989)
KRY 1492	BY4741	MATa; *his3Δ1; leu2Δ0; met15Δ0; ura3Δ*	Brachmann et. al. (1998)

KRY 1493	BY4742	MATα ; *his3Δ1; leu2Δ0; lys2Δ0; ura3Δ0*	Brachmann et. al. (1998)
KRY 1570	Uip4-13Myc	KRY1492 except *UIP4-13MYC::HIS3*	Deolal et.al. (2021)
KRY 1577	*pom34*Δ *uip4*Δ	KRY1697 except *pom34*Δ*::KanMX4*	This study
KRY 1648	Pom33-GFP	W303A, *POM33-GFP::HIS3MX*	Webster et. al. (2014)
KRY 1652	Nup188-GFP	W303B, *NUP188-GFP::HIS3MX*	Webster et. al. (2014)
KRY 1653	Nup157-GFP	W303B, *NUP157-GFP::HIS3MX*	Webster et. al. (2014)
KRY 1654	Pom33-GFP *uip4*Δ	KRY1648 except *uip4*Δ*::KanMX*4	This study
KRY 1655	Nup188-GFP *uip4*Δ	KRY1652 except *uip4*Δ*::KanMX4*	This study
KRY 1656	Nup157-GFP *uip4*Δ	KRY1653 except *uip4*Δ*::KanMX4*	This study
KRY 1679	*nup157*Δ *uip4*Δ	KRY1697 except *nup157*Δ*::KanMX4*	This study
KRY 1697	*uip4*Δ	KRY1492 except *UIP4::KanMX4*	This study
KRY 1698	*uip4*Δ	KRY1493 except *UIP4::KanMX4*	This study
KRY 1743	Nup157-GFP *atg1*Δ	KRY1653 except *atg1*Δ*::KanMX4*	This study
KRY 2035	Nup157-RITE	KRY1493 except NUP157-loxP-GFP-HygR-loxP-mRFP	This study
KRY 2036	Nup157-RITE *uip4*Δ	KRY 2035 except *uip4*Δ*::KanMX4*	This study
YLR018C	*pom34*Δ	KRY1492 except *pom34*Δ*::KanMX4*	Euroscarf
YER105C	*nup157*Δ	KRY1492 except *nup157*Δ*::KanMX4*	Euroscarf
YMR037C	*msn2*Δ	KRY1492 except *msn2*Δ*::KanMX4*	Euroscarf
YKL062W	*msn4*Δ	KRY1492 except *msn4*Δ*::KanMX4*	Euroscarf
YDR096W	*gis1*Δ	KRY1492 except *gis1*Δ*::KanMX4*	Euroscarf
YFL033C	*rim15*Δ	KRY1492 except *msn2*Δ*::KanMX4*	Euroscarf
YOR101W	*ras1*Δ	KRY1492 except *ras1*Δ*::KanMX4*	Euroscarf
YHR205W	*sch9*Δ	KRY1492 except *sch9*Δ*::KanMX4*	Euroscarf
YJR066W	*tor1*Δ	KRY1492 except *tor1*Δ*::KanMX4*	Euroscarf

2.6 STAINING AND IMAGING PROTOCOLS FOR YEAST

Trypan blue staining

Cells grown were harvested by centrifugation and the pellet was washed twice with fresh SC media. Approximately 1unit OD600 cells were resuspended in 500µl of SC media. 5µl of cells

were taken and mixed with 5µl of 0.4% Trypan blue solution, and laid on a clean glass slide. Cells were mounted with cover slip and 8-10 random fields were imaged in a microscope. The dead cells stain blue and appear darker when imaged with transmitted white light. Approximately 250-300 cells were counted to estimate the cell viability.

Live cell imaging

Cells grown were harvested by centrifugation and the pellet was washed twice with fresh SC media. Cells suspended in SC media were added to slides coated with 0.1% Concanavalin A (ConA) solution. The cells were allowed to settle for 5 minutes and excess liquid was removed using a vacuum pump. For nuclear staining, 5ul of 50ng/mL DAPI was added to the cells in dark. After 5 minutes, 4ul of Slow Fade Anti-fade mounting medium was added and coverslip placed. The edges were sealed gently using nail polish and images were acquired immediately.

For time course imaging, cells resuspended in SC media were mounted onto a 35mm cover glass bottom dish coated with ConA. After allowing the cells to settle, unbound cells were rinsed with SC media. Images were acquired in confocal microscope equipped with a temperature-controlled stage set at 30ºC.

Immunofluorescence

Immunofluorescence was performed as described in (Tirupataiah et al., 2014). Briefly, cells were fixed in growth media with 3.7% formaldehyde at 30ºC for 20min, followed by three washes with sterile distilled water. Cells were then treated with 10mM DTT and 0.1M EDTA-KOH for 10min at 30ºC. Spheroplasts were generated by treating the cells with 0.25mg/mL Zymolyase 100T at 30ºC until the cell wall was digested. Digestion of cell wall was confirmed by visualising a drop of cell suspension under a light microscope. Appropriate amount of spheroplasts were dropped onto a 0.1% poly-L-Lys coated slides. The cells were permeabilized by treating with methanol and acetone for 5min and 30sec respectively. Blocking was done using 1% BSA prepared in 1X-PBS (pH 7.4) with 0.1% Tween-20. Staining with primary antibodies was performed overnight at 4ºC in a closed, moist slide box. Staining with secondary antibodies labelled with fluorescent dye was done at room temperature for 2hrs. DAPI staining was done for 5 minutes followed by mounting with Prolong gold antifade mountant.

Transmission Electron Microscopy

For transmission electron microscopy (TEM), yeast cell cultures were grown to mid-log phase 0.5 OD600. The cells were harvested by spinning at 1000rpm for 3minutes. The cell pellet was resuspended in 40mL of ice-cold fixing solution and placed on ice for 2 hrs. The fixed cells were spun and washed with 25mL ice-cold 50mM potassium phosphate (pH 6.8) buffer twice. Next the pellet was resuspended in 1mL ice-cold 50mM potassium phosphate (pH 6.8) and transferred to a microfuge tube. The cells were pelleted and by resuspended in 750µl of freshly prepared 4% KMnO4. Post-fixation was carried out for 1 hr at room temperature in an end-over-end rotator. After this, the fixed cells were pelleted and washed twice with 1mL distilled water. Cells were treated with freshly prepared 2% uranyl acetate for 1 hr at room temperature and subsequently washed. Dehydration of cells was followed by clearing with propylene oxide and infiltration with the combination of 100% propylene oxide and 100% spur low viscosity resin. The sectioning and image acquisition was carried out at TEM facility of ACTREC, Tata Memorial Centre, Mumbai.

Fixing solution 2% glutaraldehyde
1% paraformaldehyde
1mM $MgCl_2$
50 mM potassium phosphate buffer pH 6.8

Image acquisition, processing and analysis

All images were acquired on Leica TCS SP8 using HC PL APO CS2 63X/1.40 OIL objective. Optimal laser power, image size and acquisition settings were used. At least three biological replicates for each sample were imaged for quantification and analysis.

2.6.1.1 NUCLEAR SHAPE ASSESMENT

The phenotype was scored either by manual inspection or quantified using ImageJ/FIJI (Schindelin et al., 2009). For manual quantification, the fraction of cells showing abnormal structure/distribution as compared to wild type cells imaged under same condition was reported. To quantify the nuclear shape changes, we measured the circularity of nucleus by using Analyze tool of FIJI. For this, we traced the nuclear outline using the free hand selection tool. After marking each nucleus, the selection was added to the ROI manager (Press T or Edit→ Selection→Add to Manager). After completing selection of cells, Measure function was

used and the Results appear in a new tab. The table was saved as either .csv or the data was copied and imported to Excel for further analysis.

2.6.1.2 AGGREGATION INDEX

NPC aggregation index was determined as described in (Lord and Wente, 2020). Briefly, the NE outline based on the signal from indicated nup was traced in FIJI using the freehand tool. The selection was converted to a line and fluorescence intensity values were obtained using the plot profile function. The intensity values for ~20-25 cells from at least two independent experiments were copied to excel sheet and respective background fluorescence intensity was subtracted. Next, for each NE, average intensity was subtracted from the individual values and the absolute difference was obtained. The standard deviation of this difference was divided by the average intensity of each NE and reported as the aggregation index.

2.6.1.3 NLS IMPORT RATIO

The mean intensity values of GFP in the nucleus vs cytosol was used to quantify the nuclear import of NLS-GFP construct (Webster et al., 2016). A region of definite area was drawn in the nuclear and cytosolic region of cells under inspection using the oval selection tool of FIJI. The mean fluorescence intensity was determined using the measure tool. Background fluorescence intensity from a region outside of the cell was subtracted from each value. The nuclear import of NLS-GFP was reported as the ratio of mean nuclear versus cytosolic intensity.

2.7 PROTEIN AND RELATED BIOCHEMICAL TECHNIQUES

TCA method of Protein extraction

Proteins were extracted using TCA method of protein precipitation (Abraham et al., 2019) Briefly, cells were grown in appropriate medium up to mid-log phase. 200µl of 20% TCA was added to the cell pellet and were lysed by adding glass beads and vortexing at high speed for 3 minutes. The lysate was collected in a fresh microfuge tube. The tube containing glass beads was washed twice with 200µl of 5% TCA and vortexed for 1 min. The lysate was collected and added to the previous tube. The entire lysate was spun at 13000rpm for 10 min. Supernatant

was discarded completely and the pellet was dissolved in 200µl of Laemmli buffer. 2M Tris was added drop-wise until the buffer turned blue. Proteins were denatured by boiling in Laemmli buffer for 5 minutes at 95ºC.

4X SDS loading dye (Laemmli buffer)	200mM Tris-HCl pH6.8 8% SDS w/v 40% Glycerol v/v 6mM Bromophenol Blue 4% ß-mercaptoethanol

SDS-PAGE and Western blotting

Denaturing PAGE was employed to resolve the proteins extracted. Gels for SDS-PAGE were cast using standard protocol. The stacking gel was used at 4% concentration while the concentration of resolving gel varied from 8-12% depending on the molecular weight of protein under inspection. Protein extracts were loaded onto the gel and electrophoresed at 75-80V while on stacking gel and 100-120V after the lysate enters resolving gel. Pre-stained molecular weight markers were loaded along with the samples to track the migration. SDS-PAGE was followed by a standard semi-dry method of transfer to PVDF membrane for western blotting. Protein/ epitope tag specific primary and respective secondary antibodies tagged to HRP were used. The signal was detected by chemiluminescence and membrane was imaged in ChemiDoc Imaging system.

PVDF membranes were stained reversibly using Ponceau Staining solution. This is useful to test transfer of proteins to the membrane and examine total protein. A 0.1% w/v solution in 5% GAA was used prior to addition of antibody. After developing the blot, a 2% w/v solution in 30% TCA was used to obtain more stronger binding and darker staining.

Staining protocols for acrylamide gels

The acrylamide gels were permanently stained with coomassie by soaking them in CBB staining solution for at least 1 hour and then destaining.

CBB staining solution:	Coomassie	0.25g
	Methanol	45ml
	Water	45ml
	GAA	10ml
Destaining solution:	Methanol	45ml
	Water	50ml
	GAA	5ml

Silver staining:

Prior to staining with silver nitrate, the acrylamide gels were fixed using a mixture of methanol (50%v/v) and acetic acid (12% v/v) for 2 hours. Followed by fixing, the gel was washed with distilled water for 2-4 hours. The gel was then soaked in hypo-sodium thiosulfate (20mg/ml) for 5 minutes followed by rinsing with water. The gel was then soaked in 50ml of 0.2% silver nitrate solution prepared freshly and incubated in 4ºC for 2 hours in a closed box. The gel was then quickly washed with water and the stain was developed by transferring the gel to a 50ml 6% solution of sodium carbonate containing 100µl formaldehyde (37% stock). 5% acetic acid solution was then used to stop the color darkening.

Quantification of western blot

Densitometric analysis of chemiluminescence readout after western blot was done using Gel Analyzer option of ImageJ/FIJI. Protein expression was normalized to the loading control, usually an antibody to a protein expressed by housekeeping gene. Quantification of the protein expression from western blots of at least 3 independent experiments is performed.

Pull down

The protein of interest tagged to a triple epitope bearing SFB (**S**-protein, **F**LAG and Streptavidin **b**inding peptide) tag was used to immunoprecipitate (IP) the interactors. The strain was grown to desired culture condition and cells were harvested by centrifugation at 3000rpm for 5 min at 4ºC. Cell pellet was snap frozen in liquid nitrogen and stored in -80ºC until further use. Cells equivalent to 50 units of OD600 1.0 were used to prepare the lysate based on method adapted from Kumar et al., 2020. To begin, 500µl of freshly diluted, chilled lysis buffer with protease inhibitors was added to the pellet and the tube was placed in ice for 2-3 min. The cell suspension was then transferred to a pre-chilled 2 mL microfuge tube containing glass beads

up to ~500µl mark. The cells were lysed by using a bead beater (5 cycles of 30sec pulse with 1min rest on ice). The lysate of collected transferred to a new tube and spun at 13000rpm for 20min at 4ºC. The supernatant was collected and total protein in the lysate was estimated.

3-5% of whole cell lysate was used as Input and boiled with SDS-loading dye and stored at -20ºC until further use. 4-8mg of lysate was used for IP. 100µl of streptavidin beads pre-washed with lysis buffer without protease inhibitors were added to the lysate and the mixture was incubated for at least 2hours to maximum 4hours in an end-over-end rotator placed at 4ºC. The beads were collected by spinning the tube at 2000rpm for 5 min at 4ºC. The supernatant was collected in a separate tube to assess the amount of binding. The collected beads were washed thrice with lysis buffer without inhibitors by spinning at 2000rpm for 2 min at 4ºC. 1mL of freshly prepared 2mg/mL biotin solution prepared in lysis buffer without inhibitors was added to the washed beads and incubated at 4ºC in an end-over-end rotator for 2-3 hours. The tubes were spun at 2000rpm for 2 min at 4ºC and supernatant was collected and transferred to a fresh microfuge tube. 30µl of pre-washed S-protein beads were added to it and incubated in end-over-end rotator for at least 2 hours to maximum 12 hours. The tubes were spun at 13000rpm for 5 min at 4ºC and the beads were washed thrice with lysis buffer without inhibitors. Finally, the bound proteins were eluted by boiling the beads in 2X SDS-loading dye at 95ºC for 5 min. The beads were sedimented by spinning the tube at 3000rpm for 2 min. The supernatant was collected and stored at -20ºC until further use.

For MS/MS analysis, the eluate was loaded onto an acrylamide gel. After the dye front migrated in to the resolving gel up to a 1cm distance, the gel was stained with CBB solution followed by destaining. The desired lane was excised and the gel was put in a microfuge tube containing deionised water. The samples were shipped to Taplin Biological Mass Spectrometry Facility, Harvard Medical School (https://taplin.med.harvard.edu) for LC-MS/MS analysis

Lysis Buffer composition	20mM Tris-Cl pH8.0 100mM NaCl 1mM EDTA pH8.0 0.05% Nonidet P-40
Inhibitors Mixture	2.5mM Sodium Fluoride 1mM Sodium orthovanadate 2.5mM PMSF 1X EDTA-free protease inhibitor cocktail

2.8 STATISTICAL ANALYSIS

Statistical significance was determined by using Student's t-test to compare the differences between samples, assuming that the population was selected randomly without any bias and data is distributed normally. p-value is reported where necessary and the error bars are representative of the standard error of mean throughout.

CHAPTER 3 LOSS OF *UIP4* AFFECTS NUCLEAR FUNCTION IN *SACCHAROMYCES CEREVISIAE*

3.1 OVERVIEW

In a genome wide fluorescence microscopy-based screen to identify the components that contribute to the process of regulating nuclear shape (Male et al., 2020; Deolal and Mishra, 2021), we found several non-nuclear proteins to be involved in nuclear shape regulation. The quantification of abnormal shape was represented as the fraction of cell population showing deviations from the wild-type like morphology. One such gene with uncharacterized function was UIP4. Over 50% of the *UIP4* knockout cells were scored as having abnormal nuclear shape during the genome-wide screen for factors important for regulation of nuclear morphology. *UIP4/YPL186C* encodes for a protein with a so far uncharacterized function (Source: Saccharomyces Genome Database https://www.yeastgenome.org).

The work for this project began by investigating the role of Uip4 in the regulation of nuclear shape. Initially, we established the nuclear shape abnormalities in *uip4*Δ cells. The shape of nucleus in live cells can be visualized by using a nuclear envelope protein tagged to a fluorophore. In most of the metazoans, lamin staining is an established proxy for nuclear morphology. However, since budding yeast and other lower eukaryotes lack lamin, we employed an INM protein- Esc1, to demarcate the nuclear outline (Andrulis et al., 2002). Our laboratory has established the use of GFP-Esc1 as a marker to determine nuclear shape in budding yeast (Male et al., 2020; Deolal and Mishra, 2021). Despite the absence of lamins in yeasts, the nuclear morphology is stably maintained and shape changes occur in a regulated fashion.

One of the largest and dynamic protein macro assembly that spans the NE is the SPB (Jaspersen and Winey, 2004). In fungi that undergo closed mitosis, the nucleus displays a series of morphological alterations coordinated with cell cycle stages. In such cells, the SPB is located inside the nucleus and undergoes lateral expansion (Byers and Goetsch, 1974). During mitosis, the SPB divides and the two spindles move to opposite poles within the NE, pulling the attached chromosomes with them. Normally, the round nucleus elongates to a spindle shape and appears like a dumb-bell right before splitting into two round daughter nuclei. The SPB dynamics

affects nuclear shape and size (Gonzalez et al., 2009). When spindles fail to separate normally, the NE deforms (Zheng et al., 2007). NPCs are other large multi-protein assemblies inserted into the NE and their stability is critical for nuclear geometry as described in Chapter 1. Thus, SPB and NPCs stabilize the overall nuclear structure and participate in membrane curvature by interacting with several proteins including, but not limited to, lamina and members of LINC complex (Zheng et al., 2007; Gonzalez et al., 2012; Liu et al., 2007; Lussi et al., 2011). We tested the localization and distribution of these two macromolecular assemblies at the NE- the SPB and the NPCs, in wild type and *uip4*Δ.

We employ fluorescence microscopy-based techniques to visualize and comprehend the differences between nuclei of wild type and *uip4*Δ cells. We also used Stimulated emission depletion (STED) to achieve enhanced resolution and examine the finer differences between distribution of marker protein, and transmission electron microscopy (TEM) to confirm shape abnormalities. Our results suggest that Uip4 is involved in stabilizing the assembly intermediates of NPC in yeast.

3.2 RESULTS

Loss of *UIP4* Causes abnormal nuclear shape

In preliminary experiments performed in the laboratory, we had an observation that loss of *YPL186C (UIP4)* results in alteration of nuclear morphology. We authenticated this observation of the high-throughput genome wide screen, by co-transforming wild type and *uip4*Δ cells with plasmid expressing GFP-Esc1 and mRFP-Nop1. The nuclear outline in wild type yeast cell marked with GFP tagged INM protein Esc1 appears to be round in 95% of the cells harvested from an unsynchronised population. Nop1, a nucleolar protein, demarcates the crescent shaped nuclear sub-compartment, the nucleolus (Fig5A, left). On the other hand, in *uip4*Δ cells, a large number of cells displayed abnormally shaped nuclei (Fig5A, right). To get a measure of this abnormality we quantified the irregularity in the nuclear morphology by measuring circularity index. Circularity Index (CI) is one of the most widely quantified morphological features of nucleus. It is calculated as: 4*π*area/perimeter^2. We traced the nuclear outline as defined by the distribution of Esc1. As the majority of wild type cells have circular nuclei, the CI lies close to 1 (Fig5B). Whereas in case of *uip4*Δ cells, the shape of nucleus is not circular and hence the CI is far from 1 with median of the distribution around

0.7 (Fig5B). There is also large heterogeneity in the shape of nuclei with some nuclei being heavily distorted as the distribution of CI shows.

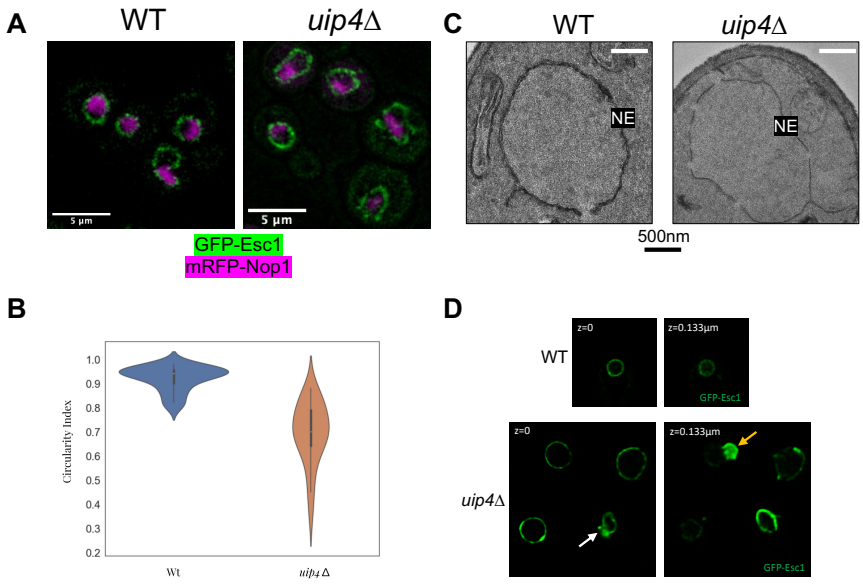

Fig5. Loss of *UIP4* leads to nuclear shape abnormalities in yeast

A. The micrographs representative of nuclear morphology in wild type and *uip4*Δ cells are shown. GFP-Esc1 marks the NE in green and the signal from mRFP-Nop1 is shown in magenta. **B.** Violin plot showing circularity index (CI) of 25-30 nuclei from wild type and *uip4*Δ cells is presented. **C.** 2D electron micrographs representative of the NE morphology in wild type and *uip4*Δ are shown. The darkly stained NE is labelled. **D**. Fluorescence micrographs acquired ~130nm apart in the Z-axis are shown for wild type and *uip4*Δ cells. The nuclear morphology appears round, disc shaped in both the planes, whereas clear deformities marked by arrows can be seen in *uip4*Δ cells.

We further assessed the nuclear shape by transmission electron microscopy. Such irregularities were also mirrored in our 2D electron micrographs of fixed cells. The nuclear envelope can be seen as a continuous, round bilayer in wild type (Fig5C, left). But in the *uip4*Δ cells, the NE appears to be discontinuous and distorted (Fig5C, right). These differences between the two cell types were also noticeable when acquiring a 3D image. The WT nuclei display ring like membrane staining when optically sectioned in the Z axis (Fig5D, top). On the other hand, *uip4*Δ cells display various membrane associated deformities such as flares (Fig5D, bottom-white arrow) and blebs (Fig5D, bottom-yellow arrow). Therefore, with these preliminary experiments we established that indeed *UIP4* is critical for maintenance of the quasi-round nuclear shape in budding yeast. *uip4*Δ cells have various kinds of nuclear shape deformities.

Defective nuclear shape has been associated with delayed mitosis (Webster et al., 2009). Therefore, we sought to monitor the nuclear shape dynamics during cell division by live cell microscopy in wild type and *uip4*Δ cells. Cells were grown in a 35mm cover glass bottom dish in the presence of SC medium at 30ºC. *S. cerevisiae* undergoes closed mitosis therefore in wild type cells the nuclei remained mostly round-elliptical with a uniform distribution of Esc1 around the nuclear periphery (Fig6A, left). On the other hand, *uip4*Δ display abnormal nuclear morphologies during nuclear transmission to the bud (Fig6A, right). These abnormal nuclei take significantly longer time to partition in to the daughter bud as revealed in the quantification of time taken by nucleus to enter the daughter cell (Fig6B). This resulted in an increased nuclear division time for *uip4*Δ as compared to the wild type. We then asked if this has any effect on the overall growth rate of cells and compared the growth of WT and *uip4*Δ cells in solid and liquid growth medium. However, we did not find any differences in the duplication time or the mitotic growth (Fig6C, 6D).

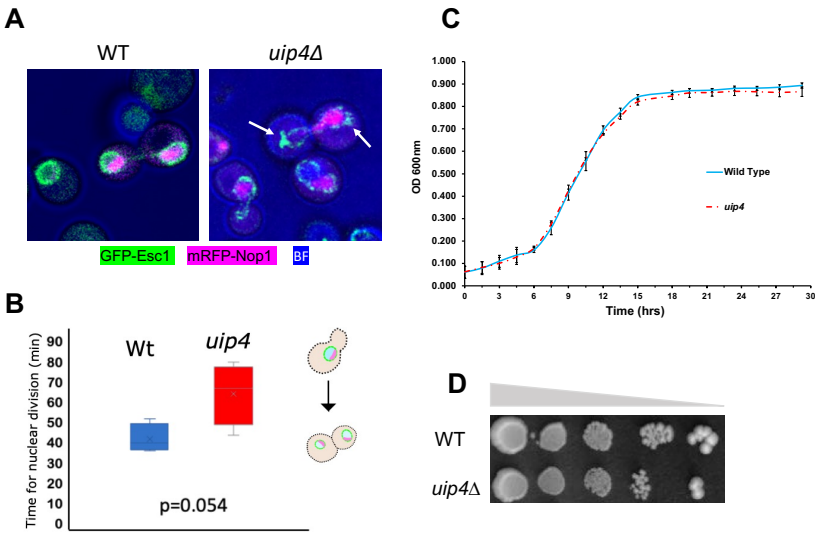

Fig6. Loss of *UIP4* does not cause mitotic growth defect

A. The micrographs representative of nuclear morphology in wild type and *uip4*Δ cells undergoing division are shown. GFP-Esc1 marks the NE in green and the signal from mRFP-Nop1 is shown in magenta. **B.** Box plot showing nuclear division time of 25-30 nuclei from wild type and *uip4*Δ cells is presented. Horizontal line represents the median time. **C.** Growth curve for wild type and *uip4*Δ cells grown in liquid medium at 30ºC is plotted. Error bars shows SEM. **D.** 10-fold serially diluted cell suspension from wild type and *uip4*Δ culture was spotted on to SC plate and image captured after 2 days of growth at 30ºC is shown.

NPCs aggregate at the NE in *uip4*Δ cells and mis-localize as cytosolic spots

So the initial findings showed that indeed loss of Uip4 has a major effect on nuclear morphology and this causes increased nuclear division time and abnormal distribution of the marker protein, Esc1, along the membrane. To test if this effect was specific to Esc1 distribution, or other NE proteins as well, we examined the distribution of components belonging to SPB and NPC. In budding yeast, the NE houses the spindle pole body (SPB), which forms attachments to the kinetochore-centrosome complexes of the chromosomes. We transformed the cells with fluorescently tagged constituent proteins of these compartments. Nup49, an FG-nup, fused to GFP marks the NPCs and DsRed tagged Spc42, a spindle protein, labels the SPB. The chromosomes organize along the central nuclear axis from the spindle pole body (SPB) to the diametrically opposite nucleolar centre (Sáez-Vásquez and Gadal, 2010). In WT cells, the spindle duplicates, migrates to opposite end of the nucleus and is distributed to the mother and the daughter cell, while the nuclear shape and integrity is retained. On the other hand we find that in *uip4*Δ, while the Spc42 duplicates and gets distributed to the daughter bud, the distribution of signal for GFP-Nup49 seems to distribute irregularly along the nuclear periphery (Fig7A, arrows) and could also be located outside of the NE.

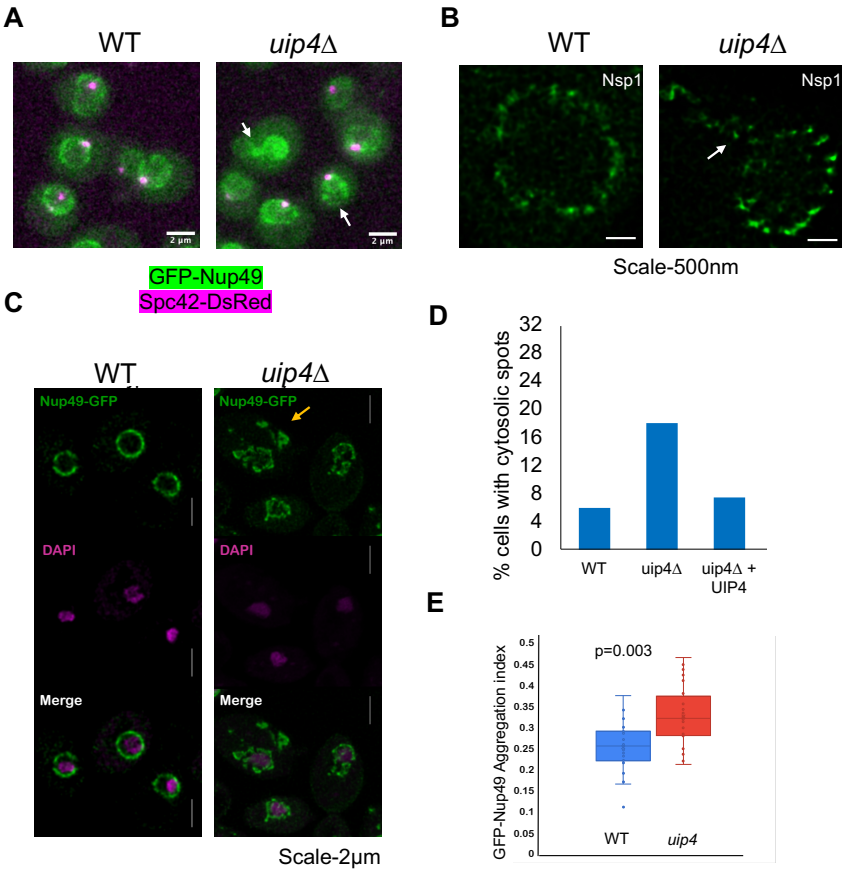

Fig7. Loss of *UIP4* results in clustering and mislocalization of nups

A. The micrographs representative of GFP-Nup49 (green) and Spc42-DsRed (magenta) in wild type and *uip4*Δ cells undergoing division are shown. **B.** A STED micrograph of a single

cell from wild type and *uip4*Δ representative of the distribution of nups is shown. A primary antibody against the nup-Nsp1 was used to locate NPCs. White arrow shows extensions of NE bearing nups. **C.** Images of wild type and *uip4*Δ cells transformed with GFP-Nup49, stained with DAPI are shown. Non-nuclear spots of Nup49 can be seen in *uip4*Δ as marked by the arrow. **D.** Histogram showing fraction of wild type and *uip4*Δ cells with cytosolic spots of Nup49 is presented (n~200). **E.** Distribution of nups in wild type and *uip4*Δ cells were quantified as aggregation index and is shown as box plot (n~30). Horizontal line represents median aggregation index. *The data shown in D, E is a cumulative representation of cells marked without any bias from multiple fields, acquired from 3 independent experiments.*

We then investigated the effect of loss of *UIP4* on the distribution of NPCs more carefully. We performed indirect immunofluorescence and stained the NPCs in wild type and *uip4*Δ cells using antibody to Nsp1-a cytoplasmic FG nucleoporin. Then we acquired the images using STED based super resolution microscopy(Hell and Wichmann, 1994). STED involves use of an additional laser beam other than the excitation laser. The high intensity and high wavelength STED laser beam has a donut shape which enhances the lateral and axial resolution of biological samples by turning the fluorophores outside of the diffraction limited spot to an 'off' state. Therefore, the fluorescent signal can be seen as clearer, resolved spots, rather than a contiguous blur. In wild type cells, the NPCs are known to distribute along the nuclear periphery almost evenly as the STED micrograph in Fig7B, left, shows. This distribution becomes uneven, and non-nuclear as well, in the *uip4*Δ cells (Fig7B, right). Apart from aggregation of NPCs at the NE, we also observed presence of cytosolic spots of Nsp1 in *uip4*Δ. In order to check if these non-nuclear extensions also have nuclear content, we imaged live cells stained with DAPI. Wild type and the mutants were transformed with a plasmid borne Nup49- GFP as a marker for the NPCs (Fig7C). Live cells were imaged and the defect was quantified in two ways- aggregation index of NPCs at the NE, and fraction of cells showing cytosolic spots of Nup49. We found that in *uip4*Δ, non- nuclear GFP signal is seen in about 18% of the population and also the distribution of Nup49 along the envelope is different (Fig7C, 7D). Although cytosolic pool of nucleoporins in wild type cells has been reported earlier (Colombi et al., 2013; Makio et al., 2013; Kumanski et al., 2021), this fraction of cell population was at least three-fold higher in *uip4*Δ cells (Fig7D). Complementation with a plasmid borne copy of *UIP4* expressed from endogenous promoter could rescue the phenotype in *uip4*Δ (Fig7D). In order to quantify the NPC aggregation, the GFP signal of the Nup49 along the NE rim was used (Lord and Wente, 2020). The comparison shows that Nup49 is distributed less evenly in the *uip4*Δ and therefore has higher aggregation index as compared to with wild type cells. Altogether, this shows that nucleoporins-Nsp1 and Nup49 show clustering along the

NE in the absence of *UIP4* and their presence can be detected in non-nuclear regions as multiple foci.

Loss of *UIP4* leads to clustering and mis-localization of multiple Nups

We then examined the distribution of inner ring nucleoporins namely Nup157 and Nup188. Both of these nups were also clustered upon loss of *UIP4* (Fig8A, 8B). The transmembrane nup, Pom33, showed a differential localisation in the *uip4*Δ cells (Fig8C). A minor fraction of Pom33 is localized to the ER in addition to the NE in wild type cells (Chadrin et al., 2010). Apart from clustering at the NE, there was a reduction in the distribution of Pom33 to the cortical ER in *uip4*Δ as compared to wild type cells, with most of Pom33 present in the NE (Fig8C, MIP). Loss of *UIP4* therefore seems to affect distribution of multiple nups.

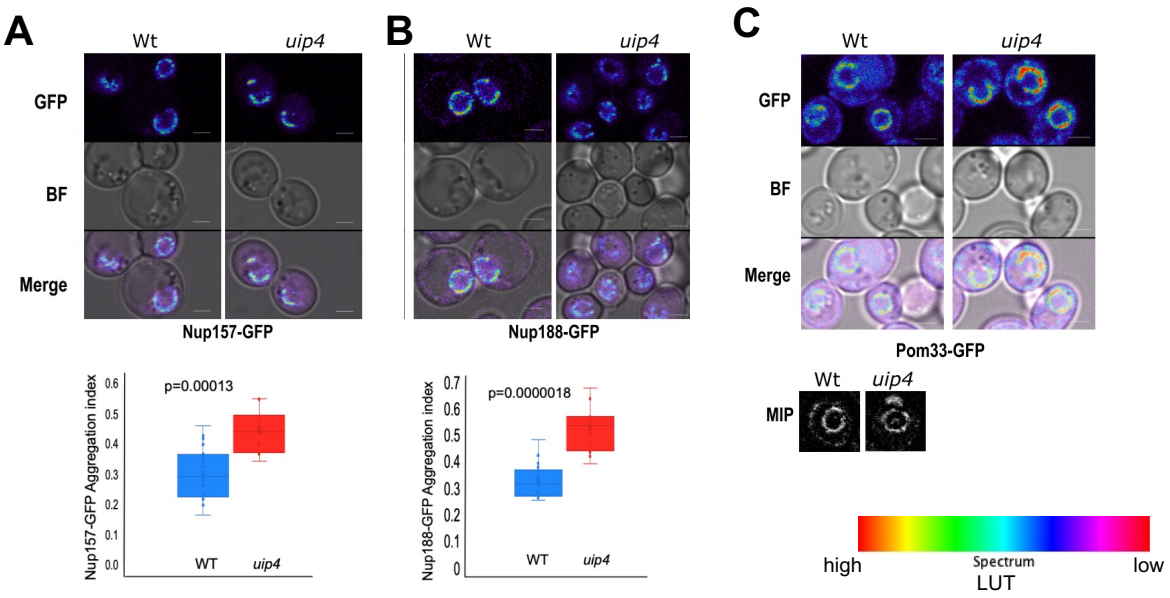

Fig8: Loss of UIP4 results in NPC clustering

Live cell imaging was done for Wt and *uip4* strains expressing indicated GFP tagged Nups from their endogenous loci (A- Nup157, B-Nup188, C-Pom33). Spectrum lookup table (LUT) is used for GFP signal (shown on bottom right) The box plot represents the aggregation index calculated from GFP signal along the NE in the mid-focal plane of 25-30 individual cells from Wt (blue) and *uip4* (red). MIP- maximum intensity projection of Pom33-GFP signal shown in grey. Scale-2µm.

We assessed the relative distribution of nucleoporins from two sub-complexes between wild type and cells lacking *UIP4*. Wild type and *uip4*Δ cells expressing GFP tagged Nup157 from its endogenous loci were transformed with Nup49-mCherry plasmid and imaged (Fig9A). Cytosolic spots of either nup were rarely observed in wild type cells harvested from mid-log

phase. While 5-8% of wild type population had single Nup49-mcherry puncta in the cytosol, Nup157-GFP was only found to be present at the NE. The NPC clusters at the nuclear periphery do not differ in their relative nup constitution between wild type and *uip4*Δ as determined based on the degree of colocalization of Nup157 and Nup49 (Fig9B). Contrary to this, the cytosolic spots observed in *uip4*Δ contain more than just Nup49 unlike in wild type (Fig9C). Colocalization analysis indicates that at least some additional NPC components are present in the puncta found in *uip4*Δ.

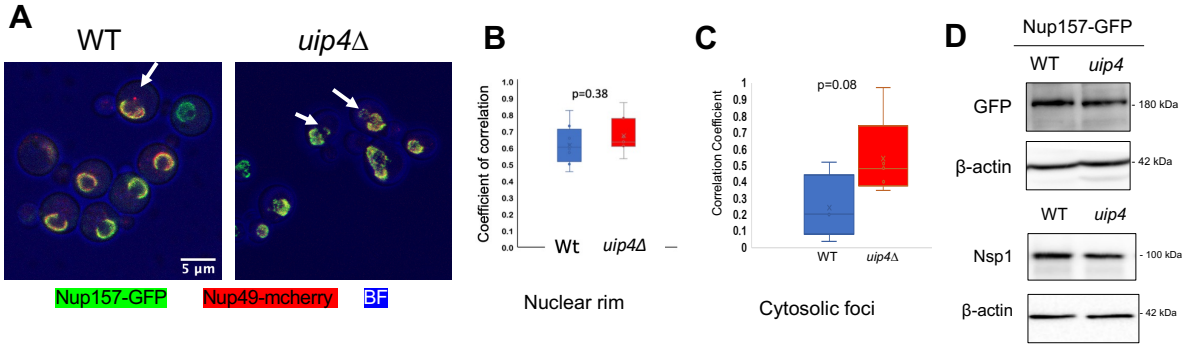

Fig9. Multiple nups are found in cytosolic foci upon loss of *UIP4*

A. The micrographs representative of Nup157-GFP (green) and Nup49-mCherry (red) localization in wild type and *uip4*Δ cells are shown. White arrow represents cytosolic foci in the two cell types. **B.** Box plot shows the coefficient of correlation between Nup157-GFP and Nup49-mCherry signal at the nuclear rim in wild type and *uip4*Δ. **C.** Box plot shows the coefficient of correlation between Nup157-GFP and Nup49-mCherry signal at the cytosolic spots in wild type and *uip4*Δ. **D.** Western blot analysis was done to compare the expression levels of Nup157 and Nsp1 in Wt and *uip4*Δ cells harvested from mid-log phase. α-GFP was used to detect endogenously tagged Nup157 and actin is the loading control.

Next, we asked if the mis localization of nups results in their clearance by degradation. Our western blot results indicate that the total protein levels for Nsp1and Nup157 do not differ much between wild type and the *uip4*Δ (Fig 9D). This absence of reduction in protein levels indicates that these foci are unlikely to be disintegrating NPCs. Overall, these results suggest that multiple components of NPC are affected upon loss of Uip4 and the cytosolic foci observed in *uip4*Δ could be either assembled NPC assembly intermediates or disintegrated NPCs.

Cytosolic spots in *uip4*Δ are a result of disrupted *de novo* NPC assembly

In order to understand the origin of these cytosolic nup foci, we monitored their dynamics in mitotically dividing live cells. We observed that the cytosolic spots form continuously and

were highly mobile. These spots also appear to merge with the NE in the *uip4*Δ cells. We then reasoned that if these cytosolic spots are due to an assembly defect, then preventing fresh protein synthesis should reduce the occurrence of these spots. On the other hand, if these are a consequence of degradation/ removal from NE, they will continue to increase even in the absence of new protein synthesis.

We monitored GFP-Nup49 in wild type and *uip4*Δ cells by time-lapse live cell imaging after addition of 10µg/ml cycloheximide (CHX), a protein translation inhibitor (Fig10A). We did not see any increase in the cytosolic foci suggesting that the cytosolic spots are intermediates of NPC assembly. While in wild type cells, the spots disappeared in 40±10min, it took 120±25min in *uip4*Δ. Further, after 2 hours there were no noticeable non-nuclear foci of Nup49. This observation suggests that in the absence of Uip4, de novo assembly of NPCs is affected and these cytosolic foci represent assembly intermediates rather than degradation intermediates. Interestingly, we also observed that after two hours of cycloheximide exposure, even in wild type cells, the NPCs began to cluster and nuclear morphology also began to distort (Fig10A), although no new cytosolic nup could be detected.

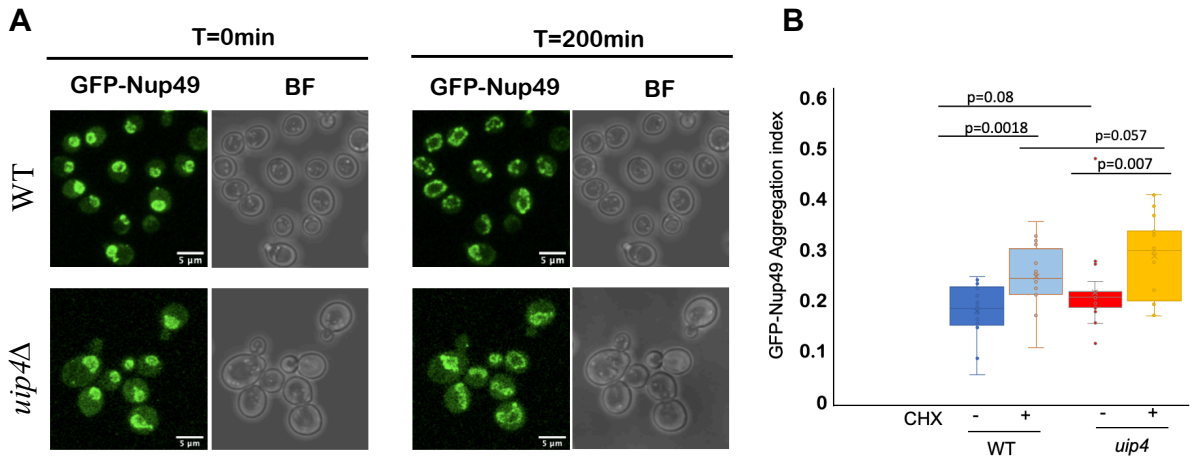

Fig10. The cytosolic foci in *uip4*Δ are a result of disrupted *de novo* NPC assembly.
A. The micrographs representative of Nup157-GFP (green) and Nup49-mCherry (red) localization in wild type and *uip4*Δ cells are shown. white arrow represents cytosolic foci in the two cell types. **B.** Box plot shows the coefficient of correlation between Nup157-GFP and Nup49-mCherry signal at the cytosolic spots in wild type and *uip4*Δ.

These results gave us a static snapshot of the defective NPC assembly. Since nups are highly dynamic and continually synthesized, we used the power of genetic manipulation in yeast coupled with microscopy-based visualization of NPC dynamics. This assay involved tagging

nup with an epitope that can undergo recombination induced tag exchange (RITE) (Verzijlbergen et al., 2010). The template has two tags in tandem and therefore all protein synthesized prior to induction of recombination will express only tag 1, in this case GFP. Once the recombination is induced, the tag1 is lost and all newly synthesized proteins will contain tag2, here an RFP (Terweij et al., 2013). Recombination is induced by addition of β-estradiol, since the recombinase is fused to human estradiol binding domain (EBD). The switching of tag is a permanent change at the genetic level, thereby allowing a clear observation of old and new pool of protein tagged with a RITE epitope.

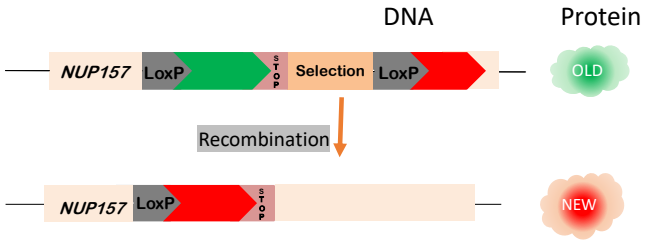

Fig11. Schematic representation of RITE in Nup157

We standardized the experiment and confirmed functionality of the tag in wild type cells. Cells expressing Nup157 tagged with GFP to RFP convertible tag imaged prior to recombination show typical ring like distribution along NE (Fig12A- column1). Once the switch was induced by addition of β-estradiol, we began to see new protein synthesis and red fluorescence started to appear at the NE and eventually all the old, green fluorescing Nup157 was replaced with new, red fluorescing Nup157 protein (Fig12A- column 2,3). The old-green, and newly synthesized-red proteins were distributed evenly as represented in the graph below the image. In the *uip4*Δ, at the start the green fluorescing Nup157 at periphery showed clustering (Fig12B- column 1). As the new protein was being synthesized after recombination, it also began to accumulate at the NE and more clusters appeared over time (Fig12B- column 2,3). This is clear from the intensity plot of the 'new' pool of Nup157, shown in red (Fig12B- column3)

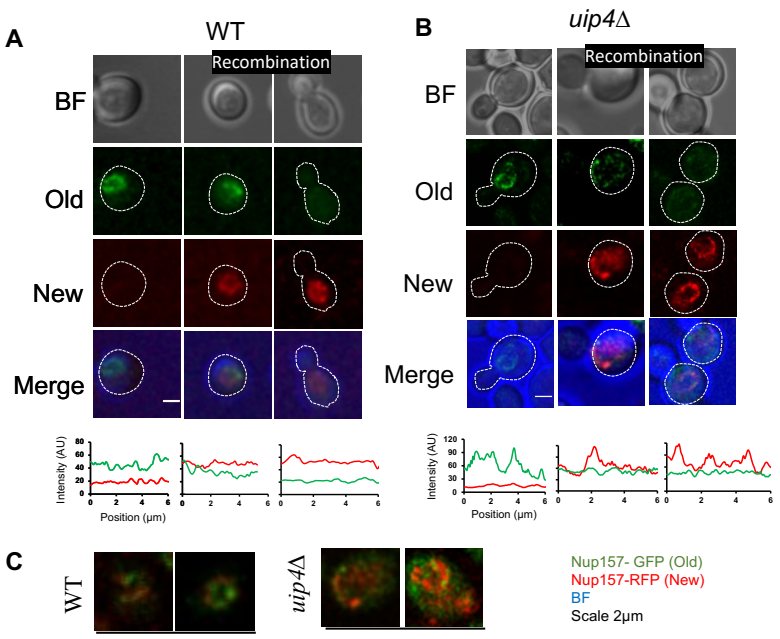

Fig12. NPC aggregation is a consequence of assembly defect in *uip4*Δ.

A, B. The micrographs represent localization of old (green) and new (red) Nup157 in wild type (A) and *uip4*Δ (B) cells. Cell shown in first column of A and B is captured before induction of recombination. The plot below the images shows relative intensity and distribution of the green and red signal along the NE. Dotted white line corresponds to outline of the cell under inspection; AU- arbitrary unit **C.** Images of a region (5μmX5μm) cropped around the nucleus of wild type and *uip4*Δ cells after recombination is shown.

So, while in wild type we see the new signal accumulation only at the NE, in the *uip4*Δ we find cells that retain the newly synthesized protein in the cytosol for longer (Fig12C). This strengthens the notion that the cytosolic spots seen in the cells lacking *UIP4* indeed represent the assembly intermediates.

*uip4*Δ cells are defective in nuclear import

The NPC functions as a gate for protein import into the nucleus. NE serves as a selective barrier between cytoplasm and nucleoplasm. In order to check the integrity of NE and functional competence of the nuclear pores, we tested the nuclear import capability of cells lacking *UIP4* using NLS-GFP construct (Stade et al., 1997). Wild type and *uip4*Δ were transformed with a large 2X-GFP bearing NLS so that it doesn't enter or exit the nucleus by diffusion. In a cell with functionally competent NPCs, upon transformation, the translated construct is retained

inside the nucleus. On the other hand, if the NPCs are dysfunctional, the construct will not be imported and GFP signal is observed in the cytosol and as such the ratio of nuclear and cytosolic GFP intensity under normal and impaired import will be different. Wild type cells accumulated NLS-GFP in the nucleus efficiently as evidenced by a bright nuclear fluorescence (Fig13A). However, loss of *UIP4* showed a defect in the nuclear import of NLS-GFP in about one fourth of the population (Fig13A). The ratio of GFP intensity in the nucleus vs cytosol was used to quantify the nuclear import (Fig13B). This indicates a compromised nuclear permeability barrier upon loss of *UIP4*.

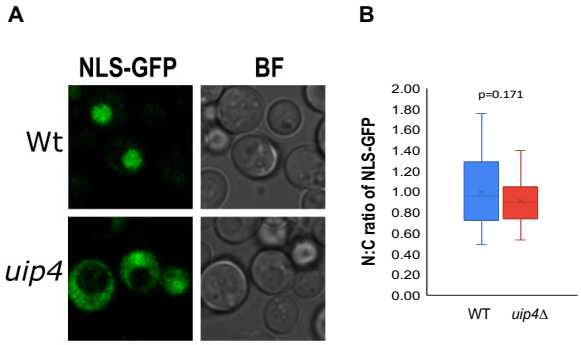

Fig13. *uip4*Δ are defective in retention of NLS-GFP in the nucleus
A. The micrographs representative of wild type and *uip4*Δ cells expressing NLS-GFP plasmid are shown. **B.** Distribution of GFP in nucleus vs cytosol of wild type and *uip4*Δ cells was quantified based on mean fluorescence intensity of GFP and is shown as box plot (n~30). Horizontal line represents median ratio.

3.3 SUMMARY

Wild type cells have a spherical nucleus, but *UIP4* deletion mutants have abnormal nuclear shape. The quantification of abnormal shape is represented as the fraction of cell population showing deviations from the wild-type like morphology. We also investigated the effect of this on distribution and function of NPCs. We used various microscopy based approached such as live cell imaging, indirect immunofluorescence and transmission electron microscopy to confirm the altered nuclear shape and NPC aggregation in *uip4*Δ. Additionally, we also observe a mislocalization of nucleoporins. Along with co-aggregation at the NE, we also observe that in case of *uip4*Δ cells, the cytosolic spots also have more nucleoporins from various sub complexes. We answered an important question about the molecular nature of these nup containing puncta by combining the power of yeast genetics and imaging techniques, we used recombination induced tag exchange to monitor the dynamics of NPC clustering in wild type

and *uip4*Δ cells. Our results show that NPC clustering and mis-localization is a result of delayed integration of NPC into the NE in cells lacking *UIP4.* This shows that in the absence of Uip4 NPCs fail to distribute properly along the NE and this results in deficient NPC function.

CHAPTER 4 REGULATED EXPRESSION OF *UIP4* IS CRUCIAL FOR NUCLEAR PORE COMPLEX FUNCTION

4.1 OVERVIEW

Regulated gene expression is a critical driving force in establishing cellular homeostasis. The expression of lamins is tightly regulated in a cell (Dechat et al., 2010). The relative amounts of lamin A/C and lamin B impact nuclear flexibility and genomic plasticity. The levels of lamins in a cell are modulated during development and differentiation (Manley et al., 2018). For example, mesenchymal stem cells alter the lamin composition and nuclear shape to regulate bone tissue homeostasis. Lamin A levels remain low during early development but increase during osteogenic differentiation (Alcorta-Sevillano et al., 2020). However, altering the lamin profile also alters genome organization, which, in turn, changes expression pattern of genes involved in the various physiological processes and nucleo-cytoskeletal interactions (Guerreiro and Kind, 2019; Fracchia et al., 2020). The overexpression of *SUN2*, an INM protein in metazoans, induces lobulation of nuclei, which blocks infection by HIV by affecting early events between reverse transcription and viral entry into nucleus (Donahue et al., 2016). In budding yeast also various studies have reported abnormal nuclear morphology upon overexpression of genes essential for sustenance of nuclear form and function. Nuclear membrane extends dramatically towards the cytoplasm resulting in formation of 'escapades' upon Esc1 overexpression (Hattier et al., 2007). Similar nuclear dysmorphia is observed when INM proteins Heh1, Heh2 or Prm3 are overexpressed (Hattier et al., 2007). Apart from the nuclear proteins, overexpression of ER proteins also affects nuclear morphology. Membrane stacks referred to as 'karmellae' have been seen upon overexpression of NE/ER protein- HMG CoA reductase type I (Wright et al., 1988). NE sheets extending inwards can be seen upon *BRL1* overexpression (Zhang et al., 2018). Brl1 is an ER protein that transiently associates with NPCs along with Brr6 and Apq12 and promotes NPC biogenesis. Such intranuclear proliferation of membrane is also observed upon overexpression of nucleoporin Nup53 (Marelli et al., 2001).

Since loss of *UIP4* compromised function of NPCs, we wanted to test if Uip4 interacts with nucleoporins or other NE proteins that contribute to NPC stability. We addressed this by some loss of function studies in known NPC assembly mutants. The classical genetic approach for exploring biological pathways typically begins by identifying mutations that cause a phenotype of interest. So, we compared the clustering and mislocalization of nups, in the double mutants with the *UIP4* single mutant. In addition to the traditional loss-of function or deletion studies, mutant phenotype can also be a result of overexpression or misexpression of the wild type gene. This provides an alternative yet powerful tool to identify pathway components that might remain undetected otherwise (Prelich, 2012). For instance, loss of Esc1 does not affect nuclear morphology but its overexpression does (Hattier et al., 2007). We used Uip4 OE as a tool to evaluate phenotypes. We tested localization of other components of the NPC. We studied the distribution of an FG Nup- Nup60, inner ring components- Nup157 and Nup188, and a transmembrane Nup- Pom33. The growth of yeast cells as a measure of fitness is usually used to dissect functional interaction between genetic pathways. Our results are indicative of a genetic interaction between *UIP4* and NUPs suggesting a functional connection between the two. Both *uip4*Δ*nup157* and *uip4*Δ*pom34*Δ display a higher NPC aggregation and nuclear import defect compared to *uip4*Δ. This shows that presence of Uip4p is required to ensure proper distribution of functional NPCs at the NE.

4.2 RESULTS

UIP4 shows genetic interaction with *nups*

To see if there is a genetic interaction between Uip4 and nups, we created double mutants of *UIP4* with *POM34* and *NUP157.* Pom34 is one of the three primary transmembrane nups in yeast (Strunov et al., 2011). Pom34 is important during the NPC biogenesis whereas Nup157 is required for ensuring proper assembly of pores at later stages (Makio et al., 2009). We find that neither the single mutants, nor the double mutants showed any growth defect under normal growth conditions (Fig14A, B).

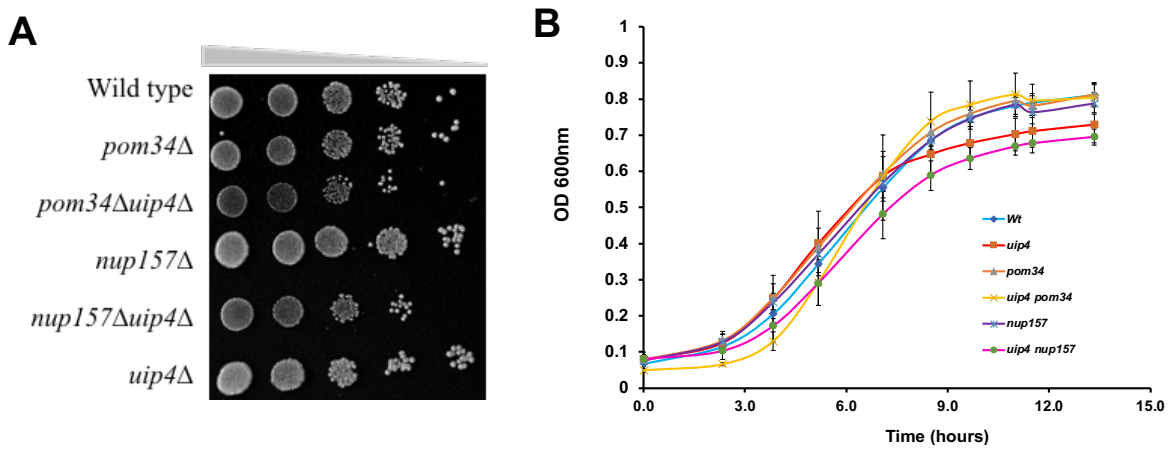

Fig14. Genetic interaction of *UIP4* with *nups*

A. Overnight cultures of the indicated strains were taken and sub-cultured by inoculating equal number of cells in a fresh medium for 4 hours. Cells were then harvested and 5µl of 10-fold dilutions were spotted on a SC-plate. The plates were incubated at 30ºC for 2 days prior to imaging.

B. Overnight cultures of the indicated strains were taken and sub-cultured in to fresh medium at 30ºC. OD600 was recorded every 90min and plotted. Three biological replicates were used. Error bars represent SEM.

Next, we tested NPC associated phenotypes. We transformed the double mutants with Nup49-GFP plasmid and imaged the cells (Fig15A). Both *uip4*Δ*nup157* and *uip4*Δ*pom34*Δ display a higher NPC aggregation and nuclear import defect compared to *uip4*Δ (Fig15B, C). This shows that presence of Uip4p is required ensure proper distribution of functional NPCs at the NE. Interestingly we see that the cytosolic spots of Nup49 are higher than the *uip4*Δ only in *uip4*Δ*nup157* and not in case of *uip4*Δ*pom34*Δ (Fig15D). This could be due to the reason that Pom34 is important for NPC biogenesis whereas Nup157 is required for proper assembly of pores. Thus, it is possible that Uip4 is involved in a later stage of NPC assembly rather than biogenesis. Our results are indicative of a genetic interaction between *UIP4* and *NUPs* suggesting a functional connection between the two.

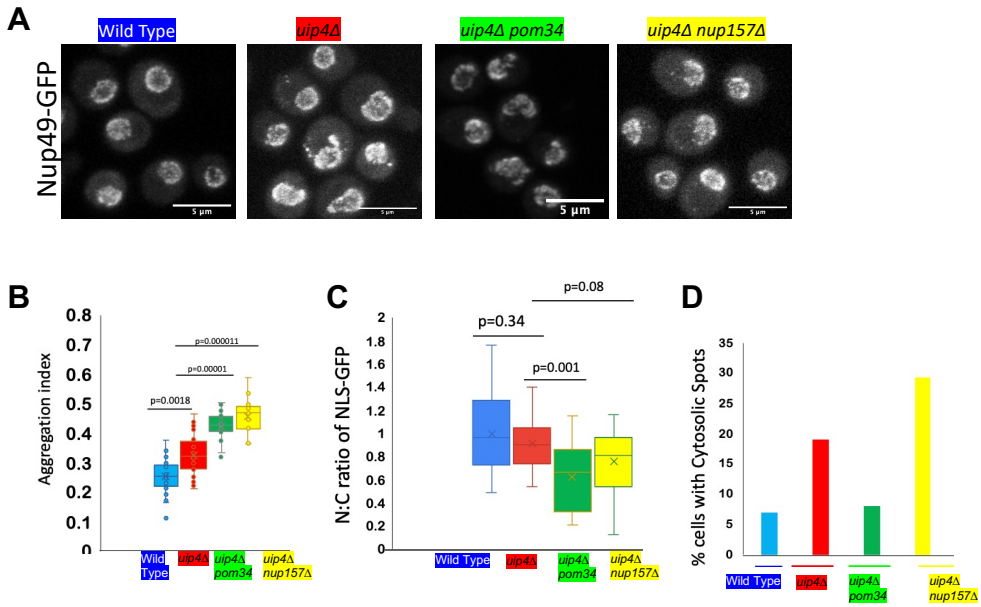

Fig15. Loss of *nups* has an additive effect on defect exhibited by *uip4*Δ

A. The micrographs are representative of the Nup49-GFP distribution as seen in the labelled strains. Various NPC associated phenotypes were quantified in the indicated strains and are plotted as shown in - **B.** Aggregation index. **C.** Nuclear retention of NLS-GFP **D.** Fraction of cells with cytosolic spots of Nup49 GFP

Overexpression of *Uip4* exacerbates structural deformities of the NE

In order to further explore the interaction between Uip4 and nups, we combined genetic analysis with overexpression studies. We tested the effect of enhancing Uip4 expression in yeast cells. In order to do so, *UIP4* was expressed from a constitutively active strong promoter-*pGPD.* We confirmed this overexpression of Uip4 by western blot and as shown in Fig16A, the expression of Uip4 is much higher. We then assessed the growth of cells over producing Uip4 since overexpression of proteins is sometimes toxic to the cells. (Fig16B, C). Overexpression of Uip4 did not have any negative effect on the mitotic division (Fig16C).

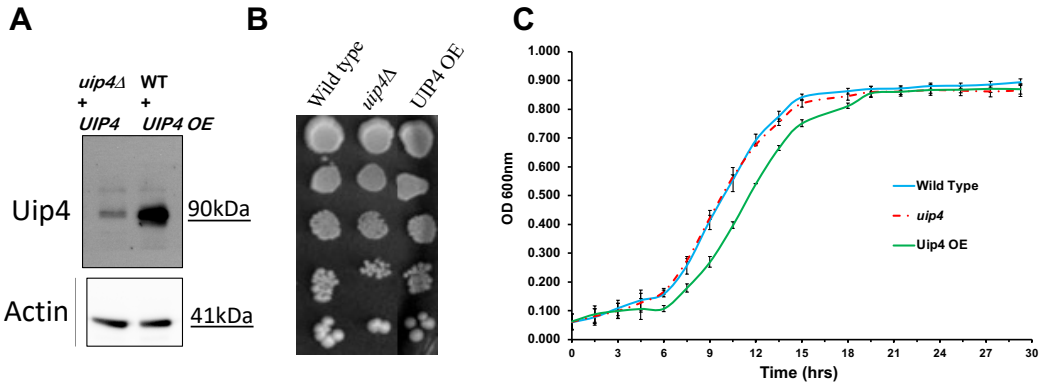

Fig16. Overexpression of *UIP4* is not toxic to the cells

A. Western blot showing expression of Uip4 from endogenous (lane 1) and strong (lane 2) promoter is presented. Actin is used as a loading control for protein level. **B**. Overnight cultures of the indicated strains were taken and sub-cultured by inoculating equal number of cells in a fresh medium for 4 hours. Cells were then harvested and 5µl of 10-fold serial dilutions were spotted on a SC-plate. The plates were incubated at 30ºC for 2 days prior to imaging. **B.** Overnight cultures of the indicated strains were taken and sub-cultured in to fresh medium at 30ºC. OD600 was recorded every 90min and plotted. Three biological replicates were used. Error bars represent SEM.

We performed additional growth experiment to test genetic interaction of *UIP4* with nups. The overexpression of Uip4 did not have any effect on growth of either wild type or nup deletion mutants at low or normal growth temperature (Fig16-B, 17). But overexpression of *UIP4* reduced the ability of *nup157*Δ and *pom34*Δ to grow at high temperature (Fig17). This negative genetic interaction suggests that *UIP4* plays a cooperative role with nups in a parallel process which is essential for growth at elevated temperature.

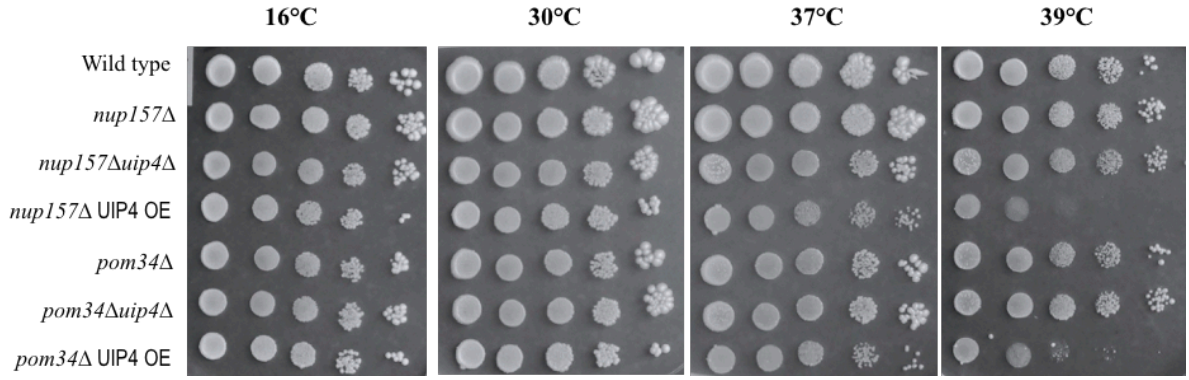

Fig17. Overexpression of *UIP4* in combination with loss of nups renders sensitivity to high temperature

Overnight cultures of the indicated strains were taken and sub-cultured by inoculating equal number of cells in a fresh medium for 4 hours. Cells were then harvested and 5µl of 10-fold serial dilutions were spotted on a SC-plate. The plates were incubated at 30ºCand 37ºC for 2 days, and at 16ºC and 39ºC for 4 days prior to imaging.

To confirm if the altered shape and cytosolic spots of Nups seen in *uip4*Δ cells are indeed due to loss of UIP4, we complemented the wild type cells with a single copy of UIP4. We found that NPC defects seen in *uip4*Δ could be restored to those seen in wild type cells (Chapter1, Fig7D). Surprisingly, we found that the defects were exacerbated when Uip4 was overproduced unlike complementation with one extra copy (Fig18). Yeast cells bearing GFP tagged protein were co-transformed either with empty pBEVY-L vector or UIP4-pBEVY-L for overexpressing Uip4. Nuclear shape changes and NPC clustering could be seen in live cells (Fig18). As both loss and overproduction of Uip4 led to distorted nuclear envelope architecture, it appears that the levels of Uip4p are important for regulating its function at the nuclear envelope.

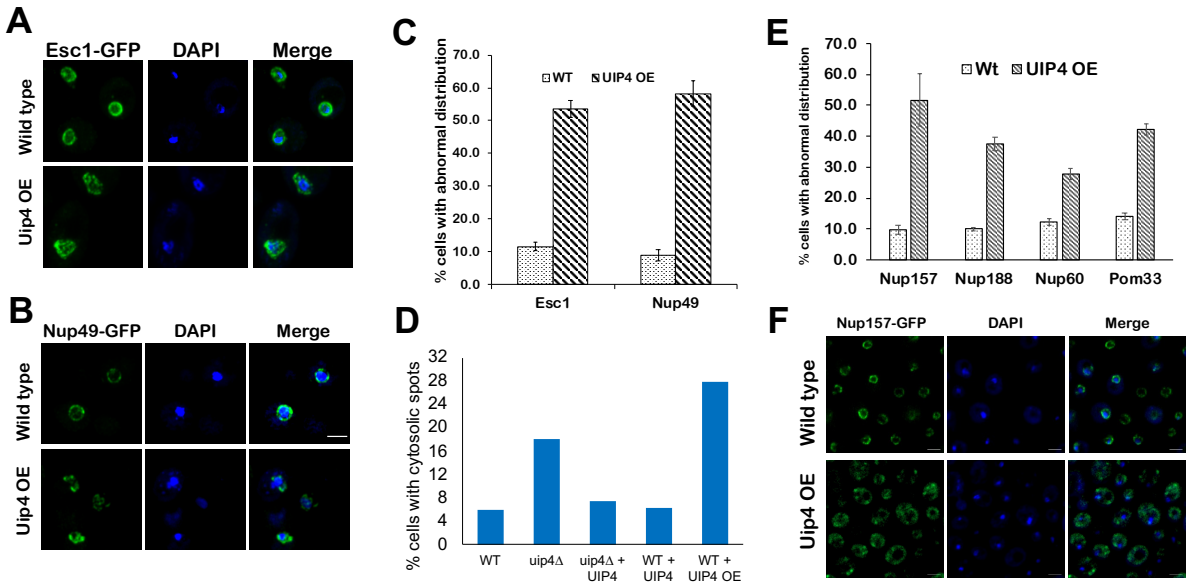

Fig18. Elevated expression of *UIP4* exacerbates nuclear deformities

A, B. The micrographs representative of GFP-Esc1 and Nup49-GFP localization respectively in wild type and *uip4*Δ cells are shown. DAPI is used as nuclear stain. **C.** Histogram showing fraction of cells with abnormal nuclear shape (Esc1) and clustering of NPCs (Nup49) is plotted. Error bars show SEM. **D.** Histogram showing fraction of labelled wild type and *uip4*Δ cells with cytosolic spots of Nup49 is presented (n~200). **E.** Histogram showing fraction of cells with clustering and mislocalization of indicated nup is plotted. Error bars show SEM. **F.** The micrographs representative of Nup157-GFP (green) localization in wild type and *uip4*Δ cells are shown. DAPI is used as nuclear stain

Validation of Nup157 localization upon Uip4 OE using nanobody labelling

Over expression of UIP4 results in clustering and mislocalization of various nups. We observed non-nuclear localization for Nup157 and reduced fluorescence intensity. In order to get better

localization precision, GFP nanobodies coupled to organic fluorophore targeted to Nup157 were used. Nanobodies are single domain-based antibodies, much smaller than the primary and secondary antibodies, that can be expressed in an *E. coli* based expression system. In a conventional confocal system, the localization of molecules cannot be determined precisely due to overlapping point spread functions of fluorophores. To overcome this, Rust *et al (2006)* introduced a technique based on blinking on fluorophores. This is referred to as STochastic Optical Reconstruction Microscopy (STORM). In this method, fluorophores are forced into a dark state by addition of a reducing agent in the imaging buffer. These fluorophores then return to the excited state stochastically or can be then turned 'on' by using a 405nm activation laser. The structure is then determined by fitting a gaussian to the centroid of all the localization points. The following work was done at the laboratory of Dr. Helge Ewers at FU, Berlin. The labelling strategy was adopted as described in Ries et al., 2012. Mid-log phase cells were fixed using PFA (4% paraformaldehyde, 2% Sucrose). The membranes were permeabilized by treating fixed cells with 0.25% triton. Anti-GFP nanobody conjugated to Alexa 647 was added to the cells. The cells were imaged using Bruker Vutara. GLOX (Glucose Oxidase) buffer with β-mercaptoethanol was used during STORM imaging. The localizations acquired were visualized using the SRX software. The images shown below represent the depth coded signal corresponding to Nup157-GFP. A previously shown, the NPCs were distributed evenly around the NE in case of wild type cells. Upon Uip4 OE, this distribution becomes asymmetric and Nup157 can be found in these clusters. Apart from this, Nup157 is also found in cytoplasmic regions. These non-nuclear spots could be a result of incorporation defect into NPCs.

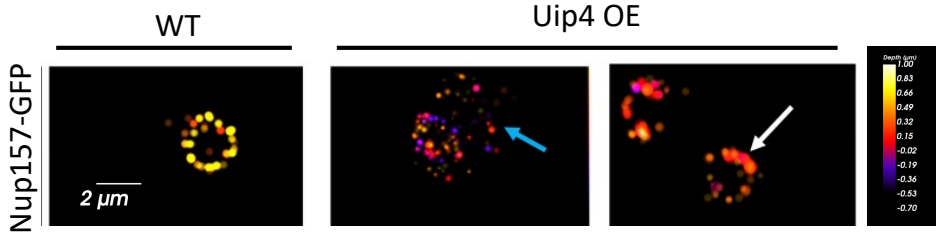

Fig19. *UIP4* OE causes redistribution of Nup157
The micrographs representative of Nup157 localization under endogenous and elevated expression of Uip4 are shown. Blue and white arrows represent mislocalized and clustered Nup157 respectively.

Blocking autophagy partially ameliorates the NPC associated defects observed upon UIP4 OE

From the imaging experiments we found that overexpression of Uip4p resulted in severe mislocalization of Nup157p (Fig18E). The signal intensity for Nup157-GFP was also greatly reduced (Fig18F, Fig19). Therefore, the levels of these proteins were checked under altered Uip4 levels. Under deletion of *UIP4,* the levels of Nup157 were found to be unaffected (Fig9D). However, under overexpression of Uip4, the levels of Nup157 were greatly reduced (Fig20A, B). The reduction of Nup157p levels explains the low intensity of the signal during live cell fluorescence imaging.

For most large protein complexes, small subunits or individual components undergo turnover. Unintegrated nucleoporins are believed to be subjected to degradation (Toyama et al., 2013). We wanted to check if the degradation of Nup157 is prevented by blocking autophagy and whether the localization of Nup157 is restored. Blocking autophagy per se does not affect the localization of Nup157 (Fig20C, left). We monitored the localization of Nup157-GFP by fluorescence microscopy in live cells and found that over expression of Uip4 in *atg1*Δ prevents mislocalization of Nup157 by reducing the degradation of Nup157 (Fig20C).

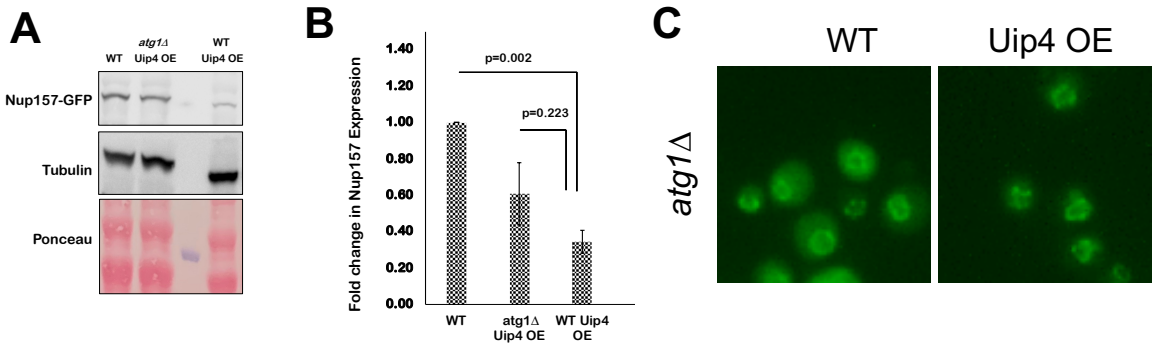

Fig20. Blocking autophagy prevents Nup157 degradation and mislocalization

A. Western blot analysis was done to compare the expression levels of Nup157 in the indicated strains harvested from mid-log phase. α-GFP was used to detect endogenously tagged Nup157 and tubulin is the loading control. Total protein in the membrane is stained with ponceau. **B.** The quantification of Nup157 expression normalized to tubulin is compared between the indicated strain. Error bars show SEM. **C.** The micrographs representative of Nup157-GFP (green) localization in wild type and upon Uip4 OE in autophagy defective cells are shown.

4.3 SUMMARY

We found that the NPC localization and NE morphology defects were exacerbated when Uip4 was overproduced. As both loss and overproduction of Uip4 led to distorted nuclear envelope architecture and defective protein import function, it appears that the levels of Uip4p are important for regulating its function at the nuclear envelope. Cells with deletion of either *NUP157* or *POM34* overexpressing *UIP4* were highly sensitive to elevated growth temperature We report that if the macroautophagy is blocked by deletion of *atg1*Δ, then the degradation and severity of Nup157 mislocalization reduces. Taken together, these results suggest that the dosage and distribution of Uip4 is critical for its function in budding yeast.

In the absence of Uip4, the NPC assembly is compromised and as such the nucleoporins stay in the cytosol for longer. These cytosolic spots of nups are integrated in to the NE overtime. Thereby suggesting that NPC assembly is compromised in *uip4*Δ. When Uip4 is overexpressed, we see increased abundance in the cytosolic pool of nups along with degradation of Nup157. This phenotype could be a result of either aggravated NPC assembly defect or compromised stability of assembly intermediates. While we cannot yet delineate the exact mechanism, our results suggest that the dosage and distribution of Uip4 is critical for its function in budding yeast.

As mentioned in the introduction, overexpression of various nuclear and ER proteins disrupts nuclear morphology. In many such cases reduction and increased expression of a protein have similar phenotype. For instance, abnormal nuclear morphology is reported in various mammalian cell types upon both overexpression and deletion or depletion of integral INM protein *SUN2* (Donahue et al., 2016; Lahaye et al., 2016). Altered *SUN2* expression affect nuclear envelope morphology, nuclear organisation and thereby susceptibility to HIV infection (Lahaye et al., 2016; Bhargava et al., 2021). Although the exact phenomenon is not known, it is believed that these seemingly similar phenotypes are exhibited by different underlying mechanisms (Bhargava et al., 2021). As both loss and overproduction of Uip4 led to distorted nuclear envelope architecture and defective protein import function, it appears that the levels of Uip4p are important for regulating its function at the nuclear envelope.

CHAPTER 5 CHARACTERIZATION OF LOCALIZATION AND EXPRESSION OF UIP4

5.1 INTRODUCTION

Under normal growth, yeast encounters starvation like conditions when all the glucose in the media has been consumed. A lot of metabolic conditioning ensures that the cell stays viable under such nutrient-limiting conditions (Galdieri et al., 2010). The shift from anaerobic (fermentable) to aerobic (respiratory) growth upon exhaustion of glucose under the standard laboratory growth conditions is referred to as diauxic shift (Perez-Samper et al., 2018). As the cells cross diauxic phase, genes that offer protection from metabolic stress are upregulated alongside activation of starvation induced autophagy (Howell and Manning, 2011; Müller et al., 2015). The movement and utilization of metabolites is also remodelled. Phosphatidic acid is utilized for synthesis of storage lipid- triacylglycerol, rather than conversion to membrane phospholipids (Romanauska and Köhler, 2018; Kwiatek et al., 2020). Such storage lipids are then packaged in lipid droplets and mobilized to various intra-cellular destinations (Wang, 2014). The cell organelles also undergo structural and functional alterations (Sun and Gresham, 2021). For instance, the number and size of mitochondria increase when the demand for respiratory processes increase in stationary phase (Dakik and Titorenko, 2016; Eiyama et al., 2013). The vacuole of metabolically aged cells grows as result of fusion (Baba et al., 1994; Aufschnaiter and Büttner, 2019). Membranous contact between organelles namely nucleus-vacuole junction (NVJ) and ER-mitochondria encounter structure (ERMES) also expand during starvation or nutrient limiting conditions such as in stationary phase (Helle et al., 2013; Hönscher et al., 2014; Kohler and Büttner, 2021).

When yeast cells are exposed to nutrient limiting conditions, they undergo a transcriptional and translational reprograming that brings about the aforementioned changes. Nutrient sensing in yeast is regulated by various pathways operating in concert with each other (Jalihal et al., 2021; Argüello-Miranda et al., 2018). Three main pathways involving the protein kinases PKA, TOR and Sch9 integrate the nutrient sensing cues from the growth medium in a Rim15 dependent manner (Toda et al., 1988; Rolland et al., 2002; Swinnen et al., 2006). Rim15 is a glucose-sensing protein kinase required for entry of cells into stationary phase (Reinders et al., 1998). Activation of Rim15 under nutrient depletion and stress conditions regulates growth and

controls gene expression in a Msn2/4 and Gis1 transcription factor dependent manner (Martínez-Pastor et al., 1996; Pedruzzi, 2000). Genes regulated by Msn2 and Gis1 offer protection against stress and are usually involved in lifespan extension (Medvedik et al., 2007).

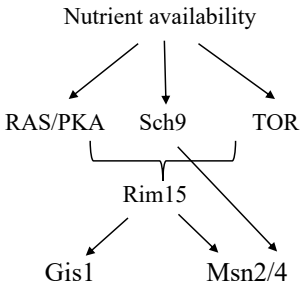

Fig21. Flow chart showing nutrient sensing pathways in yeast

In this chapter we further describe the results that show Uip4 expression is induced under nutrient limiting conditions. Modulating carbon source, nitrogen availability, cellular energy state and pH of growth media impact Uip4 expression. We show that the expression of Uip4 during transition from abundant to limiting nutrient availability is controlled by transcription factors Msn2 via the Rim15 kinase. Further, this regulated expression of Uip4 is essential for nucleus-related functions and ensuring long term viability of cells.

5.2 RESULTS

Uip4 expression is induced upon entry to stationary phase

Indirect immunofluorescence was done in cells expressing Uip4-13xMyc. Uip4 harbors an N terminal Early Set glycogen binding domain (1-87aa) and a MDN1 superfamily midasin domain (73-271aa) (Marchler-Bauer et al., 2011). It lacks a transmembrane membrane domain but has a KKXX (^{277}KKLL^{280}) motif, suggesting potential ER membrane retention. In consonance with the presence of KKLL motif, Uip4 localizes to two prominent rings resembling ER distribution (Figure 22 and Thesis- Dr. Imlitoshi Jamir).

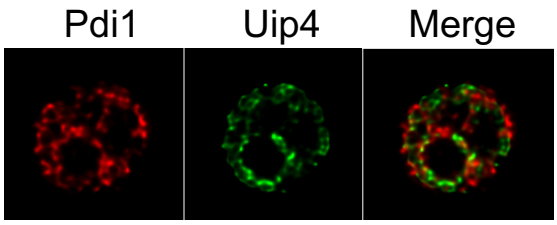

Fig22. Uip4 localizes to NE/ER

The micrograph shows deconvolved image of a cell representative of Uip4 localization. Indirect Immunofluorescence was done to determine Uip4 localisation in fixed cells. α-Pdi was used to mark ER. α-myc was used to probe Uip4 fused with 13-myc epitope.

We observed that Uip4 expression between cells varied and therefore wanted to test if the expression and/or localization of Uip4 changes based on the metabolic status. We harvested wild type cells having *UIP4-13MYC* tag and compared the level of protein expression between cells in mid-log versus stationary phase. We observed a higher expression of Uip4 in cells harvested from stationary phase as compared to those in mid-log phase (Fig23A). Uip4 is expressed at almost 6-8 times higher level during stationary phase (Fig23B). Next, we compared the localization of Uip4 in cells during mid-log phase and those in stationary phase. Consistent with increased expression, we observed a brighter signal for Uip4. Uip4 was localized exclusively to ER (Fig23C). Additionally, we did not see any overlap between non-nuclear associated Nsp1 and Uip4 (Fig23C, arrow). This suggests that Uip4 does not directly associate with the nucleoporins.

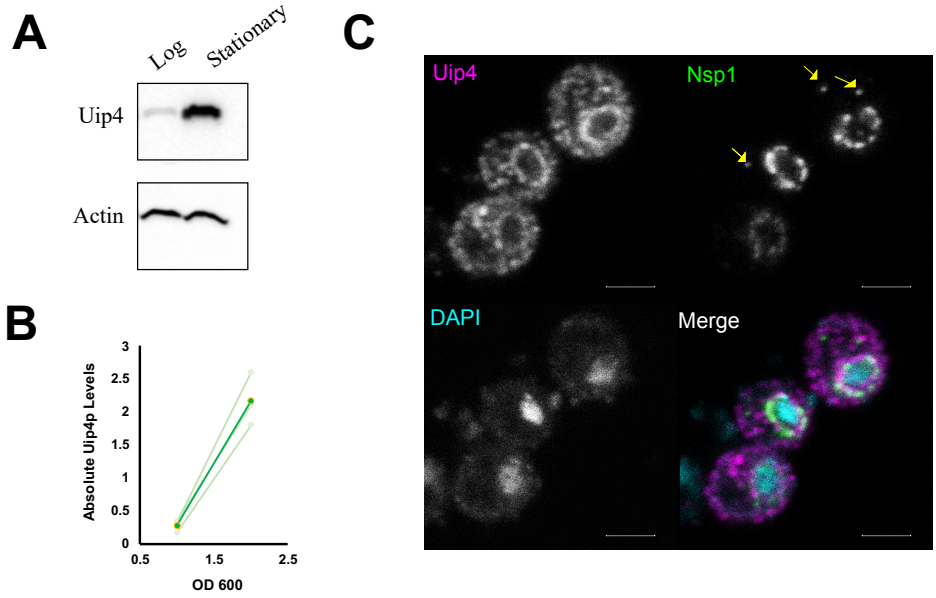

Fig23. Uip4 expression is higher in stationary phase of growth

A. Western blot analysis was done to compare the expression levels of Uip4 in the cells harvested from mid-log phase (OD $_{600}$ 0.8) and stationary phase (OD $_{600}$ 2.0). α-myc was used to detect Uip4-13myc. α-actin was used to detect actin for loading control. **B.** The quantification of Uip4 expression normalized to actin is shown between log and stationary phase. Dark green line shows the average of three individual experiments shown in light green. **C.** The micrograph shows an image panel of a representative of Uip4 localization. Indirect Immunofluorescence was done to determine Uip4 localisation in cells fixed at stationary phase. α-Nsp1 was used to mark NE/nups. α-myc was used to probe Uip4 fused with 13-myc epitope. Yellow arrows mark non-nuclear spots of Nsp1.

UIP4 is essential for pore complex function during stationary phase

Wild type cultures from stationary phase of growth also have cytosolic presence of nups that display foci like distribution distinct from the NE (Fig23C). Similar to the cells from log phase culture, we observed increased number of cells showing cytosolic foci of Nup49 in stationary phase as well, for *uip4*Δ (Fig24A). This indicates that Uip4 could be important for NPC distribution particularly during stationary phase. To assess this further, we looked at the NE integrity by import of NLS-GFP. Fluorescence imaging indicated an overall reduction in the signal intensity for cells harvested during stationary phase for both wild type and *uip4*Δ (Fig24B) Western blots also confirmed the lower level of NLS-GFP expression in both cells harvested from stationary phase as compared to those harvested in log phase (Fig24C). In addition to defective nuclear import, in *uip4*Δ cells the expression level of NLS-GFP was lower than respective wild type in all stages of growth (Fig24B, C). Importantly, in the stationary phase, the reduced NLS-GFP signal was almost entirely nuclear in wild type cells. But in *uip4*Δ the NLS-GFP signal was either from dead cells or whole cells, and hardly any cells showed nuclear accumulation, indicating a more compromised NPC function and cellular health.

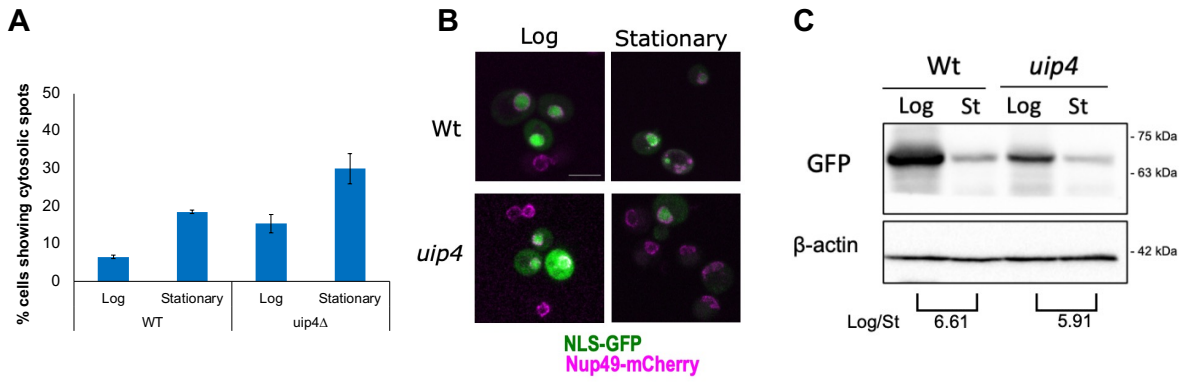

Fig24. Loss of *UIP4* shows dramatic phenotype in stationary phase

A. The bar graph represents the fraction of cells in the indicated strain harvested from either mid-log or stationary phase showing cytosolic spots of GFP-Nup49. ~100 cells from 2

independent experiments were counted. **B.** Live cell imaging was performed in Wt and uip4 cells bearing NLS-GFP plasmid harvested from either mid-log or stationary phase. The overlay images showing NLS-GFP (green) and Nup49-mCherry (magenta) are indicative of the observation. Scale-5µm **C.** Western blot showing protein level of NLS-GFP detected using α-GFP is shown for wild type and *uip4*Δ cells harvested from log and stationary (St) phase. The quantification of the NLS-GFP in Log/Stationary phase is shown (Average of 2 independent experiments). Actin is used as a loading control.

UIP4 is essential for viability of non-dividing yeast population

In order to test the significance of Uip4 induction in stationary phase, we looked at the survival of wild type and *uip4*Δ cells in the post-mitotic state. First, we quantified the fraction of dead cells in the two strains by staining with trypan blue. The uptake of dye by dead cells is used as a measure to distinguish live and dead fraction (Liesche et al., 2015). We found that a higher fraction of *uip4*Δ cells stained with trypan blue as compared to wild type cells where the dye was entirely excluded from cells harvested from an overnight culture (Fig25A). A 1 day old culture of *uip4*Δ cells had ~4% of cells that stained positive with trypan blue. To confirm that dye exclusion is actually due to reduced viability and not due to compromised cell wall function, we also assessed the growth of these cells as they were aging. CFU/ml (Colony forming units) for each strain was quantified and normalised to the number of survivors for a 1 day old culture. The fraction of survivors was calculated for each strain and we find a remarkable difference in the viability between wild type and *uip4*Δ cells as the number of days increase (Fig25B). There are significantly reduced survivors in *uip4*Δ as the cells age. These results indicate a reduced capacity of *uip4*Δ cells to survive in the post-mitotic phase.

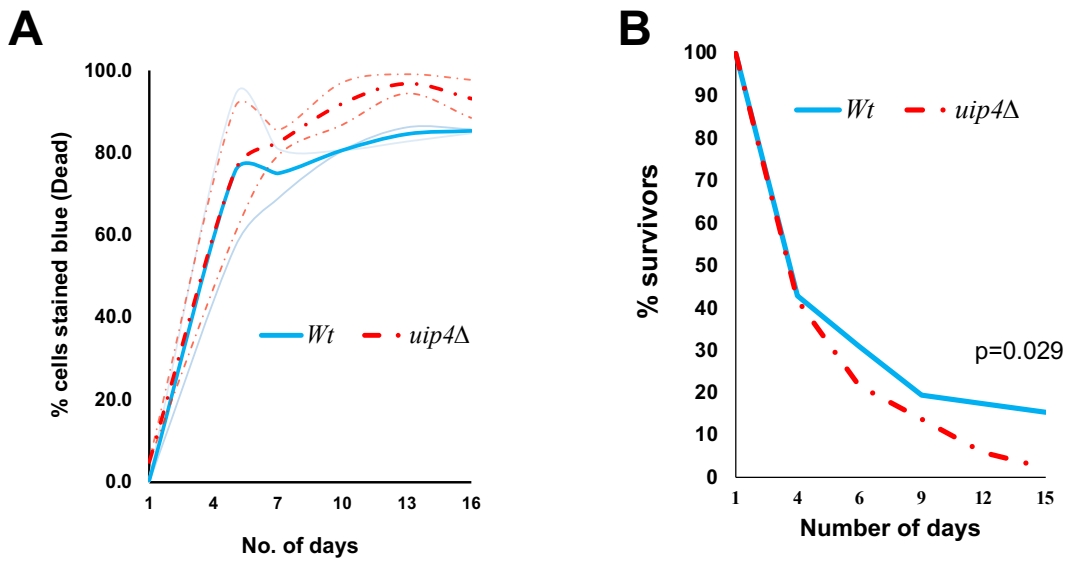

Fig25. Old *uip4*Δ cells have reduced viability

A. The plot represents the fraction of cells in the indicated strain that stained positive for trypan blue. The dark lines are the average for each strain. Values from independent experiments are shown in faint lines. **B.** The fraction of cells surviving in the indicated strains as the cells aged is plotted.

Several genes required for stationary phase survival are also required during thermal stress (Sun and Gresham, 2021). Since Uip4 was expressed more in cells harvested at stationary phase and cells lacking *UIP4* showed reduced survival, we checked the sensitivity of *uip4*Δ to growth at high temperature. Equal number of wild type and *uip4*Δ cells were spotted on SC plate and then grown in either 30ºC or 39ºC. We find that loss of UIP4 had a negative impact on the growth at 39ºC. Taken together, these results suggest that elevated expression of Uip4 in late stages of growth is important for cell survival and function.

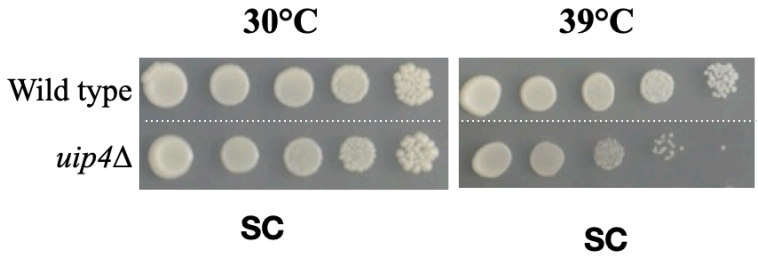

Fig26. *uip4*Δ cells have reduced viability at high temperature.

Overnight cultures of the indicated strains were taken and 5µ of 10-fold serial dilutions were spotted on a SC-plate. The plates were incubated at either 30ºC or 39ºC.

Glucose exhaustion and nutrient limitation induces Uip4 expression

We found the Uip4p levels to be lowest during log phase when the cells are actively dividing and highest during the stationary phase when the growth is seized. We then quantified the expression of Uip4 from cells harvested during different points. We measured the OD600 of the culture and plotted the growth curve to know the growth phase (Magenta curve). Corresponding to the marked points, we determined the protein level of Uip4 (Green curve). Our results reveal that Uip4 expression varied depending on the growth stage. Uip4 is highly expressed during the stationary phase of cells whereas the expression is kept minimal during log phase when the cells are actively dividing. We then quantified the abundance of *UIP4* transcripts by quantitative RT-PCR. As controls, we tested the transcriptional status of *ATG8,* an autophagy related protein and *NUP157,* a nucleoporin. Autophagy is induced upon glucose depletion and entry into stationary phase while the expression of nucleoporins remains fairly

unchanged (Galdieri et al., 2010; Toyama et al., 2013). As anticipated, we find that levels of *NUP157* mRNA do not alter much between log (OD 600- 0.8) to stationary phase (OD 600- 3.0) while transcription of *ATG8* is induced. *UIP4* mRNA increases several folds as the cells exit exponential growth phase and enter stationary phase. Our results suggest that expression of Uip4 is transcriptionally regulated.

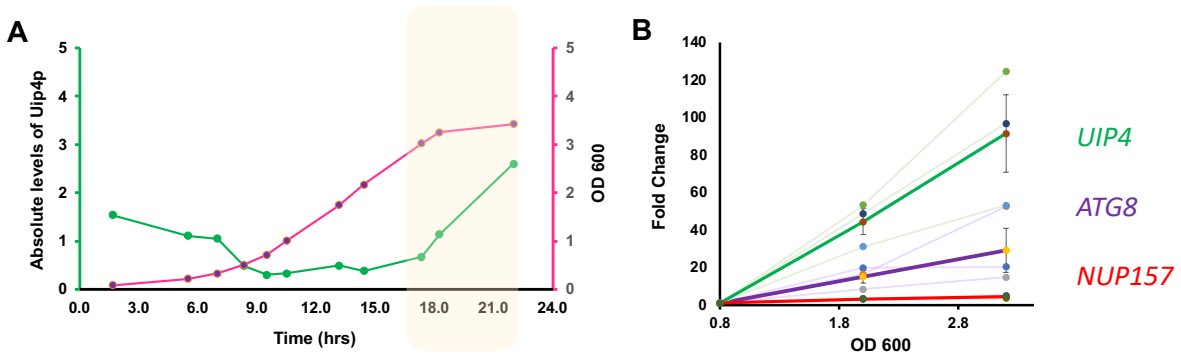

Fig27. Uip4 is highly expressed in stationary phase cells

A. The plot shows the expression of Uip4 during the growth stages. The curve in magenta shows the growth of yeast cells (Y-axis: right, magenta). The level of Uip4p corresponding to the marked time point is shown in green (Y-axis, left). Increased expression is concomitant with entry into stationary phase as highlighted. **B.** The plot shows mRNA levels of genes as displayed. Fold change in mRNA levels obtained by qRT-PCR analysis is shown in Y-axis. ACT1 was used as control. The dark lines are the average for each strain. Values from independent experiments are shown in faint lines.

We then asked if Uip4 levels are regulated depending on the available glucose in the media. To check this, we tested Uip4 levels in cells shifted to media containing low glucose. We find the Uip4 levels to increase when the cells were shifted to media containing lower than 2% glucose and reduce when shifted to higher glucose concentration. We therefore went on to check if Uip4 levels increase specifically in response to carbon limitation or also in any other nutrient limitation. We subjected cells harvested from log phase grown in 2% glucose containing media to various nutrient limiting conditions viz carbon starvation (0.75%YNB, 0.05% glucose), N- starvation (0.17%YNB, 2% Glucose), addition of Rapamycin(0.2µg/ml) to growth media and resuspending cells in water. Uip4 levels remain unchanged when left in water, even until 60 hours. On the other hand, C or N starvation induced Uip4 expression. A greater induction was observed upon N starvation as compared to C starvation. Addition of Rapamycin resulted in an even higher induction of Uip4 expression.

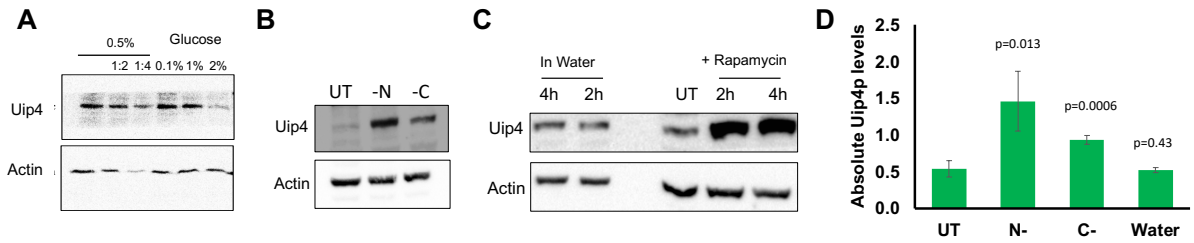

Fig28. Uip4 expression goes up during nutrient limiting conditions

A. Western blot showing the expression levels of Uip4 in the cells harvested from mid-log phase and transferred to a media containing indicated glucose concentration for 3 hours is presented. 1:2 and 1:4 dilution of lysate from culture grown in 0.5% glucose containing media are shown for better comparison. **B.** Western blot shows the expression levels of Uip4 in the cells harvested from mid-log phase and transferred to a media lacking either N source (-N is 0.17%YNB, 2% Glucose) or carbon source (-C is 0.75%SC, 0.05% Glucose) for 3 hours. UT- untreated cells **C**. Western blot showing the expression levels of Uip4 from the cells harvested from mid-log phase and then transferred either to a fresh media containing rapamycin or just resuspended in water for indicated time. UT- untreated cells **D.** The quantification of Uip4 expression normalized to actin is shown. Error bars are SEM and p-values are indicated.

Growth in alternate carbon sources enhances Uip4 expression

Yeasts are facultative anaerobes. In the laboratory conditions, yeasts utilize glucose as the primary source of energy and grow exponentially while fermenting glucose that produces ethanol and acetate (Galdieri et al., 2010). Once the glucose in the medium is depleted, they undergo a short lag phase and begin to utilize ethanol and acetate from the medium released during the process of fermentation (Gray et al., 2004; Perez-Samper et al., 2018). After this, they enter a state of quiescence that is referred to as stationary phase (Gray et al., 2004; Sun and Gresham, 2021). The cells undergo a considerable amount of change in total protein and transcript pool. Several proteins expressed largely during post diauxic shift and in stationary phase resemble those expressed under stress such as thermal, osmotic or nutrient (Gasch et al., 2000; Galdieri et al., 2010).

Next, we checked if the Uip4 levels were also increased when the cells were shifted to alternative carbon sources. We find that growing wild type cells in any alternate carbon source other than either glucose or sucrose results in increased Uip4 expression (Fig29A, B). In fact, the expression was higher in non-fermentable carbon sources that require active respiration and mitochondrial function (Fig29, B).

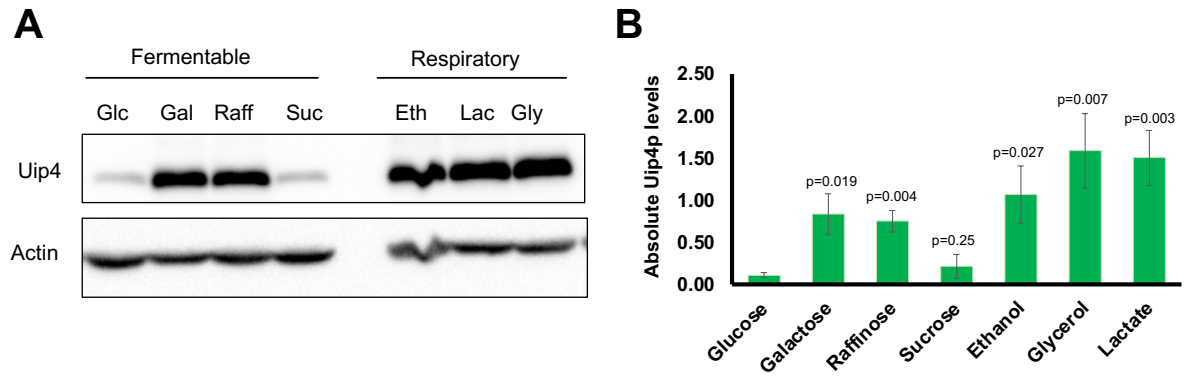

Fig29. Uip4 expression varies in alternate carbon sources

A. Western blot showing the expression levels of Uip4 in the cells harvested from mid-log phase and transferred to a media containing indicated carbon source for 5 hours is presented. **B.** The quantification of Uip4 expression normalized to actin is shown. Error bars are SEM and p-values are indicated.

Uip4 is upregulated by the transcription factor Msn2 via Ras/PKA and Sch9 kinase pathway

Genes expressed specifically under particular conditions are regulated by one or more transcription factors that bind to defined sequences or known motifs in their promoter (Hahn and Young, 2011). To understand if such regulatory control operate in the expression of Uip4p, we analysed the promoter of *UIP4* for transcription factor binding sites using the Promoter Analysis tool of Yeastract (Monteiro et al., 2020). We found various possible binding sites for transcription factor Msn2 and Gis1 as shown in Fig30. Both of these are implicated in upregulation of stress responsive genes in stationary phase of yeast growth (Pedruzzi, 2000; Durchschlag et al., 2004).

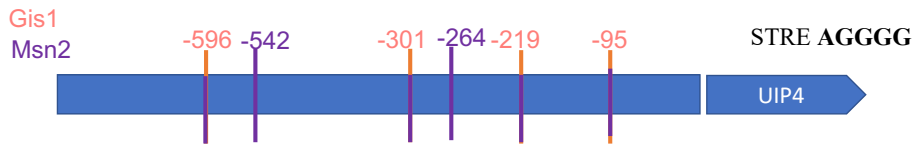

Fig30. Schematic showing Msn2 and Gis1 binding regions on *UIP4* promoter

We tested the level of Uip4 in cells harvested from stationary phase lacking one of these transcription factors (Fig31). Apart from Msn2 and Gis1, we also measured Uip4 expression in the absence of Msn4. Msn4 is also a stress responsive transcription factor, with several overlapping targets with Msn2 (Martínez-Pastor et al., 1996). We find a greater downregulation

of Uip4p in *msn2*Δ as compared to either *msn4*Δ or *gis1*Δ (Fig31A, B). We also confirmed the downregulation at the transcript level by performing quantitative RT-PCR. The abundance of *UIP4* mRNA in *msn2*Δ is highly reduced as compared to the wild type cells (Fig31C). Since the activity of Msn2 is largely dependent on the upstream kinase Rim15, we asked if the downregulation is mediated via Rim15. However, we only find a modest reduction in the Uip4 expression in *rim15*Δ (Fig31A, B). Likewise, the transcript levels also do not change much as compared to the wild type (Fig31C). This hints towards Msn2 mediated Uip4 regulation by other upstream regulators.

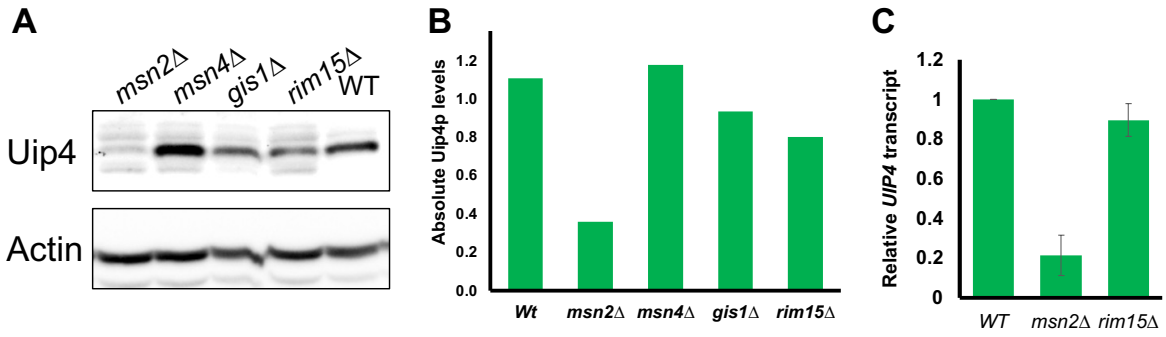

Fig31. Uip4p expression is regulated by *MSN2*

A. Western blot showing the expression levels of Uip4 in the indicated mutants in cells harvested from stationary phase. **B.** The quantification of Uip4 expression shown in panel A, normalized to actin is plotted**. C.** The fold change in *UIP4* mRNA in the indicated strains as compared to that of wild type is shown.

We therefore set out to identify the pathway which regulates the expression of Uip4 post diauxic shift. In order to do so, we looked at the protein level of Uip4 in various single gene deletion mutants of key kinases that are implicated in nutrient sensing in yeast (Fig21). In the absence of either Ras1, a GTPase involved in activation of PK-A, or Sch9 kinase, Uip4 levels are low as compared to the wild type (Fig32). Our results suggest that TOR mediated signalling is dispensable for Uip4 expression as we do not see any reduction in Uip4 expression in *tor1*Δ when compared to wild type (Fig32).

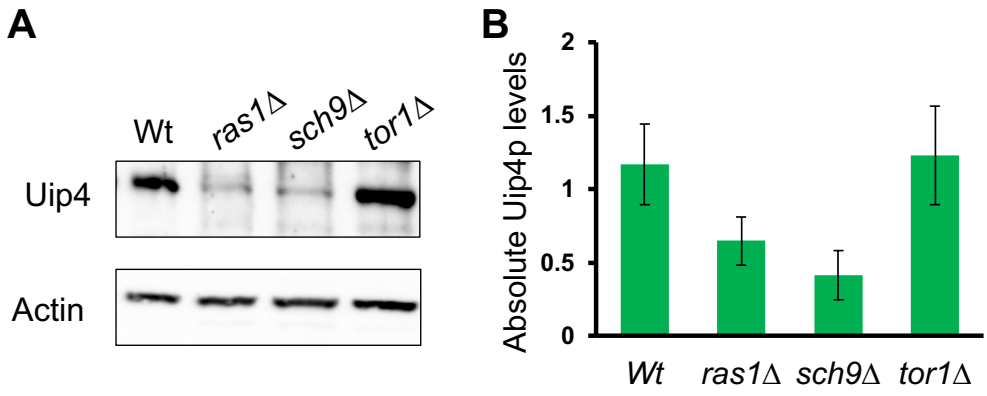

Fig32. Attenuation of PKA and Sch9 kinase signalling supresses Uip4 expression
A. Western blot showing the expression levels of Uip4 in the cells harvested from stationary phase of indicated mutants is presented. **B.** The quantification of Uip4 expression normalized to actin is shown. Error bars are SEM.

5.3 SUMMARY

In this part of the study, we have characterized the expression and localization of Uip4p. Wild type cultures from stationary phase of growth also have cytosolic presence of nups that display foci like distribution distinct from the NE. The Uip4 signal did not overlap with the cytosolic spot of Nsp1. However, loss of *UIP4* compromised NPC function. The Uip4p localization was largely unaffected during stationary phase, although, a more continuous staining of Uip4 was present at the NE/ER. The expression of Uip4p was also induced as the cells progressed towards stationary phase of growth. The identification of stationary phase-specific expression pattern is corroborated with the necessity of UIP4 for stationary phase survival. While Uip4 appears to be dispensable for mitotic growth, it is important for growth at high temperature and long-term survival. We found that Sch9 and PKA kinase pathways are important for Uip4 expression. This regulation is partly mediated via the Rim15 kinase as we see only a minor reduction of Uip4p in *rim15*Δ. This could be due to direct activation of Msn2 via Sch9 (Yorimitsu et al., 2007). The induction of Uip4 in non-fermentable carbon sources, its regulation by Msn2 and reduced survival in stationary phase and high temperature shows a pattern similar to those genes that are implicated in adaption to conditions that necessitate metabolic reprogramming (Rep et al., 2000). However, the exact mechanism and role of Uip4 in this process remains elusive and will require further investigation.

CHAPTER 6 UNDERSTANDING THE MOLECULAR FUNCTION OF UIP4

6.1 INTRODUCTION

YPL186C was first identified in a two-hybrid screen for interactors of the deSUMOylase, Ulp1p and therefore called Ulp1 interacting protein 4 (Takahashi et al., 2000). There are no known sequence based homologs of *UIP4* (Garapati and Mishra, 2018). Besides, very few interactors of Ui4p have been reported in literature and therefore the knowledge of its role and regulation to date is scant.

In order to understand the molecular function of Uip4 and the pathways where it is involved, we used both genetics and proteomics approach. Yeast-two-hybrid is a powerful tool to screen for physical interactors (Chien et al., 1991). Novel interactors for a protein of unknown function can also be identified by using a tagged version of the protein of interest as bait in a pull-down assay. In order to identify the interacting partners of Uip4 specifically during stationary phase, a proteomics approach was taken. UIP4 was tagged with SFB (Streptavidin Flag S-protein) tag at the C terminal (Kumar et al., 2020). Immunoprecipitation was performed and eluates were analysed by Mass spectrophotometry analysis.

6.2 RESULTS

Identifying interactors via yeast two hybrid

In order to look for physical interactors of Uip4, the yeast-two-hybrid approach was undertaken. Uip4 was used as a bait by cloning the full length ORF in a GBD vector (pGBD UC-1). Genomic library cloned in a GAD vector was used. UIP4 was fused to the GAL binding domain in the pGBKT7 vector and the clone was confirmed by restriction digestion and sequencing. Self-activation of the clone was tested by co transforming the clone with Empty-GAD vector. Novel interactors were screened by activation of reporter gene- *HIS3* that allowed growth of transformants on plate lacking the amino acid histidine. Identification of interactor was done by sequence analysis. The results are represented in the following table.

Table9: Novel interactors of Uip4 identified via yeast two hybrid screen.

Gene	**Function** (Source: Saccharomyces Genome Database)
PTC3	Type 2C protein phosphatase, role in DNA damage checkpoint inactivation
ISM1	Mitochondrial isoleucyl-tRNA synthetase
YPR089W	Protein of unknown function; exhibits genetic interaction with ERG11 and protein-protein interaction with Hsp82p
RPS2	Protein component of the small (40S) subunit; essential for control of translational accuracy
RTC1	Subunit of SEACAT, a subcomplex of the SEA complex, SEA is a coatomer-related complex that associates dynamically with the vacuole; has N-terminal WD-40 repeats and a C-terminal RING motif;
VHS1	Cytoplasmic serine/threonine protein kinase
CEX1	Component of nuclear aminoacylation-dependent tRNA export pathway; cytoplasmic; interacts with nuclear pore component Nup116p
CSM1	Nucleolar protein that mediates homolog segregation during meiosis
MTH1	Negative regulator of the glucose-sensing signal transduction pathway
HRB1	Poly(A+) RNA-binding protein; key surveillance factor for the selective export of spliced mRNAs from the nucleus to the cytoplasm
GSY2	Glycogen synthase; expression induced by glucose limitation, nitrogen starvation, heat shock, and stationary phase
FAA4	Long chain fatty acyl CoA Synthase
VPS36	ESCRT II subunit protein
PDH1	Putative 2-methylcitrate dehydrogenase
VPS13	peripheral membrane protein that localizes to the prospore membrane and at numerous membrane contact sites, required for mitochondrial integrity

Identifying interactors via pull down followed by MS/MS

In order to find the interacting partners of Uip4, we generated a C-terminal SFB tagged UIP4 construct expressed from its own promoter. This triple tag construct has a S protein and FLAG epitope followed by Streptavidin binding site. The clone was confirmed by sequencing and

expression was checked by western blot using Flag antibody. Uip4-SFB fusion construct was detected at a molecular weight of ~65kDa on a 10% SDS-PAGE using FLAG antibody.

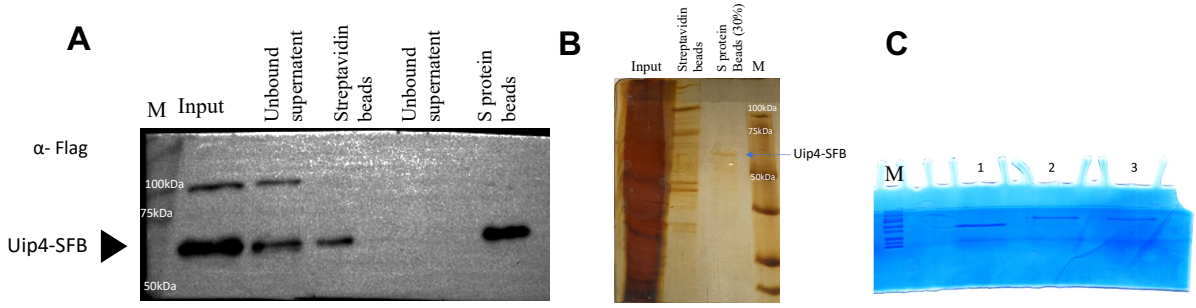

Fig33. Confirmation of Uip4-SFB expression and IP

A. The western blot shows detection of Uip4-SFB using α-Flag, through various steps of immunoprecipitation. **B.** A silver-stained acrylamide gel to confirm presence of purified interacting proteins of Uip4. **C.** The eluate was separated by SDS-PAGE and the presence of protein was confirmed by CBB staining prior to excising and sending for MS/MS analysis.

The pull-down was performed in stationary phase cells as Uip4 is highly expressed in this stage and the protocol used is described in detail in the methods sections. We obtained diverse functional interactors. Physical interactome analysis of the strong and moderate interactors of Uip4 reveals the network map shown in Fig34. Pyruvate metabolism, longevity regulation and protein processing in ER are some of the prominent functional categories observed. Hsp104, Ssa1, Ssb2 and Cct4 are involved in protein folding whereas Met6, Pdc1, Arc1, Pyc2, Leu1, Pyc1 and Acc1 are involved in carboxylic acid metabolism with Pdc1, Pyc2 and Pyc11 specifically involved in glucose metabolic process. Uip4 was found to interact with 5 cytosolic (Ssa1, Ssa2, SSsb1, Ssb2, Sz1), 1 ER (Kar2) and 1 mitochondrial (Ssc1) HSP70 class of chaperones. Apart from the HSP70 family, Uip4 also interacts with Hsp104, Hsp60, Hsp78, Hsc82 and Hsp82. The isoforms Hsp82 and Hsc82 are yeast Hsp90. Of note, we did not find any interactor identified by yeast two-hybrid in the pull-downs.

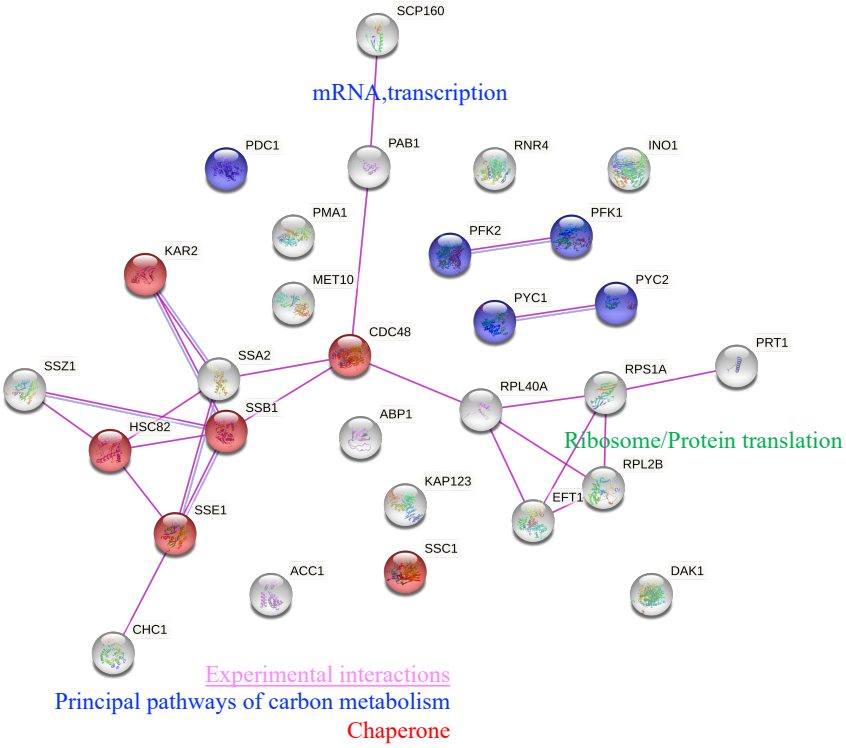

Fig34. Interactors of Uip4 obtained by pull down approach

6.3 SUMMARY

We have identified multiple novel potential functional interactors. The interactors of Uip4 fall into diverse functional groups. The interactors from two hybrid and pull down could be categorized into two major functional categories: Protein translation/folding and Carbon metabolism. Uip4 appears to be involved in pathways that are induced by specific cellular stresses such as nutrient starvation. However, it is not clear if Uip4 itself acts as a chaperone to its interacting partners or if it is important for substrate specific chaperone binding. We have also identified several interesting, novel interactors of Uip4 via a yeast-two hybrid screen approach. Interactors such as Vps13 (Involved in protein targeting to vacuole, localizes to organelle membrane contact sites), Vps36 (ESCRT II subunit component), FAA4 (Long chain fatty acyl CoA synthase) etc hint towards involvement of Uip4 in an inter-organellar communication network.

CHAPTER 7 SUMMARY

We have identified and reported a novel role of a previously uncharacterized ER protein, Uip4, in maintenance of nuclear integrity. We demonstrate that dosage of Uip4 is critical for its function. Both loss and overexpression of Uip4 lead to compromised NPCs with reduced nuclear import capacities. It is likely that altered Uip4p regulation affects the quality of NE by causing dysregulation of NPC stoichiometry. The severe clustering of NPCs upon Uip4 OE could be due to reduced Nup157p levels. Based on our observation of mis-localized NE proteins upon either loss or overexpression of Uip4, we hypothesize that Uip4 could be involved in stabilizing the assembly intermediates of NPC or the entire complex. In the absence or OE of Uip4, the incorporation of these substrates into the NE/NPC is prevented and these can be seen in cytosol. Preventing degradation of these Nups by blocking the protein homeostasis pathways, restores assembled NPC. This suggests that Uip4 is potentially involved in the quality control of NPC.

Although Uip4 was originally identified in a yeast two-hybrid screen for interactors of Ulp1, we did not find any positive interaction between Ulp1 and Uip4. Additionally, we did not detect any nucleoporin or nuclear protein that is known to directly affect NPC function. Taken together, these results indicate that although the presence of Uip4 contributes positively towards NPC assembly and stability, this effect is likely to be a consequence of either a transient association of Uip4 with nups or an indirect association.

Key results:

- Loss of Uip4 results in abnormal nuclear shape, clustering of nuclear pore complexes at the NE and mis-localization of nucleoporins.

- Over-expression of Uip4 exhibits a dominant negative phenotype. Upon Uip4 OE, the inner ring nucleoporin Nup157 undergoes degradation. This can be prevented partially when autophagy is brought down.

- Uip4p is localized to NE/ER and its levels are fairly low during the log phase of yeast growth and increase as the cells progress towards stationary phase. Uip4 levels also

increase upon shift from glucose to alternate carbon sources and nutrient limiting conditions.

- Uip4 expression in controlled by RAS/PKA and Sch9 kinase signalling and the downstream transcription factor Msn2.

- Majority of the interactors of Uip4 are involved in protein translation regulation, chaperone like-function and carbon metabolism.

CHAPTER 8 DISCUSSION

Overall cellular health is an outcome of multiple, dynamic processes that are interconnected. Organelles have a characteristic shape and must function optimally in order to detect and respond to nutritional changes. Budding yeast *Saccharomyces cerevisiae* is particularly sensitive and adaptable to altered metabolic states. Despite the knowledge of basic structural components of nuclear envelope, a clear understanding of the mechanisms that contribute towards the maintenance of shape of NE and integrity associated complexes is lacking. In particular the dynamic changes in the nuclear shape and organisation associated with altered metabolic states are poorly understood.

Previous studies have shown that the shape of nucleus and mitochondria changes in response to nutrient availability. Nuclear geometry- size and circularity, are also reported to change when carbon source is altered or cells when cells are shifted to starvation inducing media (Walters et al., 2019, 2012). However, very little is known about the mechanistic basis of changes in organellar morphology between 'fed' and 'starved' states. We have found that expression of Uip4p in yeast is controlled by glucose availability. Overexpression of Uip4 during post-diauxic shift is concomitant with altered nuclear structure and NPC function. Deterioration of nuclear shape maintenance, irregular NPC distribution, subdued nuclear permeability and lower long-term survival in cells lacking Uip4 could provide a tantalizing link between organelle morphology, metabolic sensing and cellular aging. Although we do not find any direct physical interaction of Uip4 with the nups, this does not entirely eliminate the possibility of a transient interaction between the two. Uip4 with its N-terminal Ig-like fold and C-terminal amphipathic helix might act as a flexible connection between the NPC and the nuclear membrane; thereby contributing to the stability during assembly. Membrane nups such a Pom152 also have such Ig like fold (Yewdell et al., 2011). Loss of viability under nutrient starved conditions of prolonged growth could also be due to reduced stress responsiveness in the absence of Uip4. Our results indicate that Uip4p could play a crucial role in nutrient driven organelle remodelling in *S. cerevisiae*.

Additionally, increasing protein levels of Uip4p results in a compromised turnover of Nup157 most likely via autophagy. In yeast, mechanisms of nup turnover have not been extensively investigated. Yeast is a better model to study this also because NPCs do not disintegrate in

mitosis unlike the mitotic disassembly and post-mitotic reassembly in metazoans. A lot of nuclear constituents such as histones, nucleoporins and lamins are long lived, so they are also vulnerable to accumulation of damage (Toyama et al., 2019). NPC does not turnover as an entire entity, rather as smaller subunits and individual complexes (Daigle et al., 2001; Tomioka et al., 2020). ESCRTs play a role in autophagy and have also been implicated in removal of old nucleoporins (Rusten and Stenmark, 2009; Toyama et al., 2019). We have identified novel interaction of Uip4 with ESCRT-II component Vps36 (Table9). This interaction could be a possible molecular player in the autophagy dependent regulation of NPC turnover.

We show that the timing and extent of Uip4 expression is important. Uip4 is expressed more during conditions that limit glucose availability. These include reducing glucose concentration in the growth medium, adding galactose or ethanol as carbon source, or cells in stationary phase. We have identified the pathways that regulate expression of Uip4. This work also sheds light on the heterogeneity of physiological vs non-physiological deformations induced in the cellular organelles and adds to the understanding of architectural changes of nucleus possibly as an adaptation to metabolic demands. Importantly, as Uip4 function appears to be important for survival in stationary phase/quiescent stage, it is possible that Uip4 is involved in metabolic reprogramming of cells during this period. An understanding of the physiological rewiring under altered Uip4 levels warrants further biochemical investigation and and would shed light on the molecular role of Uip4 in this phase.

In addition to identifying regulators of nuclear organization this work has opened avenues for understanding inter-organellar communication. This ER localized protein shows interaction with several cytoplasm, mitochondria and vacuole-localized proteins. Since Uip4 bears a E-set domain that senses AMPK levels, it is likely to function in coordination with pathways involved in regulation of nutrient sensing to NE homeostasis. Why nuclear shape and NPC distribution is responsive to growth conditions is not known. However, the regulation of transcription at the nuclear periphery and association of mRNAs with the NPCs might have a role in this. Which components directly mediate the response to nutrient availability to the nuclear periphery and dictate shape alterations is an open question. Together, this study hints at the key role of a NE/ER protein in nuclear structure and function regulation under altered metabolic conditions. Our work has iterated the significance of cross talk between multiple biological pathways. Future experiments will aim to identify the underlying pathways that control nuclear morphology and its components in response to physiologically relevant signals.

APPENDIX

9.1 LIST OF ANTIBODIES USED

Antibody	Host	Source	Identifier	Dilution used
Primary				
Actin	Mouse	Santa Cruz	sc-47778	WB 1:5000
GFP	Rabbit	Abcam	ab290	WB 1:10000
GFP	Rabbit	Sigma	G1544	WB 1:8000
Myc	Rabbit	Abcam	ab9106	IF 1:800, WB 1:10000
Myc	Mouse	Abcam	ab56	WB 1:5000
Nsp1	Mouse	Abcam	ab4641	IF 1:800, WB 1:10000
Pdi1	Mouse	Abcam	ab4644	IF 1:600, WB 1:10000
Tubulin	Rat	Abcam	ab6160	WB 1:10000
Secondary				
Mouse-Alexa488	Goat	Life technologies	A21202	IF 1:1000
Mouse-HRP	Goat	Abcam	ab97023	WB 1:30000
Rabbit-Cy3	Goat	Jacksons	111-165-003	IF 1:1000
Rabbit-HRP	Goat	Abcam	ab97051	WB 1:20000
Rat-HRP	Goat	Abcam	ab97057	WB 1:20000

9.2 LIST OF PRIMERS

S.no	Identifier	Sequence 5'-3'	Purpose
1	ACT1 FP	GTAACATCGTTATGTCCGGTGGTAC	RT-PCR
2	ACT1 RP	GTAACATCGTTATGTCCGGTGGTAC	
3	UIP4 FP	GTAACATCGTTATGTCCGGTGGTAC	
4	UIP4 RP	GAACTTCGTTCAATGGAGCATGTTC	
5	ATG8 FP	GAACTTCGTTCAATGGAGCATGTTC	
6	ATG8 RP	GAACTTCGTTCAATGGAGCATGTTC	
7	NUP157 FP	TAGAGAATACCGCACTACTCGATACG	
8	NUP157 RP	TAGAGAATACCGCACTACTCGATACG	
9	NUP157_ S_FP	TAGAGAATACCGCACTACTCGATACG	Screening primer for Nup157
10	NUP157_ S_RP	GTTTAAGTGTGTATATTTTGAGCTGCC	Screening primer for Nup157
11	Nup157RI TE_F1	GATCCCGTTCAAGATTATGTGAAGGA TCGTCATCATGGCCTGAAA *ggt gga tct ggt gga tct*	Forward primer for C terminal epitope tagging of NUP157
12	Nup157RI TE_R3	GAAAACTTCACAATCAAACTGCTAAA ATATACAAATAATTCCGT *TCA ggcgccggtggagtggcg*	Reverse primer for C terminal epitope tagging of NUP157
13	UIP4_F1	CATACATACATACTTGGTTGTAACAT TAAGATAGGCAAAGCAACTAAATA *C GGATCCCCGGGTTAATTAA*	Forward primer for deletion of UIP4
14	UIP4_F2	GCTCATGGTTTTCTTGGTTGACAACG AAAATGTCAAGCTCAGAGGCATCA*CG GATCCCCGGGTTAATTAA*	Forward primer for C terminal epitope tagging of UIP4
15	UIP4_R1	TAGTAGCTAAAAAAAGATGAATGTG AATCGAATCCTAAGAGAATTCAACA*G AATTCGAGCTCGTTTAAAC*	Reverse primer for C terminal epitope tagging/ deletion of UIP4
16	4RP_prom _BamHI	CGAGGATCCTATTTAGTTGCTTTGCCT ATC	Reverse primer for amplification of *pUIP4,* upstream of START
17	4RP_noST OP_EcoRI	GCCGAATTCTGATGCCTCTGAGCTTG ACATTTTCG	Reverse primer for amplification of UIP4, upstream of STOP
18	GFP_pUG 23_FP	TCAggatccATGTCTAAAGGTGAAGAAT TATTC	Forward primer for amplification of GFP from pUG23
19	GFP_pUG 23_RP	CGAgaattcTTTGTACAATTCATCCATAC CATG	Reverse primer for amplification of GFP from pUG23

20	RP_MYC Clone	AAGgtcgacGCGAATTCACTAGTGATTGAT	Reverse primer 17bp downstream of stop codon after 13MYC
21	F2_UIP4	ATTggatccATGGTCACCATTGTATTTGATCATC	Forward primer for Amplification of UIP4 from START codon
22	FP164SUIP4	GCAGTGATGTTCCACCAATA	Forward primer 164bp upstream of *UIP4* START
23	RP_S_UIP4	GCTGCCTGCCATATTTCAAT	Reverse primer 130bp downstream of *UIP4* STOP
24	FI_UIP4	AAAggatccCTAACCCCTATTTCAAAGATCTCAA	Forward primer, 600 bp upstream of START codon of UIP4
25	RP uip4	AAAgtcgacCAGTGTAGATGTAACAAAGTCGACT	Reverse primer 350 down stream of STOP codon of UIP4
26.	UIP4_tagS	GCTGCCTGCCATATTTCAAT	RP 150 bp downstream of STOP
27.	Uip4_FP_XbaI	GGGtctagaATGGTCACCATTGTATTTGAT	Forward primer, 600 bp upstream of START codon of UIP4
28	KanMX RP	AGTCTGACCATCTCATCTGT	552 bp downstream of KanMX start site Reverse primer
29	Uip4FP	CGgtcgacATGGTCACCATTGTATTTGATC	Forward primer from START codon of UIP4
30	Uip4RP	TACTGCAGTTATGATGCCTCTGAGCTTGAC	Reverse primer from up to STOP codon of UIP4

9.3 DETAILS OF RECOMBINANT DNA CONSTRUCTS/ STRAINS

Generating *pGPD*-UIP4-13MYC-pBEVYL (CKM501)

In order to clone Uip4-13Myc in a pBEVY-L for overexpression under pGPD, genomic DNA from KRY1570 was used as template and following primers were used for amplification:

UIP4-FP_XbaI From START codon of UIP4 with XbaI site
GGGtctagaATGGTCACCATTGTATTTGAT

RP-13MYC 13bp downstream of STOP codon after 13MYC with SalI site
AAGgtcgacGCGAATTCACTAGTGATTGAT

The 1476 bp PCR product was digested with XbaI and SalI and ligated into pBEVY-L digested with the same set of restriction enzymes. The clone was confirmed by restriction digestion and sequencing.

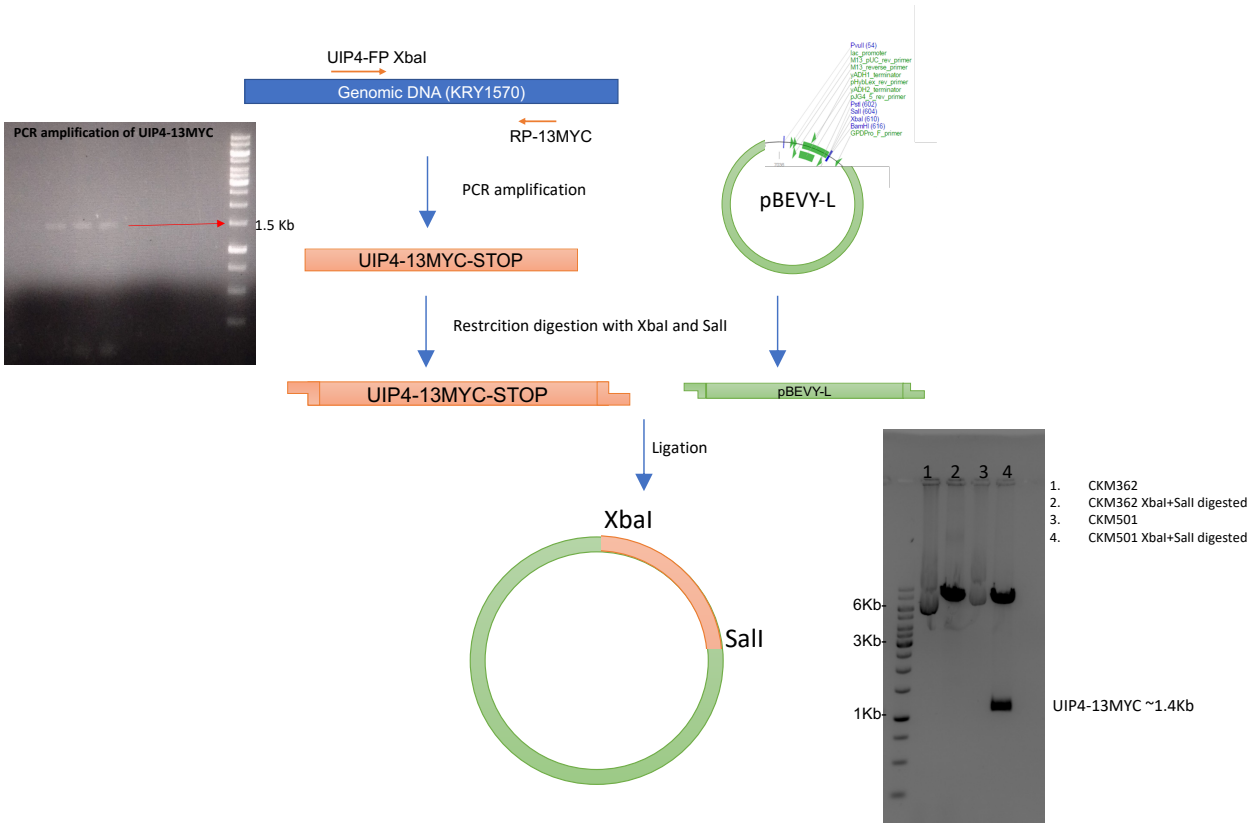

Schematic showing cloning generation of CKM501

Generating UIP4-pGBKT7 (CKM517)

UIP4 cloned in pGBKT7 vector was used as a bait for yeast two-hybrid screen. The gene was amplified using genomic DNA form KRY1492 as template.

Primers used:
Uip4FP Forward primer from START codon of UIP4
CGgtcgacATGGTCACCATTGTATTTGATC

Uip4RP Reverse primer from upto STOP codon of UIP4
TACTGCAGTTATGATGCCTCTGAGCTTGAC

The ~930 bp product obtained was ligated into pBlueScript vector. This clone was digested with SalI and PstI restriction enzymes to generate the fragment for ligation in to pGBKT7 vector. The clone was confirmed by restriction digestion and sequencing.

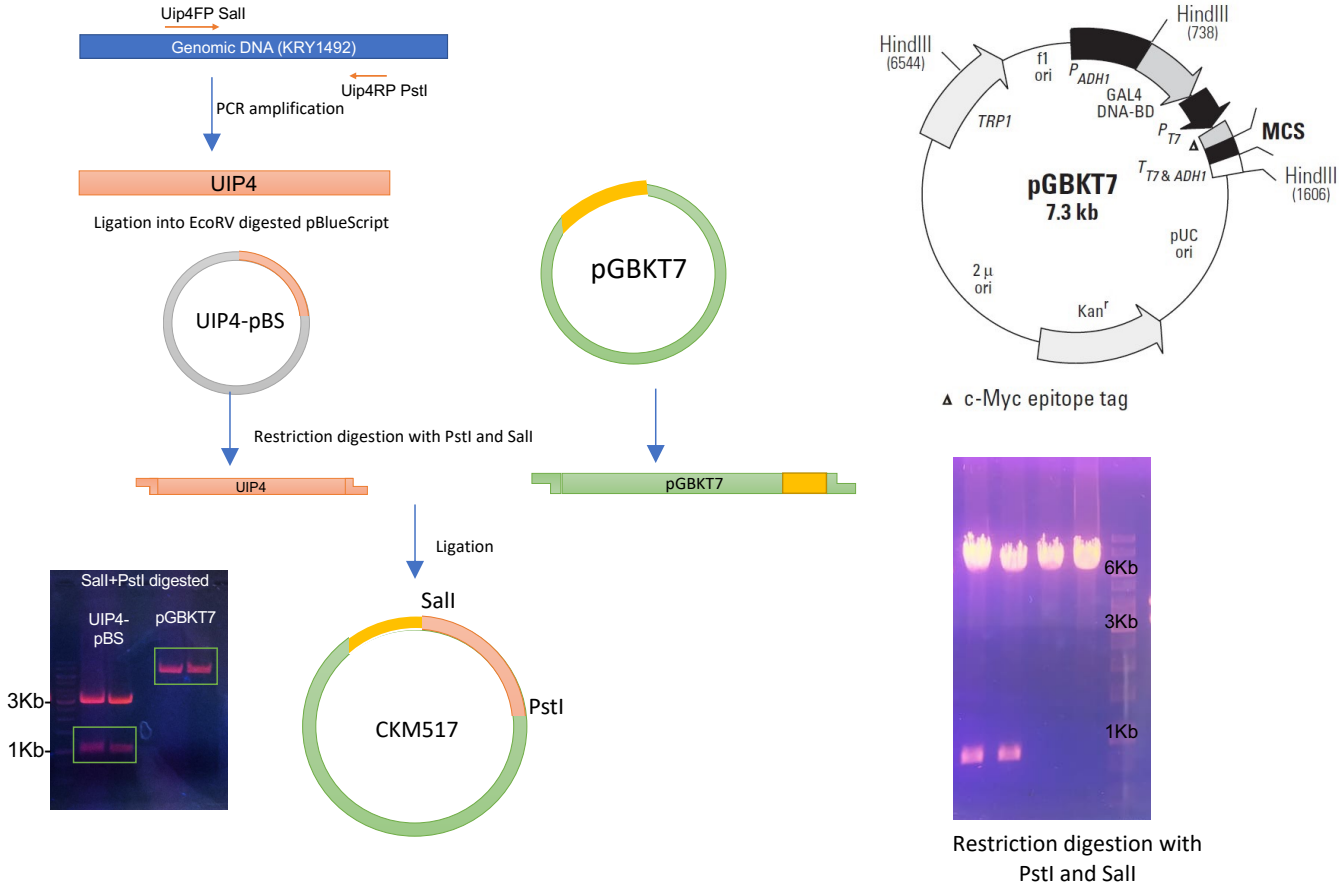

Schematic showing cloning generation of CKM517

Generating *pUIP4*-UIP4-SFB-pRS313

In order to clone Uip4-SFB in a CEN vector under its endogenous promoter, genomic DNA from KRY1492 was used as template and following primers were used for amplification of UIP4 with promoter and without STOP codon.

Uip4_FP_ XbaI Forward primer, 600 bp upstream of START codon of UIP4
GGGtctagaATGGTCACCATTGTATTTGAT

4RP_noSTOP_EcoRI Reverse primer for amplification of UIP4, upstream of STOP
GCCgaattcTGATGCCTCTGAGCTTGACATTTTCG

SFB fragment was obtained by restriction digestion of CKM638 with EcoRI and SalI. The two fragments were then ligated into pRS313 linearised with XbaI/SalI.

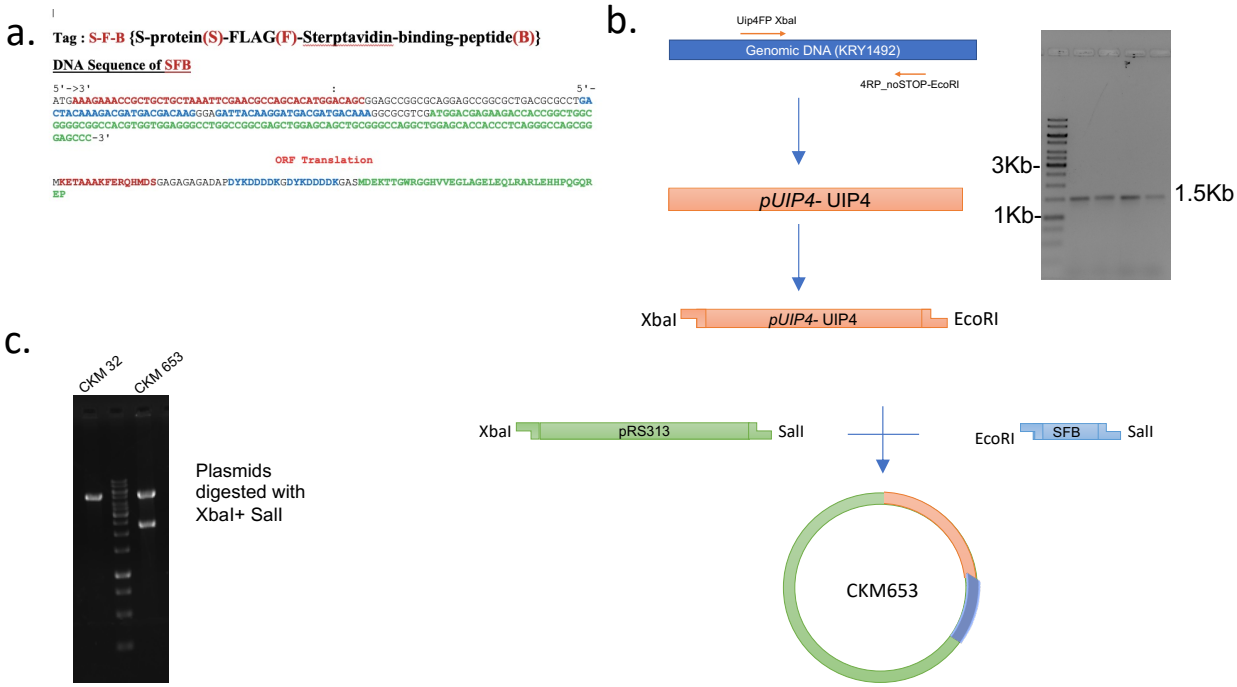

Schematic showing cloning generation of CKM653

Generating *pUIP4*-UIP4-13MYC-pRS316 (CKM670)

In order to clone Uip4-13Myc in a CEN vector under its endogenous promoter, genomic DNA from KRY1570 was used as template and following primers were used for amplification:

F1-UIP4 600bp upstream of START codon
AAAggatccCTAACCCCTATTTCAAAGATCTCAA

RP-13MYC 17bp downstream of STOP codon after 13-MYC
AAGgtcgacGCGAATTCACTAGTGATTGAT

The 2076 bp PCR product was digested with BamHI and SalI and ligated into pRS316. The clone was confirmed by restriction digestion and sequencing.

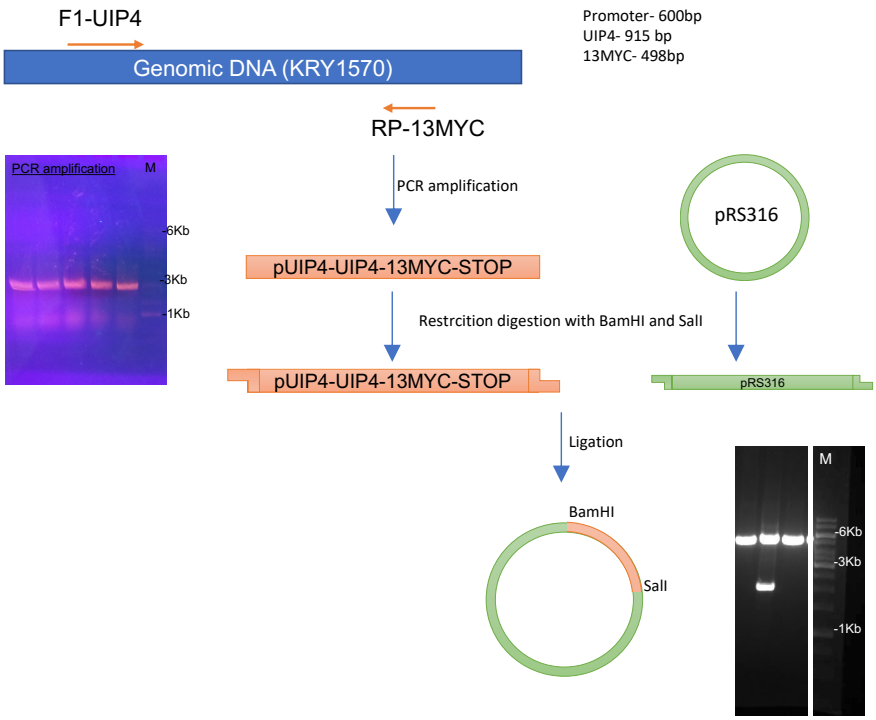

Schematic showing cloning generation of CKM670

Generating *pUIP4*-GFP-SFB-pRS313

In order to clone GFP-SFB in a CEN vector under the endogenous promoter of UIP4, pUG23 vector was used as a template to amplify GFP sequence and genomic DNA from KRY1492 was used as template to amplify the promoter of UIP4. Following primers were used for amplification of *pUIP4* :

Uip4_FP_ XbaI Forward primer, 600 bp upstream of START codon of UIP4
GGGtctagaATGGTCACCATTGTATTTGAT

4RP_prom_BamHI Reverse primer for amplification of pUIP4, upstream of START
CGAGGATCCTATTTAGTTGCTTTGCCTATC

Following primers were used for amplification of *GFP:*

GFP_pUG23_FP Forward primer for amplification of GFP from pUG23
TCAggatccATGTCTAAAGGTGAAGAATTATTC

GFP_pUG23_RP Reverse primer for amplification of GFP from pUG23
CGAgaattcTTTGTACAATTCATCCATACCATG

SFB fragment was obtained by restriction digestion of CKM638 with EcoRI and SalI.

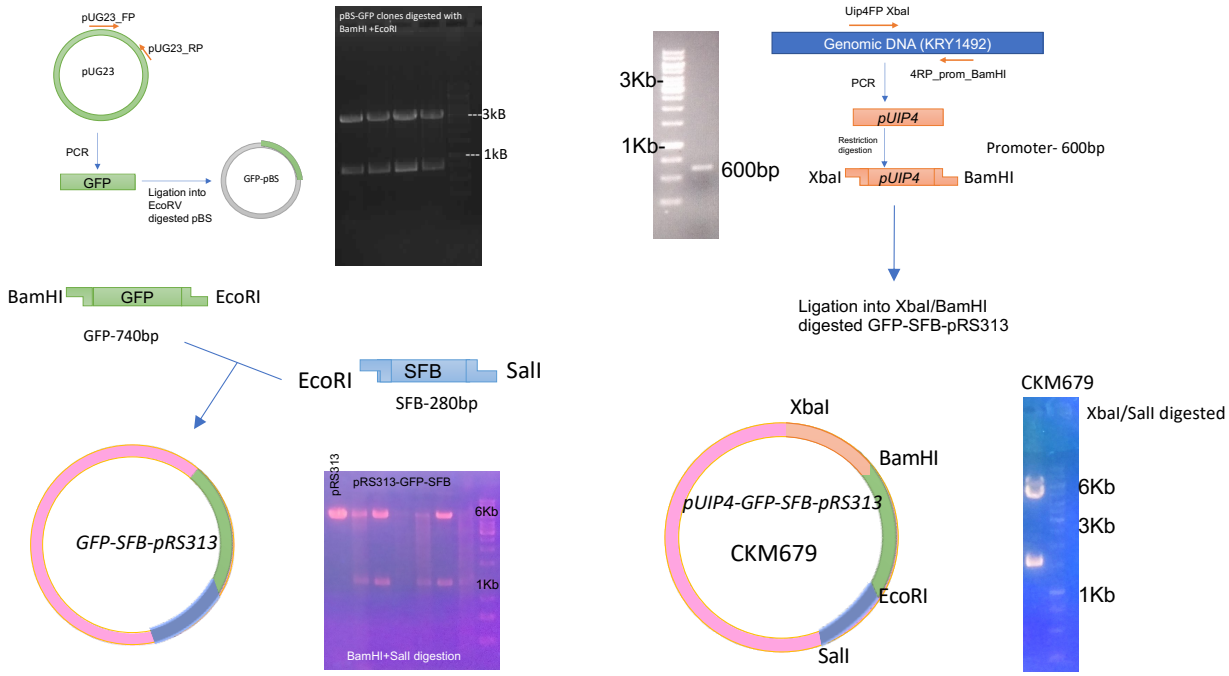

Generating *NUP157*-RITE (KRY 2035)

In order to study the dynamics of Nup157, RITE was employed. The GFP to RFP convertible tag was generated by homologous based recombination method of epitope tagging. The tag was amplified using pKV016 as template using the following primers:

Nup157RITE_F1
GATCCCGTTCAAGATTATGTGAAGGATCGTCATCATGGCCTGAAA *ggt gga tct ggt gga tct*

Nup157RITE_R3
GAAAACTTCACAATCAAACTGCTAAAATATACAAATAATTCCGT *TCA* ggcgccggtggagtggcg

The product was transformed into KRY1492 and the transformants were selected on YPD plate containing Hygromycin (25mg/100ml). Genomic DNA was isolated from the colonies obtained and the integration was confirmed by screening PCR. The following set of screening primers were used:

Nup157 screening:
Nup157 FP_S + YES RITE RP (internal from HYG^R) will give 1272 bp product only in colonies positive for tag.

Nup157FP_S + nup157RP_S(downstream of NUP157 STOP)
with tag: 4043 bp; without tag 346 bp

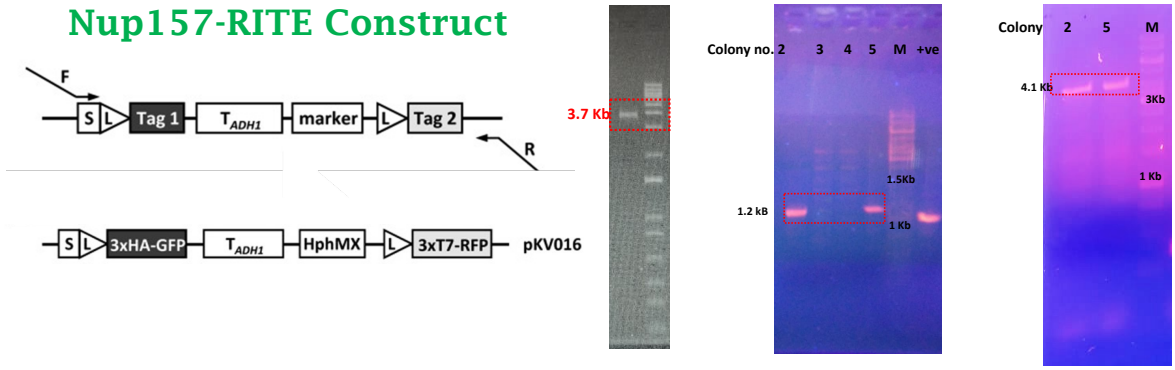

Generating *uip4Δ::KanMX*

Full length deletion knockout of UIP4 was carried out by employing homologous recombination-based strategy. The following primers were used for amplification of deletion cassette using pFA6a-KanMX as template:

UIP4_F1
CATACATACATACTTGGTTGTAACATTAAGATAGGCAAAGCAACTAAATA *CGGATCCCCGGGTTAATTAA*

UIP_R1
TAGTAGCTAAAAAAAGATGAATGTGAATCGAATCCTAAGAGAATTCAACA*GAATTCGAGCTCGTTTAAAC*

The PCR product was transformed in to the desired strain background and transformants were selected on YPD plate containing G418 (20mg/100ml). The deletion was confirmed by screening PCR using the following set of primers:

FP164SUIP4 Forward primer 164bp upstream of *UIP4* START
GCAGTGATGTTCCACCAATA

KanMX RP 552 bp downstream of KanMX start site Reverse primer
AGTCTGACCATCTCATCTGT

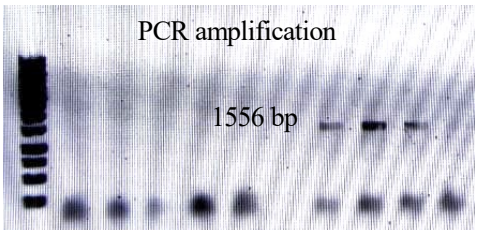

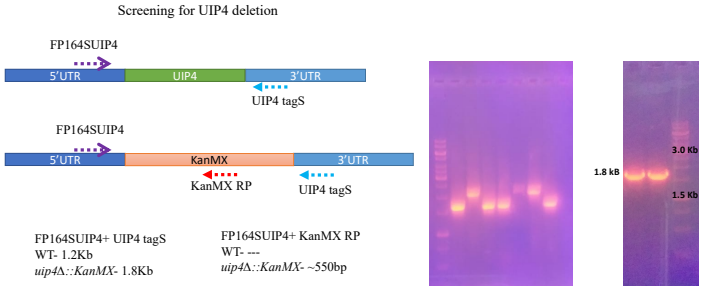

9.4 COMPLETE LIST OF PUBLICATIONS

Deolal, P., I. Jamir, and K. Mishra. 2022. Uip4p modulates nuclear pore complex function in *Saccharomyces cerevisiae*.
Doi: 10.1080/19491034.2022.2034286
In Press- Nucleus-Taylor and Francis

Deolal, P., and K. Mishra. 2022. An adaptable live-cell imaging protocol to analyze organelle morphology in Saccharomyces cerevisiae
doi: 10.1016/j.xpro.2022.101124
In Press- STAR Protocols

Deolal, P., and K. Mishra. 2021. Regulation of diverse nuclear shapes: pathways working independently, together. Commun. Integr. Biol. 14:158–175.
doi:10.1080/19420889.2021.1939942.

Deolal, P., G. Male, and K. Mishra. 2021. The challenge of staying in shape: nuclear size matters. Curr. Genet. 1–8.
doi:10.1007/s00294-021-01176-1.

Male, G., **P. Deolal,** N.K. Manda, S. Yagnik, A. Mazumder, and K. Mishra. 2020. Nucleolar size regulates nuclear envelope shape in *Saccharomyces cerevisiae*. J. Cell Sci.
doi:10.1242/jcs.242172.

REFERENCES

Abraham, N.M., and K. Mishra. 2018. Elevated dosage of Ulp1 disrupts telomeric silencing in Saccharomyces cerevisiae. *Mol. Biol. Rep.* 45:2481–2489. doi:10.1007/s11033-018-4415-1.

Abraham, N.M., K. Ramalingam, S. Murthy, and K. Mishra. 2019. Siz2 Prevents Ribosomal DNA Recombination by Modulating Levels of Tof2 in Saccharomyces cerevisiae. *mSphere*. 4. doi:10.1128/mSphere.00713-19.

Alcorta-Sevillano, N., I. Macías, C.I. Rodríguez, and A. Infante. 2020. Crucial Role of Lamin A/C in the Migration and Differentiation of MSCs in Bone. *Cells*. 9. doi:10.3390/cells9061330.

Alvarado-Kristensson, M., and C.A. Rosselló. 2019. The Biology of the Nuclear Envelope and Its Implications in Cancer Biology. *Int. J. Mol. Sci.* 20. doi:10.3390/IJMS20102586.

Andrulis, E.D., D.C. Zappulla, A. Ansari, S. Perrod, C. V. Laiosa, M.R. Gartenberg, and R. Sternglanz. 2002. Esc1, a nuclear periphery protein required for Sir4-based plasmid anchoring and partitioning. *Mol. Cell. Biol.* 22:8292–301. doi:10.1128/mcb.22.23.8292-8301.2002.

Antonin, W., C. Franz, U. Haselmann, C. Antony, and I.W. Mattaj. 2005. The integral membrane nucleoporin pom121 functionally links nuclear pore complex assembly and nuclear envelope formation. *Mol. Cell*. 17:83–92. doi:10.1016/j.molcel.2004.12.010.

Argüello-Miranda, O., Y. Liu, N.E. Wood, P. Kositangool, and A. Doncic. 2018. Integration of Multiple Metabolic Signals Determines Cell Fate Prior to Commitment. *Mol. Cell*. 71:733-744.e11. doi:10.1016/j.molcel.2018.07.041.

Arii, J., M. Watanabe, F. Maeda, N. Tokai-Nishizumi, T. Chihara, M. Miura, Y. Maruzuru, N. Koyanagi, A. Kato, and Y. Kawaguchi. 2018. ESCRT-III mediates budding across the inner nuclear membrane and regulates its integrity. *Nat. Commun.* 9:3379. doi:10.1038/s41467-018-05889-9.

Aufschnaiter, A., and S. Büttner. 2019. The vacuolar shapes of ageing: From function to morphology. *Biochim. Biophys. Acta - Mol. Cell Res.* 1866:957–970.

doi:10.1016/j.bbamcr.2019.02.011.

Baba, M., K. Takeshige, N. Baba, and Y. Ohsumi. 1994. Ultrastructural analysis of the autophagic process in yeast: detection of autophagosomes and their characterization. *J. Cell Biol.* 124:903–13. doi:10.1083/jcb.124.6.903.

Bahmanyar, S., and C. Schlieker. 2020. Lipid and protein dynamics that shape nuclear envelope identity. 31. American Society for Cell Biology.

Barzilai, S., S.K. Yadav, S. Morrell, F. Roncato, E. Klein, L. Stoler-Barak, O. Golani, S.W. Feigelson, A. Zemel, S. Nourshargh, and R. Alon. 2017. Leukocytes Breach Endothelial Barriers by Insertion of Nuclear Lobes and Disassembly of Endothelial Actin Filaments. *Cell Rep.* 18:685–699. doi:10.1016/j.celrep.2016.12.076.

Belgareh, N., and V. Doye. 1997. Dynamics of Nuclear Pore Distribution in Nucleoporin Mutant Yeast Cells. *J. Cell Biol.* 136:747–759. doi:10.1083/jcb.136.4.747.

Belgareh, N., G. Rabut, S.W. Baï, M. van Overbeek, J. Beaudouin, N. Daigle, O. V. Zatsepina, F. Pasteau, V. Labas, M. Fromont-Racine, J. Ellenberg, and V. Doye. 2001. An evolutionarily conserved NPC subcomplex, which redistributes in part to kinetochores in mammalian cells. *J. Cell Biol.* 154:1147–1160. doi:10.1083/jcb.200101081.

Bhargava, A., A. Williart, M. Maurin, M. Piel, X. Lahaye, N.M. Correspondence, P.M. Davidson, M. Jouve, and N. Manel. 2021. Inhibition of HIV infection by structural proteins of the inner nuclear membrane is associated with reduced chromatin dynamics. *Cell Rep.* 36. doi:10.1016/j.celrep.2021.109763.

Blofield, B.A., L. Short, H.J. Samour, D. Ball, and C.M. Hawkey. 1992. Phylogenetic and haematological implications of differences in the morphology of the heterophil nucleus in reptiles. *J. Zool.* doi:10.1111/j.1469-7998.1992.tb07497.x.

Bortle, K. Van, and V.G. Corces. 2012. Nuclear Organization and Genome Function. doi:10.1146/annurev-cellbio-101011-155824.

Brandt, A., F. Papagiannouli, N. Wagner, M. Wilsch-Bräuninger, M. Braun, E.E. Furlong, S. Loserth, C. Wenzl, F. Pilot, N. Vogt, T. Lecuit, G. Krohne, and J. Großhans. 2006.

Developmental control of nuclear size and shape by kugelkern and kurzkern. *Curr. Biol.* doi:10.1016/j.cub.2006.01.051.

Byers, B., and L. Goetsch. 1974. Duplication of Spindle Plaques and Integration of the Yeast Cell Cycle. *Cold Spring Harb. Symp. Quant. Biol.* 38:123–131. doi:10.1101/SQB.1974.038.01.016.

Cantwell, H., and G. Dey. 2021. Nuclear size and shape control. *Semin. Cell Dev. Biol.* doi:10.1016/j.semcdb.2021.10.013.

Capelson, M., and M.W. Hetzer. 2009. The role of nuclear pores in gene regulation, development and disease. *EMBO Rep.* 10:697–705. doi:10.1038/embor.2009.147.

Carlton, J.G., A. Caballe, M. Agromayor, M. Kloc, and J. Martin-Serrano. 2012. ESCRT-III Governs the Aurora B–Mediated Abscission Checkpoint Through CHMP4C. *Science (80-.).* 336:220–225. doi:10.1126/science.1217180.

Casey, A.K., S. Chen, P. Novick, S. Ferro-Novick, and S.R. Wente. 2015. Nuclear pore complex integrity requires Lnp1, a regulator of cortical endoplasmic reticulum. *Mol. Biol. Cell*. 26. doi:10.1091/mbc.E15-01-0053.

Castro-Garza, J., M.L. Luévano-Martínez, L. Villarreal-Treviño, J. Gosálvez, J.L. Fernández, M.I. Dávila-Rodríguez, C. García-Vielma, S. González-Hernández, and E.I. Cortés-Gutiérrez. 2018. Mycobacterium tuberculosis promotes genomic instability in macrophages. *Mem. Inst. Oswaldo Cruz*. doi:10.1590/0074-02760170281.

Chadrin, A., B. Hess, M. San Roman, X. Gatti, B. Lombard, D. Loew, Y. Barral, B. Palancade, and V. Doye. 2010. Pom33, a novel transmembrane nucleoporin required for proper nuclear pore complex distribution. *J. Cell Biol.* 189:795–811. doi:10.1083/jcb.200910043.

Chen, B., C. Co, and C.-C. Ho. 2015. Cell shape dependent regulation of nuclear morphology. *Biomaterials*. 67:129–36. doi:10.1016/j.biomaterials.2015.07.017.

Cheng, S., Y. Liu, C.S. Crowley, T.O. Yeates, and T.A. Bobik. 2008. Bacterial microcompartments: Their properties and paradoxes. *BioEssays*. 30:1084–1095. doi:10.1002/bies.20830.

Chien, C.T., P.L. Bartel, R. Sternglanz, and S. Fields. 1991. The two-hybrid system: a method to identify and clone genes for proteins that interact with a protein of interest. *Proc. Natl. Acad. Sci. U. S. A.* 88:9578–82.

Chopra, K., S. Bawaria, and R. Chauhan. 2019. Evolutionary divergence of the nuclear pore complex from fungi to metazoans. *Protein Sci.* 28:571–586. doi:10.1002/pro.3558.

Chytilova, E., J. Macas, and D.W. Galbraith. 1999. Green fluorescent protein targeted to the nucleus, a transgenic phenotype useful for studies in plant biology. *Ann. Bot.* doi:10.1006/anbo.1999.0866.

Clever, M., T. Funakoshi, Y. Mimura, M. Takagi, and N. Imamoto. 2012. The nucleoporin ELYS/Mel28 regulates nuclear envelope subdomain formation in HeLa cells. *Nucleus*. 3:187–199. doi:10.4161/nucl.19595.

Cohen, M., N. Feinstein, K.L. Wilson, and Y. Gruenbaum. 2003. Nuclear Pore Protein gp210 Is Essential for Viability in HeLa Cells and Caenorhabditis elegans. *Mol. Biol. Cell*. 14:4230–4237. doi:10.1091/mbc.e03-04-0260.

Cohen, S., A.M. Valm, and J. Lippincott-Schwartz. 2018. Interacting organelles. 53. Elsevier Current Trends.

Collings, D.A., C.N. Carter, J.C. Rink, A.C. Scott, S.E. Wyatt, and N. Strömgren Allen. 2000. Plant nuclei can contain extensive grooves and invaginations. *Plant Cell*. doi:10.1105/tpc.12.12.2425.

Colombi, P., B.M. Webster, F. Fröhlich, and C.P. Lusk. 2013. The transmission of nuclear pore complexes to daughter cells requires a cytoplasmic pool of Nsp1. *J. Cell Biol.* 203:215–32. doi:10.1083/jcb.201305115.

Conrad, M.N., C.-Y. Lee, J.L. Wilkerson, and M.E. Dresser. 2007. MPS3 mediates meiotic bouquet formation in Saccharomyces cerevisiae. *Proc. Natl. Acad. Sci.* 104:8863–8868. doi:10.1073/pnas.0606165104.

D'Angelo, M.A., M. Raices, S.H. Panowski, M.W. Hetzer, H. Aguilaniu, L. Gustafsson, M. Rigoulet, T. Nystrom, F. Alber, S. Dokudovskaya, L.M. Veenhoff, W. Zhang, J. Kipper, D. Devos, A. Suprapto, O. Karni-Schmidt, R. Williams, B.T. Chait, et al., W. Antonin,

C. Franz, U. Haselmann, C. Antony, I.W. Mattaj, M.J. Beanan, S. Strome, M. Beck, F. Forster, M. Ecke, J.M. Plitzko, F. Melchior, G. Gerisch, W. Baumeister, O. Medalia, B. Burke, J. Ellenberg, B. Chakravarti, D.N. Chakravarti, S.L. Commerford, A.L. Carsten, E.P. Cronkite, S.L. Crittenden, K.A. Leonhard, D.T. Byrd, J. Kimble, M.A. D'Angelo, M.W. Hetzer, M.A. D'Angelo, D.J. Anderson, E. Richard, M.W. Hetzer, N. Daigle, J. Beaudouin, L. Hartnell, G. Imreh, E. Hallberg, J. Lippincott-Schwartz, J. Ellenberg, I. Dalle-Donne, G. Aldini, M. Carini, R. Colombo, R. Rossi, A. Milzani, S.R. Danielson, J.K. Andersen, L.I. Davis, G. Blobel, A. Dillin, D.K. Crawford, C. Kenyon, P. Frosst, T. Guan, C. Subauste, K. Hahn, L. Gerace, V. Galy, I.W. Mattaj, P. Askjaer, P. Grandi, T. Dang, N. Pane, A. Shevchenko, M. Mann, D. Forbes, E. Hurt, E. Haithcock, Y. Dayani, E. Neufeld, A.J. Zahand, N. Feinstein, A. Mattout, Y. Gruenbaum, J. Liu, A. Harel, A.V. Orjalo, T. Vincent, A. Lachish-Zalait, et al. 2009. Age-Dependent Deterioration of Nuclear Pore Complexes Causes a Loss of Nuclear Integrity in Postmitotic Cells. *Cell*. 136:284–295. doi:10.1016/j.cell.2008.11.037.

Daigle, N., J. Beaudouin, L. Hartnell, G. Imreh, E. Hallberg, J. Lippincott-Schwartz, and J. Ellenberg. 2001. Nuclear pore complexes form immobile networks and have a very low turnover in live mammalian cells. *J. Cell Biol.* 154:71–84. doi:10.1083/jcb.200101089.

Dakik, P., and V.I. Titorenko. 2016. Communications between Mitochondria, the Nucleus, Vacuoles, Peroxisomes, the Endoplasmic Reticulum, the Plasma Membrane, Lipid Droplets, and the Cytosol during Yeast Chronological Aging. *Front. Genet.* 7:177. doi:10.3389/fgene.2016.00177.

Daniel Gietz, R., and R.A. Woods. 2002. Transformation of yeast by lithium acetate/single-stranded carrier DNA/polyethylene glycol method. *Methods Enzymol.* 350:87–96. doi:10.1016/S0076-6879(02)50957-5.

Dawson, T.R., M.D. Lazarus, M.W. Hetzer, and S.R. Wente. 2009. ER membrane-bending proteins are necessary for de novo nuclear pore formation. *J. Cell Biol.* 184:659–75. doi:10.1083/jcb.200806174.

Dechat, T., S.A. Adam, P. Taimen, T. Shimi, and R.D. Goldman. 2010. Nuclear lamins. *Cold Spring Harb. Perspect. Biol.* 2:a000547. doi:10.1101/cshperspect.a000547.

Deolal, P., and K. Mishra. 2021. Regulation of diverse nuclear shapes : pathways working

independently , together. *Commun. Integr. Biol.* 14:158–175. doi:10.1080/19420889.2021.1939942.

Dittmer, T., and T. Misteli. 2011. The lamin protein family. *Genome Biol.* doi:10.1186/gb-2011-12-5-222.

Dittmer, T.A., N.J. Stacey, K. Sugimoto-Shirasu, and E.J. Richards. 2007. LITTLE NUCLEI genes affecting nuclear morphology in Arabidopsis thaliana. *Plant Cell*. 19:2793–2803. doi:10.1105/tpc.107.053231.

Donahue, D.A., S. Amraoui, F. di Nunzio, C. Kieffer, F. Porrot, S. Opp, F. Diaz-Griffero, N. Casartelli, and O. Schwartz. 2016. SUN2 Overexpression Deforms Nuclear Shape and Inhibits HIV. *J. Virol.* doi:10.1128/jvi.03202-15.

Doucet, C.M., J.A. Talamas, M.W. Hetzer, F. Alber, S. Dokudovskaya, L.M. Veenhoff, W. Zhang, J. Kipper, D. Devos, A. Suprapto, O. Karni-Schmidt, R. Williams, B.T. Chait, et al., D.J. Anderson, M.W. Hetzer, D.J. Anderson, M.W. Hetzer, D.J. Anderson, M.W. Hetzer, D.J. Anderson, J.D. Vargas, J.P. Hsiao, M.W. Hetzer, W. Antonin, W. Antonin, J. Ellenberg, E. Dultz, W. Antonin, C. Franz, U. Haselmann, C. Antony, I.W. Mattaj, B. Antonny, M. Beck, F. Forster, M. Ecke, J.M. Plitzko, F. Melchior, G. Gerisch, W. Baumeister, O. Medalia, N. Belgareh, G. Rabut, S.W. Bai, M. van Overbeek, J. Beaudouin, N. Daigle, O.V. Zatsepina, F. Pasteau, V. Labas, M. Fromont-Racine, et al., I.C. Berke, T. Boehmer, G. Blobel, T.U. Schwartz, T. Boehmer, S. Jeudy, I.C. Berke, T.U. Schwartz, S.G. Brohawn, N.C. Leksa, E.D. Spear, K.R. Rajashankar, T.U. Schwartz, S.G. Brohawn, J.R. Partridge, J.R. Whittle, T.U. Schwartz, H.J. Chial, M.P. Rout, T.H. Giddings, M. Winey, J.M. Cronshaw, A.N. Krutchinsky, W. Zhang, B.T. Chait, M.J. Matunis, M.A. D'Angelo, D.J. Anderson, E. Richard, M.W. Hetzer, M.A. D'Angelo, M. Raices, S.H. Panowski, M.W. Hetzer, L.I. Davis, G. Blobel, T.R. Dawson, M.D. Lazarus, M.W. Hetzer, S.R. Wente, J.O. De Craene, J. Coleman, P.E. de Martin, M. Pypaert, S. Anderson, et al. 2010. Cell cycle-dependent differences in nuclear pore complex assembly in metazoa. *Cell*. 141:1030–41. doi:10.1016/j.cell.2010.04.036.

Durchschlag, E., W. Reiter, G. Ammerer, and C. Schüller. 2004. Nuclear Localization Destabilizes the Stress-regulated Transcription Factor Msn2 * ♦. *J. Biol. Chem.* 279:55425–55432. doi:10.1074/JBC.M407264200.

Eiyama, A., N. Kondo-Okamoto, and K. Okamoto. 2013. Mitochondrial degradation during starvation is selective and temporally distinct from bulk autophagy in yeast. *FEBS Lett.* 587:1787–1792. doi:10.1016/J.FEBSLET.2013.04.030.

Fernandez-Martinez, J., and M.P. Rout. 2009. Nuclear pore complex biogenesis. *Curr. Opin. Cell Biol.* 21:603–12. doi:10.1016/j.ceb.2009.05.001.

Fields, S., and O. Song. 1989. A novel genetic system to detect protein–protein interactions. *Nature*. 340:245–246. doi:10.1038/340245a0.

Filesi, I., F. Gullotta, G. Lattanzi, M.R. D'Apice, C. Capanni, A.M. Nardone, M. Columbaro, G. Scarano, E. Mattioli, P. Sabatelli, N.M. Maraldi, S. Biocca, and G. Novelli. 2005. Alterations of nuclear envelope and chromatin organization in mandibuloacral dysplasia, a rare form of laminopathy. *Physiol. Genomics*. doi:10.1152/physiolgenomics.00060.2005.

Fracchia, A., T. Asraf, M. Salmon-Divon, and G. Gerlitz. 2020. Increased Lamin B1 Levels Promote Cell Migration by Altering Perinuclear Actin Organization. *Cells*. doi:10.3390/cells9102161.

Franz, C., R. Walczak, S. Yavuz, R. Santarella, M. Gentzel, P. Askjaer, V. Galy, M. Hetzer, I.W. Mattaj, and W. Antonin. 2007. MEL-28/ELYS is required for the recruitment of nucleoporins to chromatin and postmitotic nuclear pore complex assembly. *EMBO Rep.* 8:165–172. doi:10.1038/sj.embor.7400889.

Frost, A., M.G. Elgort, O. Brandman, C. Ives, S.R. Collins, L. Miller-Vedam, J. Weibezahn, M.Y. Hein, I. Poser, M. Mann, A.A. Hyman, and J.S. Weissman. 2012. Functional repurposing revealed by comparing S. pombe and S. cerevisiae genetic interactions. *Cell*. 149:1339–52. doi:10.1016/j.cell.2012.04.028.

Galdieri, L., S. Mehrotra, S. Yu, and A. Vancura. 2010. Transcriptional Regulation in Yeast during Diauxic Shift and Stationary Phase. *Omi. A J. Integr. Biol.* 14:629–638. doi:10.1089/omi.2010.0069.

Garapati, H.S., and K. Mishra. 2018. Comparative genomics of nuclear envelope proteins. *BMC Genomics*. 19:823. doi:10.1186/s12864-018-5218-4.

Gardner, J.M., and S.L. Jaspersen. 2014. Manipulating the Yeast Genome: Deletion, Mutation, and Tagging by PCR. *In* Methods in molecular biology (Clifton, N.J.). Humana Press, New York, NY. 45–78.

Gasch, A.P., P.T. Spellman, C.M. Kao, O. Carmel-Harel, M.B. Eisen, G. Storz, D. Botstein, and P.O. Brown. 2000. Genomic Expression Programs in the Response of Yeast Cells to Environmental Changes. *Mol. Biol. Cell*. 11:4241–4257. doi:10.1091/mbc.11.12.4241.

Goldman, R.D., D.K. Shumaker, M.R. Erdos, M. Eriksson, A.E. Goldman, L.B. Gordon, Y. Gruenbaum, S. Khuon, M. Mendez, R. Varga, and F.S. Collins. 2004. Accumulation of mutant lamin A progressive changes in nuclear architecture in Hutchinson-Gilford progeria syndrome. *Proc. Natl. Acad. Sci. U. S. A.* doi:10.1073/pnas.0402943101.

Gonzalez, Y., K. Meerbrey, J. Chong, Y. Torii, N.N. Padte, and S. Sazer. 2009. Nuclear shape, growth and integrity in the closed mitosis of fission yeast depend on the Ran-GTPase system, the spindle pole body and the endoplasmic reticulum. *J. Cell Sci.* doi:10.1242/jcs.049999.

Gonzalez, Y., A. Saito, and S. Sazer. 2012. Fission yeast Lem2 and Man1 perform fundamental functions of the animal cell nuclear lamina. *Nucleus*. doi:10.4161/nucl.18824.

Gray, J. V., G.A. Petsko, G.C. Johnston, D. Ringe, R.A. Singer, and M. Werner-Washburne. 2004. “Sleeping Beauty”: Quiescence in Saccharomyces cerevisiae. *Microbiol. Mol. Biol. Rev.* 68:187–206. doi:10.1128/MMBR.68.2.187-206.2004.

Gu, M., D. LaJoie, O.S. Chen, A. von Appen, M.S. Ladinsky, M.J. Redd, L. Nikolova, P.J. Bjorkman, W.I. Sundquist, K.S. Ullman, and A. Frost. 2017. LEM2 recruits CHMP7 for ESCRT-mediated nuclear envelope closure in fission yeast and human cells. *Proc. Natl. Acad. Sci.* 114:E2166–E2175. doi:10.1073/pnas.1613916114.

Gu, N.-H., W.-L. Zhao, G.-S. Wang, and F. Sun. 2019. Comparative analysis of mammalian sperm ultrastructure reveals relationships between sperm morphology, mitochondrial functions and motility. *Reprod. Biol. Endocrinol.* 17:66. doi:10.1186/s12958-019-0510-y.

Guerreiro, I., and J. Kind. 2019. Spatial chromatin organization and gene regulation at the

nuclear lamina. *Curr. Opin. Genet. Dev.* 55:19–25. doi:10.1016/j.gde.2019.04.008.

Hahn, S., and E.T. Young. 2011. Transcriptional Regulation in Saccharomyces cerevisiae : Transcription Factor Regulation and Function, Mechanisms of Initiation, and Roles of Activators and Coactivators. *Genetics*. 189:705–736. doi:10.1534/genetics.111.127019.

Hattier, T., E.D. Andrulis, and A.M. Tartakoff. 2007. Immobility, inheritance and plasticity of shape of the yeast nucleus. *BMC Cell Biol.* 8:47. doi:10.1186/1471-2121-8-47.

Hawryluk-Gara, L.A., E.K. Shibuya, and R.W. Wozniak. 2005. Vertebrate Nup53 Interacts with the Nuclear Lamina and Is Required for the Assembly of a Nup93-containing Complex. *Mol. Biol. Cell*. 16:2382–2394. doi:10.1091/mbc.e04-10-0857.

Hell, S.W., and J. Wichmann. 1994. Breaking the diffraction resolution limit by stimulated emission: stimulated-emission-depletion fluorescence microscopy. *Opt. Lett.* 19:780. doi:10.1364/OL.19.000780.

Helle, S.C.J., G. Kanfer, K. Kolar, A. Lang, A.H. Michel, and B. Kornmann. 2013. Organization and function of membrane contact sites. *Biochim. Biophys. Acta*. 1833:2526–41. doi:10.1016/j.bbamcr.2013.01.028.

Hobson, C.M., M. Kern, E.T. O'Brien, A.D. Stephens, M.R. Falvo, and R. Superfine. 2020. Correlating nuclear morphology and external force with combined atomic force microscopy and light sheet imaging separates roles of chromatin and lamin A/C in nuclear mechanics. *Mol. Biol. Cell*. 31:1788–1801. doi:10.1091/mbc.E20-01-0073.

Hönscher, C., M. Mari, K. Auffarth, M. Bohnert, J. Griffith, W. Geerts, M. van der Laan, M. Cabrera, F. Reggiori, and C. Ungermann. 2014. Cellular Metabolism Regulates Contact Sites between Vacuoles and Mitochondria. 30. 86–94 pp.

Howell, J.J., and B.D. Manning. 2011. mTOR couples cellular nutrient sensing to organismal metabolic homeostasis. *Trends Endocrinol. Metab.* 22:94–102. doi:10.1016/j.tem.2010.12.003.

Jalihal, A.P., P. Kraikivski, T.M. Murali, and J.J. Tyson. 2021. Modeling and analysis of the macronutrient signaling network in budding yeast. *Mol. Biol. Cell*. 32. doi:10.1091/mbc.E20-02-0117.

James, P., J. Halladay, and E.A. Craig. 1996. Genomic Libraries and a Host Strain Designed for Highly Efficient Two-Hybrid Selection in Yeast. *Genetics*. 144:1425–1436. doi:10.1093/genetics/144.4.1425.

Janin, A., D. Bauer, F. Ratti, G. Millat, and A. Méjat. 2017. Nuclear envelopathies: a complex LINC between nuclear envelope and pathology. *Orphanet J. Rare Dis.* 12:147. doi:10.1186/s13023-017-0698-x.

Jaspersen, S.L., and M. Winey. 2004. THE BUDDING YEAST SPINDLE POLE BODY: Structure, Duplication, and Function. *Annu. Rev. Cell Dev. Biol.* 20:1–28. doi:10.1146/annurev.cellbio.20.022003.114106.

John J. Scarcelli, 1, 1 Christine A. Hodge, 2 and Charles N. Cole1, J.J. Scarcelli, C.A. Hodge, and C.N. Cole. 2007. The yeast integral membrane protein Apq12 potentially links membrane dynamics to assembly of nuclear pore complexes. *J. Cell Biol.* 178:799–812. doi:10.1083/jcb.200702120.

Kabachinski, G., and T.U. Schwartz. 2015. The nuclear pore complex - structure and function at a glance. *J. Cell Sci.* 128:423–429. doi:10.1242/jcs.083246.

Katta, S.S., C.J. Smoyer, and S.L. Jaspersen. 2014. Destination: inner nuclear membrane. *Trends Cell Biol.* 24:221–229. doi:10.1016/j.tcb.2013.10.006.

Ketelaar, T., C. Faivre-Moskalenko, J.J. Esseling, N.C.A. de Ruijter, C.S. Grierson, M. Dogterom, and A.M.C. Emons. 2002. Positioning of Nuclei in Arabidopsis Root Hairs. *Plant Cell*. 14:2941–2955. doi:10.1105/tpc.005892.

Kim, S.J., J. Fernandez-Martinez, P. Sampathkumar, A. Martel, T. Matsui, H. Tsuruta, T.M. Weiss, Y. Shi, A. Markina-Inarrairaegui, J.B. Bonanno, J.M. Sauder, S.K. Burley, B.T. Chait, S.C. Almo, M.P. Rout, and A. Sali. 2014. Integrative structure-function mapping of the nucleoporin Nup133 suggests a conserved mechanism for membrane anchoring of the nuclear pore complex. *Mol. Cell. Proteomics*. 13:2911–26. doi:10.1074/mcp.M114.040915.

Knockenhauer, K.E.K.E.E., T.U.T.U.U. Schwartz, C. Ader, S. Frey, W. Maas, H.B. Schmidt, D. Görlich, M. Baldus, F. Alber, S. Dokudovskaya, L.M. Veenhoff, W. Zhang, J. Kipper, D.P. Devos, A. Suprapto, O. Karni-Schmidt, R. Williams, B.T. Chait, et al.,

N.P. Allen, L. Huang, A. Burlingame, M.F. Rexach, T.D. Allen, J.M. Cronshaw, S. Bagley, E. Kiseleva, M.W. Goldberg, S. Amlacher, P. Sarges, D. Flemming, V. van Noort, R. Kunze, D.P. Devos, M. Arumugam, P. Bork, E.C. Hurt, K.R. Andersen, E. Onischenko, J.H. Tang, P. Kumar, J.Z. Chen, A. Ulrich, J.T. Liphardt, K. Weis, T.U.T.U.U. Schwartz, H. Asakawa, H.-J. Yang, T.G. Yamamoto, C. Ohtsuki, Y. Chikashige, K. Sakata-Sogawa, M. Tokunaga, M. Iwamoto, Y. Hiraoka, T. Haraguchi, N. Belgareh, G. Rabut, S.W. Baï, M. Van Overbeek, J. Beaudouin, N. Daigle, O.V. Zatsepina, F. Pasteau, V. Labas, M. Fromont-Racine, et al., I.C. Berke, T. Boehmer, G. Blobel, T.U.T.U.U. Schwartz, A. Bestembayeva, A. Kramer, A.A. Labokha, D. Osmanović, I. Liashkovich, E.V. Orlova, I.J. Ford, G. Charras, A. Fassati, B.W. Hoogenboom, S. Bilokapic, T.U.T.U.U. Schwartz, S. Bilokapic, T.U.T.U.U. Schwartz, A. Boni, A.Z. Politi, P. Strnad, W. Xiang, M.J. Hossain, J. Ellenberg, S.G. Brohawn, N.C. Leksa, E.D. Spear, K.R. Rajashankar, T.U.T.U.U. Schwartz, S.G. Brohawn, J.R. Partridge, et al. 2016. The Nuclear Pore Complex as a Flexible and Dynamic Gate. *Cell*. 164:1162–1171. doi:10.1016/j.cell.2016.01.034.

Koch, B.A., E. Staley, H. Jin, and H.G. Yu. 2020. The ESCRT-III complex is required for nuclear pore complex sequestration and regulates gamete replicative lifespan in budding yeast meiosis. *Nucleus*. 11:219–236. doi:10.1080/19491034.2020.1812872.

Kohler, V., and S. Büttner. 2021. Remodelling of Nucleus-Vacuole Junctions During Metabolic and Proteostatic Stress. *Contact*. 4:25152564211016610. doi:10.1177/25152564211016608.

Krull, S., J. Thyberg, B. Björkroth, H.-R. Rackwitz, and V.C. Cordes. 2004. Nucleoporins as Components of the Nuclear Pore Complex Core Structure and Tpr as the Architectural Element of the Nuclear Basket. *Mol. Biol. Cell*. 15:4261–4277. doi:10.1091/mbc.e04-03-0165.

Kumanski, S., B. Viart, S. Kossida, and M. Moriel-Carretero. 2021. Lipid Droplets Are a Physiological Nucleoporin Reservoir. *Cells*. 10:472. doi:10.3390/cells10020472.

Kumar, K., R. Moirangthem, and R. Kaur. 2020. Histone H4 dosage modulates DNA damage response in the pathogenic yeast Candida glabrata via homologous recombination pathway. *PLOS Genet.* 16:e1008620. doi:10.1371/journal.pgen.1008620.

Kwiatek, J.M., G.-S.S. Han, and G.M. Carman. 2020. Phosphatidate-mediated regulation of lipid synthesis at the nuclear/endoplasmic reticulum membrane. 1865.

Lahaye, X., T. Satoh, M. Gentili, S. Cerboni, A. Silvin, C. Conrad, A. Ahmed-Belkacem, E.C. Rodriguez, J.-F. Guichou, N. Bosquet, M. Piel, R. Le Grand, M.C. King, J.-M. Pawlotsky, and N. Manel. 2016. Nuclear Envelope Protein SUN2 Promotes Cyclophilin-A-Dependent Steps of HIV Replication. *Cell Rep.* 15:879–892. doi:10.1016/j.celrep.2016.03.074.

Lattanzi, G., S. Benedetti, M.R. D'Apice, L. Maggi, N. Carboni, E. Scarano, and L. Politano. 2016. Emerging perspectives on laminopathies. *Cell Health Cytoskelet.* doi:10.2147/CHC.S59507.

Leitch, A.R. 2000. Higher Levels of Organization in the Interphase Nucleus of Cycling and Differentiated Cells. *Microbiol. Mol. Biol. Rev.* doi:10.1128/mmbr.64.1.138-152.2000.

Liesche, J., M. Marek, and T. GÃ¼nther-Pomorski. 2015. Cell wall staining with Trypan blue enables quantitative analysis of morphological changes in yeast cells. *Front. Microbiol.* 6. doi:10.3389/fmicb.2015.00107.

Liu, Q., N. Pante, T. Misteli, M. Elsagga, M. Crisp, D. Hodzic, B. Burke, and K.J. Roux. 2007. Functional association of Sun1 with nuclear pore complexes. *J. Cell Biol.* 178:785–798. doi:10.1083/jcb.200704108.

Lone, M.A., A.E. Atkinson, C.A. Hodge, S. Cottier, F. Martínez-Montañés, S. Maithel, L. Mène-Saffrané, C.N. Cole, and R. Schneiter. 2015. Yeast Integral Membrane Proteins Apq12, Brl1, and Brr6 Form a Complex Important for Regulation of Membrane Homeostasis and Nuclear Pore Complex Biogenesis. *Eukaryot. Cell*. 14:1217–27. doi:10.1128/EC.00101-15.

Longtine, M.S., A. Mckenzie III, D.J. Demarini, N.G. Shah, A. Wach, A. Brachat, P. Philippsen, and J.R. Pringle. 1998. Additional modules for versatile and economical PCR-based gene deletion and modification in Saccharomyces cerevisiae. *Yeast*. 14:953–961. doi:10.1002/(SICI)1097-0061(199807)14:10<953::AID-YEA293>3.0.CO;2-U.

Lord, C.L., B.L. Timney, M.P. Rout, and S.R. Wente. 2015. Altering nuclear pore complex function impacts longevity and mitochondrial function in S. cerevisiae. *J. Cell Biol.*

208:729–44. doi:10.1083/jcb.201412024.

Lord, C.L., and S.R. Wente. 2020. Nuclear envelope–vacuole contacts mitigate nuclear pore complex assembly stress. *J. Cell Biol.* 219. doi:10.1083/jcb.202001165.

Lussi, Y.C., I. Hügi, E. Laurell, U. Kutay, and B. Fahrenkrog. 2011. The nucleoporin Nup88 is interacting with nuclear lamin A. *Mol. Biol. Cell*. 22:1080–1090. doi:10.1091/mbc.e10-05-0463.

Maeshima, K., H. Iino, S. Hihara, T. Funakoshi, A. Watanabe, M. Nishimura, R. Nakatomi, K. Yahata, F. Imamoto, T. Hashikawa, H. Yokota, and N. Imamoto. 2010. Nuclear pore formation but not nuclear growth is governed by cyclin-dependent kinases (Cdks) during interphase. *Nat. Struct. Mol. Biol.* 17:1065–1071. doi:10.1038/nsmb.1878.

Maeshima, K., H. Iino, S. Hihara, and N. Imamoto. 2011. Nuclear size, nuclear pore number and cell cycle. *Nucleus*. 2:113–118. doi:10.4161/nucl.2.2.15446.

Maeshima, K., K. Yahata, Y. Sasaki, R. Nakatomi, T. Tachibana, T. Hashikawa, F. Imamoto, and N. Imamoto. 2006. Cell-cycle-dependent dynamics of nuclear pores: pore-free islands and lamins. *J. Cell Sci.* 119:4442–4451. doi:10.1242/jcs.03207.

De Magistris, P., and W. Antonin. 2018. The Dynamic Nature of the Nuclear Envelope. *Curr. Biol.* 28:R487–R497. doi:10.1016/j.cub.2018.01.073.

Makhija, E., D.S. Jokhun, and G. V. Shivashankar. 2016. Nuclear deformability and telomere dynamics are regulated by cell geometric constraints. *Proc. Natl. Acad. Sci. U. S. A.* doi:10.1073/pnas.1513189113.

Makio, T., D.L. Lapetina, and R.W. Wozniak. 2013. Inheritance of yeast nuclear pore complexes requires the Nsp1p subcomplex. *J. Cell Biol.* 203:187–96. doi:10.1083/jcb.201304047.

Makio, T., L.H. Stanton, C.-C. Lin, D.S. Goldfarb, K. Weis, and R.W. Wozniak. 2009. The nucleoporins Nup170p and Nup157p are essential for nuclear pore complex assembly. *J. Cell Biol.* 185:459–73. doi:10.1083/jcb.200810029.

Male, G., P. Deolal, N.K. Manda, S. Yagnik, A. Mazumder, and K. Mishra. 2020. Nucleolar size regulates nuclear envelope shape in Saccharomyces cerevisiae. *J. Cell Sci.*

doi:10.1242/jcs.242172.

Manley, H.R., M.C. Keightley, and G.J. Lieschke. 2018. The Neutrophil Nucleus: An Important Influence on Neutrophil Migration and Function. *Front. Immunol.* 9. doi:10.3389/fimmu.2018.02867.

Mansfeld, J., S. Güttinger, L.A. Hawryluk-Gara, N. Panté, M. Mall, V. Galy, U. Haselmann, P. Mühlhäusser, R.W. Wozniak, I.W. Mattaj, U. Kutay, and W. Antonin. 2006. The Conserved Transmembrane Nucleoporin NDC1 Is Required for Nuclear Pore Complex Assembly in Vertebrate Cells. *Mol. Cell*. 22:93–103. doi:10.1016/j.molcel.2006.02.015.

Marchler-Bauer, A., S. Lu, J.B. Anderson, F. Chitsaz, M.K. Derbyshire, C. DeWeese-Scott, J.H. Fong, L.Y. Geer, R.C. Geer, N.R. Gonzales, M. Gwadz, D.I. Hurwitz, J.D. Jackson, Z. Ke, C.J. Lanczycki, F. Lu, G.H. Marchler, M. Mullokandov, M. V. Omelchenko, C.L. Robertson, J.S. Song, N. Thanki, R.A. Yamashita, D. Zhang, N. Zhang, C. Zheng, and S.H. Bryant. 2011. CDD: a Conserved Domain Database for the functional annotation of proteins. *Nucleic Acids Res.* 39:D225–D229. doi:10.1093/nar/gkq1189.

Marelli, M., C.P. Lusk, H. Chan, J.D. Aitchison, and R.W. Wozniak. 2001. A link between the synthesis of nucleoporins and the biogenesis of the nuclear envelope. *J. Cell Biol.* 153:709–24. doi:10.1083/jcb.153.4.709.

Martínez-Pastor, M.T., G. Marchler, C. Schüller, A. Marchler-Bauer, H. Ruis, and F. Estruch. 1996. The Saccharomyces cerevisiae zinc finger proteins Msn2p and Msn4p are required for transcriptional induction through the stress response element (STRE). *EMBO J.* 15:2227–35. doi:http://www.ncbi.nlm.nih.gov/pmc/articles/pmc450147/.

Martins, F., J. Sousa, C.D. Pereira, O.A.B. da Cruz e Silva, and S. Rebelo. 2020. Nuclear envelope dysfunction and its contribution to the aging process. *Aging Cell*. 19:1–17. doi:10.1111/acel.13143.

Matsuoka, M. 2005. Human T-cell leukemia virus type I (HTLV-I) infection and the onset of adult T-cell leukemia (ATL). *Retrovirology*. doi:10.1186/1742-4690-2-27.

Medvedik, O., D.W. Lamming, K.D. Kim, and D.A. Sinclair. 2007. MSN2 and MSN4 Link Calorie Restriction and TOR to Sirtuin-Mediated Lifespan Extension in Saccharomyces cerevisiae. *PLoS Biol.* 5:e261. doi:10.1371/journal.pbio.0050261.

Meier, I., A.H. Griffis, N.R. Groves, and A. Wagner. 2016. Regulation of nuclear shape and size in plants. *Curr. Opin. Cell Biol.* 40:114–123. doi:10.1016/j.ceb.2016.03.005.

Mekhail, K., and D. Moazed. 2010. The nuclear envelope in genome organization, expression and stability. *Nat. Rev. cell Biol.* 11:317–328. doi:10.1038/nrm2894.

Méndez-lópez, I., and H.J. Worman. 2012. Inner nuclear membrane proteins : impact on human disease. 153–167. doi:10.1007/s00412-012-0360-2.

MESEROLL, R.A., and O. Cohen-Fix. 2016. The Malleable Nature of the Budding Yeast Nuclear Envelope: Flares, Fusion, and Fenestrations. *J. Cell. Physiol.* 231:2353–2360. doi:10.1002/jcp.25355.

Mészáros, N., J. Cibulka, M.J. Mendiburo, A. Romanauska, M. Schneider, and A. Köhler. 2015. Nuclear Pore Basket Proteins Are Tethered to the Nuclear Envelope and Can Regulate Membrane Curvature. *Dev. Cell*. doi:10.1016/j.devcel.2015.02.017.

Miller, C. 1998. Assessment of aryl hydrocarbon receptor complex interactions using pBEVY plasmids: expressionvectors with bi-directional promoters for use in Saccharomyces cerevisiae. *Nucleic Acids Res.* 26:3577–3583. doi:10.1093/nar/26.15.3577.

Miller, D.L., E.L. Styer, S.J. Decker, and T. Robeck. 2002. Ultrastructure of the spermatozoa from three odontocetes: a killer whale (Orcinus orca), a Pacific white-sided dolphin (Lagenorhynchus obliquidens) and a beluga (Delphinapterus leucas). *Anat. Histol. Embryol.* 31:158–68. doi:10.1046/j.1439-0264.2002.00385.x.

Monteiro, P.T., J. Oliveira, P. Pais, M. Antunes, M. Palma, M. Cavalheiro, M. Galocha, C.P. Godinho, L.C. Martins, N. Bourbon, M.N. Mota, R.A. Ribeiro, R. Viana, I. Sá-Correia, and M.C. Teixeira. 2020. YEASTRACT+: a portal for cross-species comparative genomics of transcription regulation in yeasts. *Nucleic Acids Res.* 48:D642–D649. doi:10.1093/nar/gkz859.

Müller, M., O. Schmidt, M. Angelova, K. Faserl, S. Weys, L. Kremser, T. Pfaffenwimmer, T. Dalik, C. Kraft, Z. Trajanoski, H. Lindner, and D. Teis. 2015. The coordinated action of the MVB pathway and autophagy ensures cell survival during starvation. *Elife*. 4:e07736. doi:10.7554/ELIFE.07736.

De Noronha, C.M.C., M.P. Sherman, H.W. Lin, M. V. Cavrois, R.D. Moir, R.D. Goldman, and W.C. Greene. 2001. Dynamic disruptions in nuclear envelope architecture and integrity induced by HIV-1 Vpr. *Science (80-.).* doi:10.1126/science.1063957.

Olmos, Y., L. Hodgson, J. Mantell, P. Verkade, and J.G. Carlton. 2015. ESCRT-III controls nuclear envelope reformation. *Nature*. 522:236–239. doi:10.1038/nature14503.

Otsuka, S., and J. Ellenberg. 2018. Mechanisms of nuclear pore complex assembly – two different ways of building one molecular machine. *FEBS Lett.* 592:475–488. doi:10.1002/1873-3468.12905.

Patel, A., H.O. Lee, L. Jawerth, S. Maharana, M. Jahnel, M.Y. Hein, S. Stoynov, J. Mahamid, S. Saha, T.M. Franzmann, A. Pozniakovski, I. Poser, N. Maghelli, L.A. Royer, M. Weigert, E.W. Myers, S. Grill, D. Drechsel, A.A. Hyman, and S. Alberti. 2015. A Liquid-to-Solid Phase Transition of the ALS Protein FUS Accelerated by Disease Mutation. *Cell*. 162:1066–1077. doi:10.1016/j.cell.2015.07.047.

Pedruzzi, I. 2000. Saccharomyces cerevisiae Ras/cAMP pathway controls post-diauxic shift element-dependent transcription through the zinc finger protein Gis1. *EMBO J.* 19:2569–2579. doi:10.1093/emboj/19.11.2569.

Perez-Samper, G., B. Cerulus, A. Jariani, L. Vermeersch, N.B. Simancas, M.M.M. Bisschops, J. Van Den Brink, D. Solis-Escalante, B. Gallone, D. De Maeyer, E. Van Bael, T. Wenseleers, J. Michiels, K. Marchal, P. Daran-Lapujade, and K.J. Verstrepen. 2018. The Crabtree Effect Shapes the Saccharomyces cerevisiae Lag Phase during the Switch between Different Carbon Sources. doi:10.1128/mBio.01331-18.

Prelich, G. 2012. Gene overexpression: Uses, mechanisms, and interpretation. *Genetics*. 190:841–854. doi:10.1534/genetics.111.136911.

Rasala, B.A., A. V. Orjalo, Z. Shen, S. Briggs, and D.J. Forbes. 2006. ELYS is a dual nucleoporin/kinetochore protein required for nuclear pore assembly and proper cell division. *Proc. Natl. Acad. Sci.* 103:17801–17806. doi:10.1073/pnas.0608484103.

Rasala, B.A., C. Ramos, A. Harel, and D.J. Forbes. 2008. Capture of AT-rich Chromatin by ELYS Recruits POM121 and NDC1 to Initiate Nuclear Pore Assembly. *Mol. Biol. Cell*. 19:3982–3996. doi:10.1091/mbc.e08-01-0012.

Reinders, A., N. Bürckert, T. Boller, A. Wiemken, and C. De Virgilio. 1998. Saccharomyces cerevisiae cAMP-dependent protein kinase controls entry into stationary phase through the Rim15p protein kinase. *Genes Dev.* 12:2943–2955. doi:10.1101/gad.12.18.2943.

Rempel, I.L., M.M. Crane, D.J. Thaller, A. Mishra, D.P. Jansen, G. Janssens, P. Popken, A. Akşit, M. Kaeberlein, E. van der Giessen, A. Steen, P.R. Onck, C.P. Lusk, and L.M. Veenhoff. 2019. Age-dependent deterioration of nuclear pore assembly in mitotic cells decreases transport dynamics. *Elife*. 8. doi:10.7554/eLife.48186.

Rempel, I.L., A. Steen, and L.M. Veenhoff. 2020. Poor old pores—The challenge of making and maintaining nuclear pore complexes in aging. *FEBS J.* 287:1058–1075. doi:10.1111/febs.15205.

Rep, M., M. Krantz, J.M. Thevelein, and S. Hohmann. 2000. The Transcriptional Response of Saccharomyces cerevisiae to Osmotic Shock. *J. Biol. Chem.* 275:8290–8300. doi:10.1074/jbc.275.12.8290.

Ries, J., C. Kaplan, E. Platonova, H. Eghlidi, and H. Ewers. 2012. A simple, versatile method for GFP-based super-resolution microscopy via nanobodies. *Nat. Methods*. 9:582–584. doi:10.1038/nmeth.1991.

Robijns, J., G. Houthaeve, K. Braeckmans, and W.H. De Vos. 2018. Loss of Nuclear Envelope Integrity in Aging and Disease. *Int. Rev. Cell Mol. Biol.* 336:205–222. doi:10.1016/bs.ircmb.2017.07.013.

Rolland, F., J. WINDERICKX, and J. THEVELEIN. 2002. Glucose-sensing and -signalling mechanisms in yeast. *FEMS Yeast Res.* 2:183–201. doi:10.1016/S1567-1356(02)00046-6.

Romanauska, A., and A. Köhler. 2018. The Inner Nuclear Membrane Is a Metabolically Active Territory that Generates Nuclear Lipid Droplets. *Cell*. 174:700-715.e18. doi:10.1016/j.cell.2018.05.047.

Rout, M.P., J.D. Aitchison, A. Suprapto, K. Hjertaas, Y. Zhao, and B.T. Chait. 2000. The yeast nuclear pore complex: composition, architecture, and transport mechanism. *J. Cell Biol.* 148:635–51. doi:10.1083/jcb.148.4.635.

Rout, M.P., and S.R. Wente. 1994. Pores for thought: nuclear pore complex proteins. *Trends Cell Biol.* 4:357–365. doi:10.1016/0962-8924(94)90085-X.

Rusten, T.E., and H. Stenmark. 2009. How do ESCRT proteins control autophagy? *J. Cell Sci.* 122:2179–83. doi:10.1242/jcs.050021.

Sáez-Vásquez, J., and O. Gadal. 2010. Genome organization and function: A view from yeast and arabidopsis. *Mol. Plant*. doi:10.1093/mp/ssq034.

Sakuma, S., and M.A. D'Angelo. 2017. The roles of the nuclear pore complex in cellular dysfunction, aging and disease. *Semin. Cell Dev. Biol.* doi:10.1016/j.semcdb.2017.05.006.

Sambrook, J., and D.W. Russell. 2006. The Inoue Method for Preparation and Transformation of Competent E. Coli : "Ultra-Competent" Cells. *Cold Spring Harb. Protoc.* 2006:pdb.prot3944. doi:10.1101/pdb.prot3944.

Santiago-Moreno, J., M. Esteso, S. Villaverde-Morcillo, A. Toledano-Díaz, C. Castaño, R. Velázquez, A. López-Sebastián, A. Goya, and J. Martínez. 2016. Recent advances in bird sperm morphometric analysis, and its role in male gamete characterization and reproduction technologies. *Asian J. Androl.* doi:10.4103/1008-682X.188660.

Scarcelli, J.J., C.A. Hodge, and C.N. Cole. 2007. The yeast integral membrane protein Apq12 potentially links membrane dynamics to assembly of nuclear pore complexes. *J. Cell Biol.* 178.

Schindelin, J., I. Arganda-Carrera, E. Frise, K. Verena, L. Mark, P. Tobias, P. Stephan, R. Curtis, S. Stephan, S. Benjamin, T. Jean-Yves, J.W. Daniel, H. Volker, E. Kevin, T. Pavel, and C. Albert. 2009. Fiji - an Open platform for biological image analysis. *Nat. Methods*. 9. doi:10.1038/nmeth.2019.Fiji.

Schneiter, R., and C.N. Cole. 2010. Integrating complex functions: coordination of nuclear pore complex assembly and membrane expansion of the nuclear envelope requires a family of integral membrane proteins. *Nucleus*. 1:387–92. doi:10.4161/nucl.1.5.12333.

Scourfield, E.J., and J. Martin-Serrano. 2017. Growing functions of the ESCRT machinery in cell biology and viral replication. *Biochem. Soc. Trans.* 45:613–634.

doi:10.1042/BST20160479.

Sikorski, R.S., and P. Hieter. 1989. A system of shuttle vectors and yeast host strains designed for efficient manipulation of DNA in Saccharomyces cerevisiae. *Genetics*. 122:19–27. doi:10.1093/genetics/122.1.19.

Skinner, B.M., and E.E.P. Johnson. 2017. Nuclear morphologies: their diversity and functional relevance. *Chromosoma*. 126:195–212. doi:10.1007/s00412-016-0614-5.

Stade, K., C.S. Ford, C. Guthrie, and K. Weis. 1997. Exportin 1 (Crm1p) Is an Essential Nuclear Export Factor. *Cell*. 90:1041–1050. doi:10.1016/S0092-8674(00)80370-0.

Strunov, A.A., E.A. Onishchenko, and E. V. Kiseleva. 2011. Inhibition of POM152 and POM34 expression in budding yeast arrests the assembly of the nuclear pore complex and increases its inner diameter. *Russ. J. Genet. Appl. Res.* doi:10.1134/S2079059711030117.

Sun, S., and D. Gresham. 2021. Cellular quiescence in budding yeast. *Yeast*. 38:12–29. doi:10.1002/yea.3545.

Swinnen, E., V. Wanke, J. Roosen, B. Smets, F. Dubouloz, I. Pedruzzi, E. Cameroni, C. De Virgilio, and J. Winderickx. 2006. Rim15 and the crossroads of nutrient signalling pathways in Saccharomyces cerevisiae. *Cell Div.* 1:3. doi:10.1186/1747-1028-1-3.

Taimen, P., K. Pfleghaar, T. Shimi, D. Moller, K. Ben-Harush, M.R. Erdos, S.A. Adam, H. Herrmann, O. Medalia, F.S. Collins, A.E. Goldman, and R.D. Goldman. 2009. A progeria mutation reveals functions for lamin A in nuclear assembly, architecture, and chromosome organization. *Proc. Natl. Acad. Sci.* 106:20788–20793. doi:10.1073/pnas.0911895106.

Takahashi, Y., J. Mizoi, A. Toh-e, and Y. Kikuchi. 2000. Yeast Ulpl, an Smt3-Specific Protease, Associates with Nucleoporins. *J. Biochem.* 128:723–725. doi:10.1093/oxfordjournals.jbchem.a022807.

Talamas, J.A., and M.W. Hetzer. 2011. POM121 and Sun1 play a role in early steps of interphase NPC assembly. *J. Cell Biol.* 194:27–37. doi:10.1083/jcb.201012154.

Tamura, K., Y. Fukao, M. Iwamoto, T. Haraguchi, and I. Hara-Nishimura. 2010.

Identification and characterization of nuclear pore complex components in Arabidopsis thaliana. *Plant Cell*. doi:10.1105/tpc.110.079947.

Tamura, K., and I. Hara-Nishimura. 2011. Involvement of the nuclear pore complex in morphology of the plant nucleus. *Nucleus*. 2:168–172. doi:10.4161/nucl.2.3.16175.

Terweij, M., T. Van Welsem, S. Van Deventer, K.F. Verzijlbergen, V. Menendez-Benito, D. Ontoso, P. San-Segundo, J. Neefjes, F. van Leeuwen, V. Menendez-benito, D. Ontoso, P. San-segundo, J. Neefjes, F. van Leeuwen, V. Menendez-Benito, D. Ontoso, P. San-Segundo, J. Neefjes, and F. van Leeuwen. 2013. Recombination-induced tag exchange (RITE) cassette series to monitor protein dynamics in Saccharomyces cerevisiae. *G3 (Bethesda).* 3:1261–72. doi:10.1534/g3.113.006213.

Thaller, D.J., and C. Patrick Lusk. 2018. Fantastic nuclear envelope herniations and where to find them. *Biochem. Soc. Trans.* 46:877–889. doi:10.1042/BST20170442.

Theera-Umpon, N., and S. Dhompongsa. 2007. Morphological Granulometric Features of Nucleus in Automatic Bone Marrow White Blood Cell Classification. *IEEE Trans. Inf. Technol. Biomed.* 11:353–359. doi:10.1109/TITB.2007.892694.

Thiry, M., and D.L.J. Lafontaine. 2005. Birth of a nucleolus: the evolution of nucleolar compartments. *Trends Cell Biol.* 15:194–199. doi:10.1016/J.TCB.2005.02.007.

Tirupataiah, S., I. Jamir, I. Srividya, and K. Mishra. 2014. Yeast Nkp2 is required for accurate chromosome segregation and interacts with several components of the central kinetochore. *Mol. Biol. Rep.* 41. doi:10.1007/s11033-013-2918-3.

Titus, L.C., T.R. Dawson, D.J. Rexer, K.J. Ryan, and S.R. Wente. 2010. Members of the RSC chromatin-remodeling complex are required for maintaining proper nuclear envelope structure and pore complex localization. *Mol. Biol. Cell*. 21:1072–87. doi:10.1091/mbc.E09-07-0615.

Toda, T., S. Cameron, P. Sass, and M. Wigler^. 1988. SCH9y a gene of Saccharomyces cerevisiae that encodes a protein distinct from, but functionally and structurally related to, cAMP-dependent protein kinase catalytic subunits.

Tolksdorf, G., H. Stein, and K. Lennert. 1980. Morphological and immunological definition

of a malignant lymphoma derived from germinal-centre cells with cleaved nuclei (centrocytes). *Br. J. Cancer*. 41:168–182. doi:10.1038/bjc.1980.27.

Tomioka, Y., T. Kotani, H. Kirisako, Y. Oikawa, Y. Kimura, H. Hirano, Y. Ohsumi, and H. Nakatogawa. 2020. TORC1 inactivation stimulates autophagy of nucleoporin and nuclear pore complexes. *J. Cell Biol.* 219. doi:10.1083/JCB.201910063.

Toyama, B.H., R. Arrojo e Drigo, V. Lev-Ram, R. Ramachandra, T.J. Deerinck, C. Lechene, M.H. Ellisman, and M.W. Hetzer. 2019. Visualization of long-lived proteins reveals age mosaicism within nuclei of postmitotic cells. *J. Cell Biol.* 218:433–444. doi:10.1083/jcb.201809123.

Toyama, B.H., J.N. Savas, S.K. Park, M.S. Harris, N.T. Ingolia, J.R. Yates, and M.W. Hetzer. 2013. Identification of long-lived proteins reveals exceptional stability of essential cellular structures. *Cell*. 154:971–982. doi:10.1016/j.cell.2013.07.037.

Ulbrich, C., M. Diepholz, J. Baßler, D. Kressler, B. Pertschy, K. Galani, B. Böttcher, and E. Hurt. 2009. Mechanochemical Removal of Ribosome Biogenesis Factors from Nascent 60S Ribosomal Subunits. *Cell*. 138:911–922. doi:10.1016/j.cell.2009.06.045.

Verzijlbergen, K.F., V. Menendez-Benito, T. van Welsem, S.J. van Deventer, D.L. Lindstrom, H. Ovaa, J. Neefjes, D.E. Gottschling, and F. van Leeuwen. 2010. Recombination-induced tag exchange to track old and new proteins. *Proc. Natl. Acad. Sci. U. S. A.* 107:64–8. doi:10.1073/pnas.0911164107.

Walters, A.D., K. Amoateng, R. Wang, J.H. Chen, G. McDermott, C.A. Larabell, O. Gadal, and O. Cohen-Fix. 2019. Nuclear envelope expansion in budding yeast is independent of cell growth and does not determine nuclear volume. *Mol. Biol. Cell*. 30:131–145. doi:10.1091/mbc.E18-04-0204.

Walters, A.D., A. Bommakanti, and O. Cohen-Fix. 2012. Shaping the nucleus: Factors and forces. *J. Cell. Biochem.* doi:10.1002/jcb.24178.

Wang, C.-W. 2014. Stationary phase lipophagy as a cellular mechanism to recycle sterols during quiescence. *Autophagy*. 10:2075–2076. doi:10.4161/auto.36137.

Wang, R., A. Kamgoue, C. Normand, I. Léger-Silvestre, T. Mangeat, and O. Gadal. 2016.

High resolution microscopy reveals the nuclear shape of budding yeast during cell cycle and in various biological states. *J. Cell Sci.* 129:4480–4495. doi:10.1242/jcs.188250.

Webster, B.M., P. Colombi, J. Jäger, and C.P. Lusk. 2014. Surveillance of nuclear pore complex assembly by ESCRT-III/Vps4. *Cell*. 159:388–401. doi:10.1016/j.cell.2014.09.012.

Webster, B.M., D.J. Thaller, J. Jäger, S.E. Ochmann, S. Borah, C.P. Lusk, and B.M. Webster. 2016. Chm7 and Heh1 collaborate to link nuclear pore complex quality control with nuclear envelope sealing. *EMBO J.* 35:2447–2467. doi:10.15252/embj.201694574.

Webster, M., K.L. Wikin, and O. Cohen-Fix. 2009. Sizing up the nucleus: Nuclear shape, size and nuclear-envelope assembly. *J. Cell Sci.* doi:10.1242/jcs.037333.

Wente, S.R., and G. Blobel. 1990. A Temperature-sensitive NUPll6 Null Mutant Forms a Nuclear Envelope Seal over the Yeast Nuclear Pore Complex Thereby Blocking Nucleocytoplasmic Traffic.

Wente, S.R., and G. Blobel. 1993. A temperature-sensitive NUP116 null mutant forms a nuclear envelope seal over the yeast nuclear pore complex thereby blocking nucleocytoplasmic traffic. *J. Cell Biol.* 123:275–284. doi:10.1083/jcb.123.2.275.

Worman, H.J., C. Ostlund, and Y. Wang. 2010. Diseases of the nuclear envelope. *Cold Spring Harb. Perspect. Biol.* 2:a000760. doi:10.1101/cshperspect.a000760.

Woulfe, J.M. 2007. Abnormalities of the nucleus and nuclear inclusions in neurodegenerative disease: a work in progress. *Neuropathol. Appl. Neurobiol.* 33:2–42. doi:10.1111/j.1365-2990.2006.00819.x.

Wright, R., M. Basson, L. D'Ari, and J. Rine. 1988. Increased amounts of HMG-CoA reductase induce "karmellae": a proliferation of stacked membrane pairs surrounding the yeast nucleus. *J. Cell Biol.* 107:101–114. doi:10.1083/jcb.107.1.101.

Yavuz, S., R. Santarella-Mellwig, B. Koch, A. Jaedicke, I.W. Mattaj, and W. Antonin. 2010. NLS-mediated NPC functions of the nucleoporin Pom121. *FEBS Lett.* 584:3292–3298. doi:10.1016/j.febslet.2010.07.008.

Yeates, T.O., C.A. Kerfeld, S. Heinhorst, G.C. Cannon, and J.M. Shively. 2008. Protein-based organelles in bacteria: carboxysomes and related microcompartments. *Nat. Rev. Microbiol.* 6:681–691. doi:10.1038/nrmicro1913.

Yewdell, W.T., P. Colombi, T. Makhnevych, and C.P. Lusk. 2011. Lumenal interactions in nuclear pore complex assembly and stability. *Mol. Biol. Cell*. 22:1375–88. doi:10.1091/mbc.E10-06-0554.

Yorimitsu, T., S. Zaman, J.R. Broach, and D.J. Klionsky. 2007. Protein Kinase A and Sch9 Cooperatively Regulate Induction of Autophagy in Saccharomyces cerevisiae. *Mol. Biol. Cell*. 18:4180–4189. doi:10.1091/mbc.e07-05-0485.

Zhang, W., A. Khan, J. Vitale, A. Neuner, K. Rink, C. Lüchtenborg, B. Brügger, T.H. Söllner, and E. Schiebel. 2021. A short perinuclear amphipathic α-helix in Apq12 promotes nuclear pore complex biogenesis. *Open Biol.* 11. doi:10.1098/rsob.210250.

Zhang, W., A. Neuner, D. Rüthnick, T. Sachsenheimer, C. Lüchtenborg, B. Brügger, and E. Schiebel. 2018. Brr6 and Brl1 locate to nuclear pore complex assembly sites to promote their biogenesis. *J. Cell Biol.* 217:877–894. doi:10.1083/jcb.201706024.

Zheng, L., C. Schwartz, V. Magidson, A. Khodjakov, and S. Oliferenko. 2007. The spindle pole bodies facilitate nuclear envelope division during closed mitosis in fission yeast. *PLoS Biol.* doi:10.1371/journal.pbio.0050170.

Zhou, L., and N. Panté. 2010. The nucleoporin Nup153 maintains nuclear envelope architecture and is required for cell migration in tumor cells. *FEBS Lett.* 584:3013–3020. doi:10.1016/j.febslet.2010.05.038.

Zink, D., A.H. Fischer, and J.A. Nickerson. 2004. Nuclear structure in cancer cells. *Nat. Rev. Cancer*. doi:10.1038/nrc1430.

Understanding the role of Uip4p, a novel NE/ER protein in the maintenance of nuclear organization and cellular homeostasis in Saccharomyces cerevisiae

by Pallavi Deolal

Submission date: 15-Jan-2022 01:15PM (UTC+0530)
Submission ID: 1742065779
File name: Pallavi_Deolal.pdf (36.1M)
Word count: 24450
Character count: 127774

Understanding the role of Uip4p, a novel NE/ER protein in the maintenance of nuclear organization and cellular homeostasis in Saccharomyces cerevisiae

ORIGINALITY REPORT

27%	25%	25%	3%
SIMILARITY INDEX	INTERNET SOURCES	PUBLICATIONS	STUDENT PAPERS

PRIMARY SOURCES

1	www.biorxiv.org Internet Source	12%
2	www.ncbi.nlm.nih.gov Internet Source	6%
3	Pallavi Deolal, Imlitoshi Jamir, Krishnaveni Mishra. "Uip4p modulates nuclear pore complex function in Saccharomyces cerevisiae", Cold Spring Harbor Laboratory, 2021 Publication	2%
4	Submitted to University of Hyderabad, Hyderabad Student Paper	1%
5	www.tandfonline.com Internet Source	1%
6	hdl.handle.net Internet Source	<1%
7	scholarbank.nus.edu.sg	

This is to certify that primary sources 1, 2, 3 & 5 are papers published by Ms. Pallavi Deolal and constitute a major part of her thesis & should be excluded from the final score. Krishnaveni Mishra.

	Internet Source	<1%
8	edoc.ub.uni-muenchen.de Internet Source	<1%
9	V. Ramachandran, P. K. Herman. "Antagonistic Interactions Between the cAMP-Dependent Protein Kinase and Tor Signaling Pathways Modulate Cell Growth in Saccharomyces cerevisiae", Genetics, 2010 Publication	<1%
10	string-db.org Internet Source	<1%
11	www.rothsteinlab.com Internet Source	<1%
12	C. Miller. "Assessment of aryl hydrocarbon receptor complex interactions using pBEVY plasmids: expressionvectors with bi-directional promoters for use in Saccharomyces cerevisiae", Nucleic Acids Research, 08/01/1998 Publication	<1%
13	sro.sussex.ac.uk Internet Source	<1%
14	2013.igem.org Internet Source	<1%

15	Submitted to Higher Education Commission Pakistan Student Paper	<1%
16	lra.le.ac.uk Internet Source	<1%
17	MÃ³nica M. BelinchÃ³n, Juana M. Gancedo. " Glucose controls multiple processes in through diverse combinations of signaling pathways ", FEMS Yeast Research, 2007 Publication	<1%
18	Lisa A. Strawn, Heather L. True. "Deletion of RNQ1 gene reveals novel functional relationship between divergently transcribed Bik1p/CLIP-170 and Sfi1p in spindle pole body separation", Current Genetics, 2006 Publication	<1%
19	d-nb.info Internet Source	<1%
20	chemogenomics.pharmacy.ubc.ca Internet Source	<1%
21	Maxuel O. Andrade. "The HD-GYP domain of RpfG mediates a direct linkage between the Rpf quorum-sensing pathway and a subset of diguanylate cyclase proteins in the phytopathogen Xanthomonas axonopodis pv citri", Molecular Microbiology, 10/2006 Publication	<1%

22	Pallavi Deolal, Krishnaveni Mishra. "Regulation of diverse nuclear shapes: pathways working independently, together", Communicative & Integrative Biology, 2021 Publication	<1 %
23	Submitted to University of Huddersfield Student Paper	<1 %
24	Submitted to University of Sheffield Student Paper	<1 %
25	eprints.soton.ac.uk Internet Source	<1 %
26	journals.plos.org Internet Source	<1 %
27	mail.scialert.net Internet Source	<1 %
28	wrap.warwick.ac.uk Internet Source	<1 %
29	worldwidescience.org Internet Source	<1 %
30	www.repo.uni-hannover.de Internet Source	<1 %
31	Submitted to Birmingham-Southern College Student Paper	<1 %
32	Submitted to National University of Ireland, Galway	<1 %

	Student Paper	
33	ediss.uni-goettingen.de Internet Source	<1 %
34	era.ed.ac.uk Internet Source	<1 %
35	Mahboobeh Forouzanfar, Farzaneh Rabiee, Kamran Ghaedi, Siamak Beheshti et al. " overexpression facilitated neural differentiation of mouse embryonic stem cells ", Cell Biology International, 2015 Publication	<1 %
36	Malgorzata Ciska, Susana Moreno Díaz de la Espina. "NMCP/LINC proteins", Plant Signaling & Behavior, 2014 Publication	<1 %
37	summit.sfu.ca Internet Source	<1 %
38	purehost.bath.ac.uk Internet Source	<1 %
39	Submitted to Queen's University of Belfast Student Paper	<1 %
40	Submitted to University of Hong Kong Student Paper	<1 %
41	Ying Qi, Mark A. Gregory, Zhaoliang Li, Jeffrey P. Brousal, Kimberly West, Stephen R. Hann. "p19ARF directly and differentially controls	<1 %

	the functions of c-Myc independently of p53", Nature, 2004 Publication	
42	link.springer.com Internet Source	<1%
43	tel.archives-ouvertes.fr Internet Source	<1%

Exclude quotes	On	Exclude matches	< 14 words
Exclude bibliography	On		